UNIVERSITÀ DI PARMA

UNIVERSITÀ DEGLI STUDI DI PARMA

DOTTORATO DI RICERCA IN
SCIENZE DEL FARMACO

CICLO XXXVIII

Additive manufacturing of solid formulations tailoring oral administration for preclinical research

Coordinatore:
Chiar.mo Prof. Fabio Sonvico

Tutore:
Chiar.ma Prof.ssa Alessandra Rossi

Co-tutore:
Dott.ssa Anna Giulia Balducci

Dottorando:
Davide De Angelis

Anni Accademici 2022/2023 – 2024/2025

Table of contents

List of acronyms

3DP: 3D printed

API: active pharmaceutical ingredient

Ac-Di-Sol®: croscarmellose sodium

ACN: acetonitrile

ASD: amorphous solid dispersion

BJT: binder jetting

CA: citric acid

$CaCl_2$: calcium chloride

CAD: computer assisted design

CD: cyclodextrin

Chol: cholesterol

CLIP: continuous liquid interface production

DED: directed energy deposition

DLP: digital light processing

DLS: dynamic light scattering

DPE: direct powder extrusion

FaSSGF: fasted state simulated gastric fluid

FDM: fused deposition modeling

FFF: fused filament fabrication

FIH: first-in-human

GRAS: generally recognized as safe

H_2O: water

HME: hot melt extrusion

HPC: hydroxypropyl cellulose high viscosity (-H, -L, -SL and -SSL refer to different grades of viscosity and molecular weight)

HPMC: hydroxypropylmethyl cellulose

KH_2PO_4: potassium phosphate monobasic

KCl: potassium chloride

K-CL: Kollidon® CL

LVER: linear viscoelastic region

MCC: micro crystalline cellulose

MEX: material extrusion

MJT: material jetting

MWCO: molecular weight cut-off

NaCl: sodium chloride

NaCMC: carboxymethylcellulose sodium salt

Na_2HPO_4: sodium phosphate dibasic

NCEs: new chemical entities

PBF: powder bed fusion

PBS: phosphate buffer saline

PC: soy phosphatidylcholine

PDI: polydispersity index

PEG: polyethylene glycol

PEO: polyethylene oxide

PVA: polyvinyl alcohol

PVP: polyvinyl pyrrolidone

RPM: revolutions per minute

SA: sodium alginate

SBE-CD: sulfobutyl-ether-β-cyclodextrin

SHL: sheet lamination

SiO_2: silicon dioxide

SSE: semi-solid extrusion

SDS: sodium dodecyl sulfate

SLA: stereolithography

SLS: selective laser sintering

STD: standard

.stl: stereolitography interface format

TLE: thin layer evaporation

TPP: two-photon polymerization

UHPLC: ultra-high performance liquid chromatography

VPP: vat photopolymerization

Abstract

This doctoral thesis is the result of an industrial Ph.D. in collaboration with Chiesi Farmaceutici S.p.A. where the applications of advanced 3D printing technologies, specifically semi-solid extrusion (SSE) and direct powder extrusion (DPE), for the design, fabrication and characterization of oral solid dosage forms intended for preclinical *in vivo* studies are investigated. The research addresses the intrinsic limitations of early-stage drug research, such as restricted material availability, rodent administration dimensional constraints, and the need for precise modulation of drug release kinetics to support pharmacokinetic and pharmacodynamic investigations. Two model drugs, caffeine (BCS Class I) and naproxen (BCS Class II), were selected to be formulated targeting sustained and immediate release profiles, respectively. The 3D-printed dosage forms were engineered to match the dimensions of size 9 capsules, commonly used for oral administration in rodent models, with a target dose of 1.65 mg per unit and with all excipients chosen from the GRAS list, to support potential *in vivo* administration.

A comprehensive workflow was established, encompassing formulation design, 3D modeling, printing process optimization, and characterization of the printlets. For caffeine, both matrix and reservoir-type hydrogels were investigated using SSE. DPE was employed to fabricate matrix-based formulations using thermoplastic polymers and powder blends. For naproxen, various strategies were explored: SSE formulations included cyclodextrin complexes, lipidic excipients, liposomal carriers, and liquisolid hydrogels. DPE technology was used to produce matrix-based formulations with suitable size and drug content. Both API's printed formulations underwent complete characterization, including solid-state analyses (X-ray diffraction, differential scanning calorimetry), rheological evaluation, imaging (scanning electron microscopy and micro-computed tomography), drug content assay, and dissolution testing in simulated gastric fluid. Finally, the best promising caffeine 3D printed prototypes were further evaluated *in vivo* in rat models to assess pharmacokinetic profiles and systemic drug exposure.

The caffeine SSE reservoir formulations achieved sustained release profiles *in vitro*, reaching between 40% and 76% of release in 120 minutes. In contrast, DPE matrix formulations matched the reference capsule in release kinetics, but demonstrated superior performance in *in vivo* studies, prolonging systemic drug exposure. *In vivo* administration studies in rats confirmed the feasibility of using 3D-printed formulations for

preclinical pharmacokinetic investigations, highlighting the importance of physiological conditions in modulating drug release.

Regarding naproxen, the SSE optimized liquisolid hydrogels enabled the fabrication of low infill density solid forms with rapid drug release in simulated gastric fluid. On the contrary, DPE technology produced matrix-based forms where further refinements are needed to achieve immediate release performance.

This thesis establishes proof-of-concept for the use of SSE and DPE 3D printing technologies in the preparation of oral solid dosage forms for preclinical research. The study highlighted the critical role of formulation composition, printing parameters, and 3D model design in achieving the desired release kinetics. The minimal material requirements and rapid adaptability of 3D printing technologies present significant advantages for preclinical research, facilitating efficient screening and optimization of novel compounds. The ability to tailor drug loading and release kinetics in miniaturized dosage forms demonstrates the potential of additive manufacturing to advance the prototyping and customization of pharmaceutical formulations, thereby supporting their strategic research and enabling the integration of these technologies into future proprietary research projects.

1. Introduction

1.1. Preclinical drug discovery area and intrinsic limitations

The drug research and development process of creating a new drug is long (usually takes 10–15 years on average) and expensive (on average from $ 161 million to $ 4.5 billion), driven by complexity and multidisciplinary [1]. The process can be divided into three main pharmaceutical phases: drug discovery, drug development and dosage form commercialization [2]. Drug discovery research process usually starts with target validation and, after translational phases, hopefully ends up with clinical trials, all up to product marketing (see Figure 1) [3].

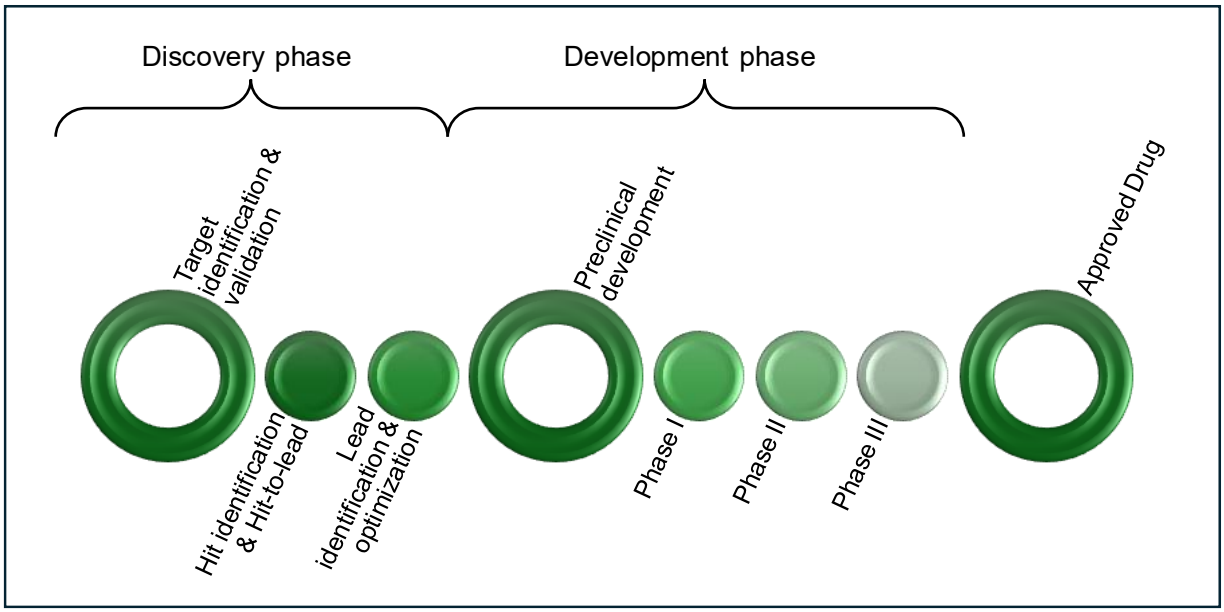

Figure 1. Drug discovery process (adapted from Antolović et al. [3]).

Early-phase drug development embraces the areas of drug discovery, preclinical studies, first-in-human (FIH) and phase I/II clinical trials [4]. Within these preliminary phases, new chemical entities (NCEs) are evaluated both with relevant *in vitro* and *in vivo* models in preclinical studies to assess their efficacy, safety and pharmacokinetic behavior among other factors, before moving on to early human studies and clinical trials [5]. Preclinical investigation usually takes one to three years to be completed and during this period a high rate of drug failure is present, due to several challenges, creating an important financial burden for the pharmaceutical industry [6]. Partial physico-chemical characterization, limited amount of drug available, short timelines and adverse drug properties (*i.e.* low solubility and permeability) are principal challenges to deal with during

pre-clinical formulation development [6]. Moreover, regarding preclinical animal models, physiological variations between animals' species must be taken into account, since they could deeply impact on the performance of a formulation (see Table 1). Especially with oral route, which is the most convenient, cost-effective and safe way to administer drugs, physiological differences could strongly impact the performance of the formulation, due to gastrointestinal environment inter-species variation limiting dissolution rate ad solubility of the dosed drug [7].

Table 1. Physiological differences between human and preclinical test species (adapted from Gao et al. [7])

Parameters	Humans	Rats	Dogs
Fasted gastric pH	0.95-3.2	1.5-3.0	3.5-4.5
Fed gastric pH	4.3-5.4	3.8-5.0	3.5-5.5
Duodenum pH	5.0-7.0	6.5-7.0	5.5-7.5
Stomach capacity (L)	1-1.6	0.0013 [8]	1.0
Gastric emptying time (min)	16-140	10-30	100
Small intestine transit time (min)	240	90	60-120
Total GI residence time (min)	2400	1200	770

1.2. Traditional formulations for preclinical studies

Rodents are the most common preclinical used animal model because of their handling easiness, low cost and physiological similarities with humans, often supported by *in vitro* test with biorelevant media, to improve *in vitro-in vivo* correlation [8]. The most used, cost-effective and safe administration route with rodents is the oral one, carried out with various types of formulations, like solutions (preferably with pH within 2 and 9), suspensions, capsules, mini-tablets and oils or neat co-solvents. Due to solubility limitations and potentially stability problems associated with liquid formulations, solid oral dosage forms could be preferrable and more convenient within pre-clinical studies with rodents [9]. Pure active pharmaceutical ingredients (APIs) can be directly administered to rats in filled size 9 capsules, using a proper dosing syringe [10]. In this way, the drug bioavailability will be precisely evaluated without excipients interference, making oral solid administration route the perfect tool for early drug screening [9].

On the other hand, manual filled capsules alongside with mini-tablets could present some challenges, involving fixed and limited dosages, being time and material consuming, avoiding formulation preparation easiness, being subjected to low API intrinsic solubility and being limited to gastric environment release [11].

1.3. 3D printing formulations in early drug discovery

The adoption of 3D printing, as an alternative formulation and manufacturing tool, may offer effective solutions to these challenges, enabling rapid and flexible production of oral solid dosage forms (also defined as printlets) to speed up preclinical evaluation, saving both costs and materials amount [5]. The optimal formulation for early phase development should offer high dose flexibility, ensure sufficient bioavailability, facilitate ease of administration and enable rapid study progression while remaining cost-effective. 3D printing technology enables oral solid formulation production with a wide variety of dosages, excipients composition and combinations, aiding the test of important factors like drug-excipients compatibility, drug release and subsequent pharmacokinetic behavior in selected preclinical animal models. Furthermore, the extensive design flexibility provided by 3D printing facilitates the manufacturing of dosage forms with geometries and dimensions specifically adapted to the requirements of preclinical testing environment [12]. 3D printing wide adaptability could be carried out within preclinical research areas tailoring drug dosage and release kinetics simply modifying printlet morphology or infill design and density. Changing the amount of material employed for the printing process permits easy modification of dosage form, according to the study requirements, and provides an efficient and precise method for data generation by means of drug dose modifications. Moreover, the change of solid dosage form design and density could have important effects on drug release, enabling precise control over release kinetics in a short timeframe, aiding to ensure optimal drug efficacy and safety, important characteristics to be kept supervised during drug delivery system investigation. With new 3D printing technologies is possible to print several different formulations in a unique process to obtain a single dosage form, for time- and site-dependent controlled release of drugs in the gastrointestinal tract [13].

Conventional manufacturing technologies for solid oral dosage forms have limitations, especially when requiring fast release and/or the combination of multi-kinetics profiles, as well as coatings or complex manufacturing processes [2]. On top of that, an important

amount of API is requested, barely available in early drug discovery phases. On the contrary, 3D printing permits to easily adapt to release kinetics requests with various possibilities, low API's amount and short efforts [14]. If a fast release of both low solubility and bioavailability drugs is requested, different possibilities could be investigated. For example, amorphous solid dispersions (ASDs) could be prepared *in situ* with 3D printing using a low amount of material. This is hard to obtain with conventional methods like hot melt extrusion or spray drying. Even low density and highly porous formulations could be easily prepared with 3D printing in a fast and reproducible way [15]. If a modified or pulsatile release formulation is required, 3D printing offers the advantage of creating intricate structural compositions or modifying coatings composition, amount or thickness, tailoring release kinetics in terms of time and site of release [16]. Other important features of pharmaceutical 3D printing that stands out from traditional formulative techniques are the possibility to obtain personalized medications to improve drug efficacy respect to patients individual necessities, as well as improve patient acceptability and therapeutic adherence to medicinal treatments, together with the possibility to decentralize pharmaceutical compounding, but these peculiarities are not relevant for the preclinical drug discovery area [5].

1.4. 3D printing technologies

Following the guidelines of the International Organization for Standardization (ISO), in cooperation with the American Society for Testing and Materials (ASTM), 3D printing is a terminology often used in non-technical context synonymously with additive manufacturing, respectively defined as a "process of joining materials to make parts from 3D model data, usually layer upon layer, as opposed to subtractive manufacturing and formative manufacturing methodologies". The guidelines identify seven main 3D printing categories: binder jetting (BJT), directed energy deposition (DED), material extrusion (MEX), material jetting (MJT), powder bed fusion (PBF), sheet lamination (SHL) and vat photopolymerization (VPP). They can be further divided into subcategories, where different names could be used for the same technology (Figure 2). Among them, only BJT, MEX, MJT, PBF and VPP are commonly used as pharmaceutical formulation technologies [9,17,18]. Each printing technology follows processing steps that encompass the development of the printed form through to its physical production. The first step is the final object modeling, normally performed with computer-aided design

(CAD) software. A 3D model is created for reproduction using the chosen technology and exported in a stereolithography file format (*stl*), which breaks down the surface of the object into triangles and provides information about their spatial coordinates. Next, the *stl* file is processed and the 3D model is converted into a layered structure through a slicing process. These sliced layers are then printed sequentially according to instructions contained in a newly generated *gcode* file, with each layer being added on top of the previous one. The obtained model must then be post-processed in order to obtain solidification and stabilization of the final structure [19,20].

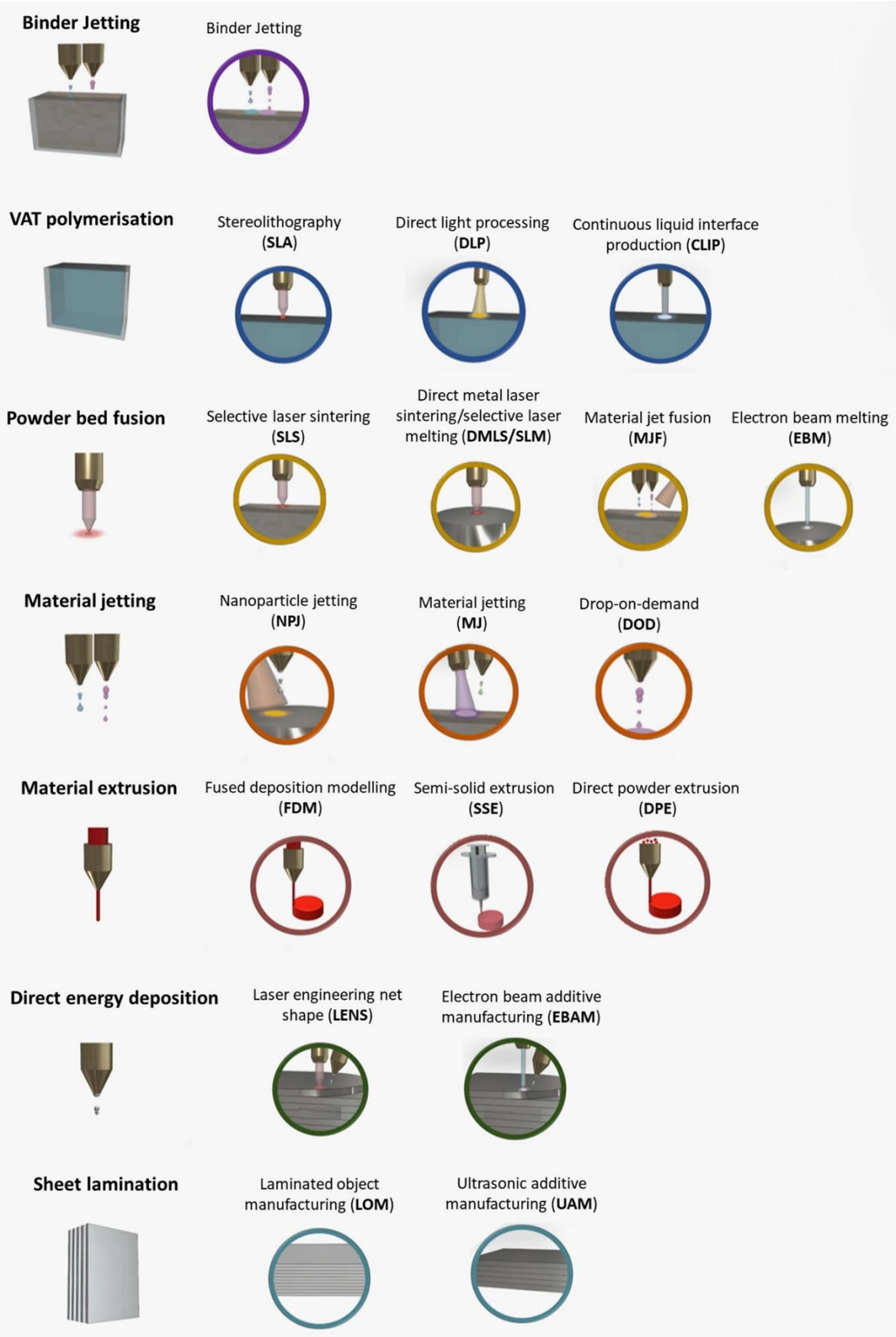

Figure 2. Graphical representation of different 3D printing categories and subcategories, reproduced from Seoane-Viaño et al. [9].

1.4.1. Binder jetting (BJT)

BJT is an additive technology defined as “a process in which a liquid bonding agent is selectively deposited to join powder materials” [17]. The world’s first approved 3D printed drug, Spritam®, was produced in 2015 by Aprecia Pharmaceuticals, adapting binder jetting technology as an alternative mass manufacturing process, the ZipDose® technology [9].

BJT technology is performed dropping the selected binder in form of droplets from the moving printhead onto a thin layer of powder, according to the sliced CAD model. The particles within the powder layer are consolidated through their interaction with the deposited binder solution. Once the initial layer is formed, an additional powder layer is applied above the previously lowered base, and the binder jetting process is repeated, thereby fusing successive cross-sections together (Figure 3) [21].

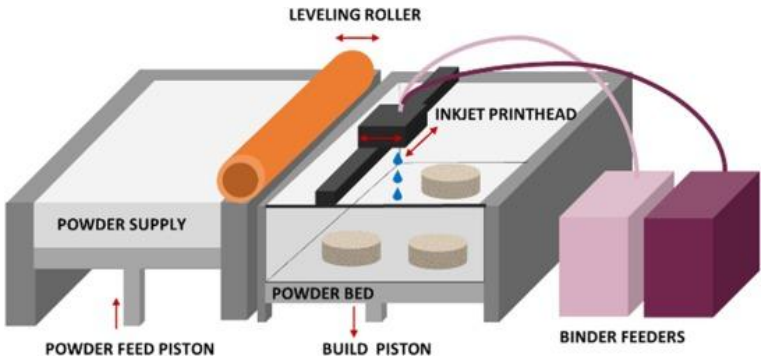

Figure 3. Schematic representation of 3D printing by binder jetting technology (reproduced from Kozakiewicz-Latała et al. [21]).

The drug could be both dispersed in the powder blend or dissolved in the binder solution. The binder agent acts forming solid bridges dissolving particles which could then recrystallize after solution evaporation, creating structures characterized by high porosity and low density. Because of that feature, this printing technique is advantageous for the fabrication of rapidly dissolvable tablets with high drug content [22]. Moreover, depending on the API and the excipients eventual interactions, drug recrystallization could be avoided, maintaining it in an amorphous state, an important characteristic to be monitored when working with poorly soluble compounds, as it may affect the dissolution process and subsequent drug release [23]. On the other hand, this high porosity could lead to defects as low printing resolution and high fragility of final printed form. In addition to that,

the employment of water-based binders is not always possible, relying on organic solvents more frequently, which brings with itself the problem of solvent drying and removal. Long drying processes could be necessary to avoid the presence of residual solvents in the final printed solid forms. At the same time, the prolonged exposure to high temperatures could lead to physico-chemical properties modifications of the API, which must be accurately monitored [24]. Nevertheless, advantages of binder jetting as 3D printing technology consist of the possibility to carry out the printing process at room temperature (avoiding potential drug degradation) and without the need of support because the powder that is not printed serves as support itself. Finally, other considerable challenges with BJT printers are that they are large, material consuming and appear to be designed only for large-scale manufacturing [25].

1.4.2. Material jetting (MJT)

Material jetting is defined as a “process in which droplets of feedstock material are selectively deposited” [17]. The receiving surface could be a previously prepared substrate (in this case we’re talking about 2D printing) or the printbed itself (in this other case it’s referred as 3D printing) [9]. Material jetting is often referred to as Inkjet printing and can be subdivided into two main different technologies, based on the physical process by which the liquid droplets are formed, known as continuous inkjet printing and drop-on-demand. Both these MJT methods rely on the “Theory of Instability” developed by Lord Rayleigh in 1878, which describes the separation of a stream of liquid or jet into droplets [26]. Moreover, some material jetting technologies require photocurable bio-inks to solidify the three dimensional printed structure, with limitations in terms of biocompatibility of excipients and photo-activators [25].

Continuous inkjet printing was developed during the 1960s and was based on a continuous stream of liquid that is ejected through a nozzle that further breaks up, forming a uniform stream of droplets under surface tension [27]. Droplet separation from the continuous stream is facilitated by imparting an electrical charge to the droplets as they transit an electrostatic field. Subsequently, these charged droplets are precisely deflected from the main trajectory at controlled angles, directing them onto the surface of substrate to produce the intended 3D printing model. For droplet separation management, any undesired drops are diverted into a gutter, where they are collected and recycled [20]. On the other hand, drop-on-demand printing was developed during the 1970s and is based

on the ejection of droplets from the nozzles only when they are needed. This technology utilizes piezoelectric, electrostatic, electrodynamic, or thermal actuators (Figure 4) to create droplets by applying pressure pulses to the ink solution [27]. Drop-on-demand inkjet printing is being used in the biomedical and pharmaceutical fields mainly due to its features of low cost, high throughput, scalability and easy processability. Moreover, due to the ability of precisely control amount and size of droplets generated, there is high potential for personalized medicine, working precisely with high potent or low dose drugs, reducing waste of material [28]. Several challenges that this printing technology brings along are mainly related to the ink formulation, printing mechanism, final droplet deposition and solidification process. Especially the selection of the proper formulation composition is quite important. The selection of appropriate solvent alone or in combination must consider the physicochemical parameters of the desired drug, especially its solubility and behavior during solvent evaporation. In addition, where excipients are used, the obtained formulation viscosity and surface tension are key features both related to droplet formation and deposition, spreading through the printing substrates or enabling layer-to-layer adhesion on the printbed. Formulation stability to materials, residence time and printing technology must be considered, especially with thermal actuators, where the temperature is considerably raised [29].

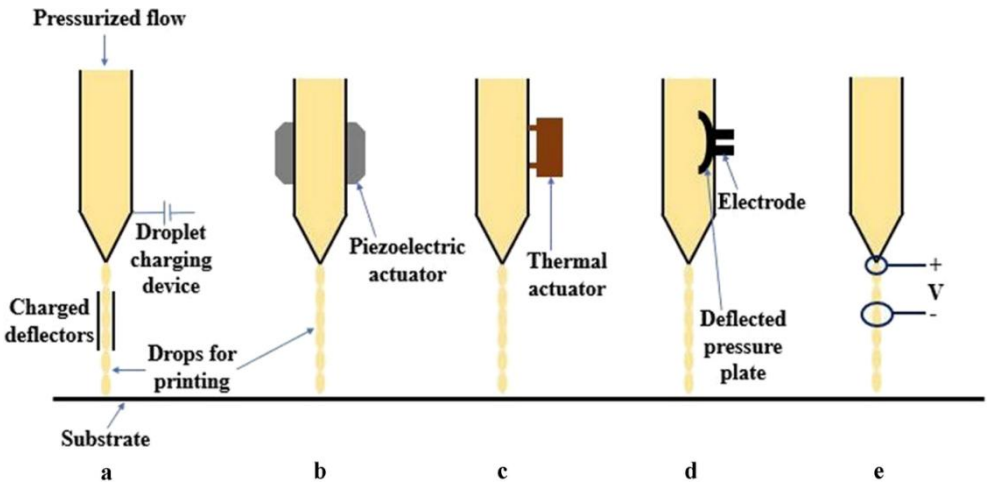

Figure 4. Schematic representation of various 3D material jetting technologies (reproduced from Muhindo et al. [27]).

1.4.3. Powder Bed Fusion (PBF)

Currently defined as “a process in which thermal energy selectively fuses regions of a powder bed” [17], this technology commonly uses a laser to reproduce the CAD model,

melting the formulation particles together. Between all the subcategories, the most well-known and employed in the pharmaceutical area is the selective laser sintering (SLS) [9]. The printer setting is similar to BJT, but instead of inducing bonds with a jetting liquid formulation, the 3D structure is created by fusing the formulation particles together through the input of high thermal energy, most commonly CO_2 lasers (Figure 5) [22].

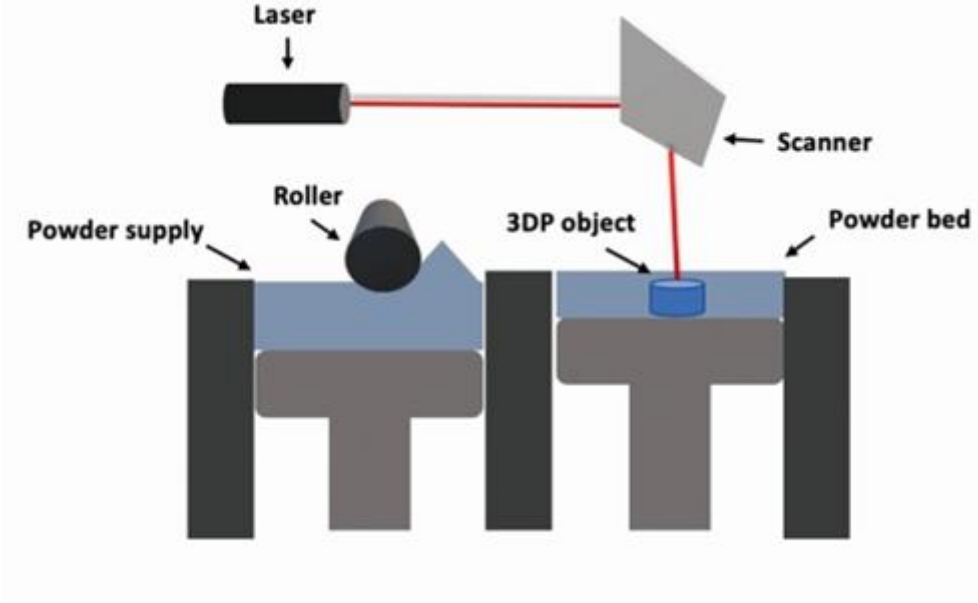

Figure 5. Schematic representation of selective laser sintering technology (reproduced from Pitzanti et el. [24]).

Like with binder jetting, a powder bed is generated by the formulation with the aid of a roller. Then, the laser selectively melts the particles in specific areas, according to the CAD model. After that, the building platform is moved downwards, and a new layer of formulation is dropped off the previous one, continuing the melting and curing process, in order to generate the 3D model. At the end of the process, when the printed form temperature is reduced, the solid dosage form generated could be removed from the powder bed and immediately used without post processing requirements. Moreover, there is low wastage of formulation, since the powder bed could be reusable for other printing processes. On the other hand, the amount of formulation required is high and needs to possess adequate flow properties to be moved between the chambers. Moreover, with SLS printing, external support is not required because the powder bed itself serves as support during the process. Other advantages of SLS printing technology are related to the fact that it is a one step, solvent free process with fast production, high resolution and

high throughput [24,30]. Generally, polymeric blends are required with SLS printing, due to their thermal properties. Thermoplastic polymers must be able to efficiently absorb energy at the laser wavelength for successful sintering, protecting the drug from thermal degradation. Ideally, polymers should have high melting enthalpy and low thermal conduction. Laser sintering of blends is especially employed to print immediate release formulations characterized by high porosity, but extended-release formulations could be printed as well, combining appropriate polymers and excipients. For many years SLS was mainly related to supports, implants or medical devices, due to its capability of printing complex and detailed structures with high risk of drug degradation. Additional limitations for using this technology, particularly in preclinical research, include the requirement for large quantities of material as well as the significant cost and size of the printers [25,31].

1.4.4. Vat Photopolymerization (VPP)

The definition of vat photopolymerization states “process in which liquid photopolymer in a vat is selectively cured by light-activated polymerization” [17]. The technique involves stereolithography (SLA), digital light processing (DLP), continuous liquid interface production (CLIP), volumetric 3D printing and two-photon polymerization (TPP) as subcategories (Figure 6). All of them encompass the use of a photosensitive liquid resin which is illuminated, following a specific path, by a light-source and allowing for photopolymerization reaction and consequently inducing resin solidification in consecutive (or simultaneous for volumetric 3D printing) layers [31,32]. VPP is the 3D printing technology that produces the highest resolution structures within micrometer range, with optimal accuracy, giving the possibility to print very complex structures [25].

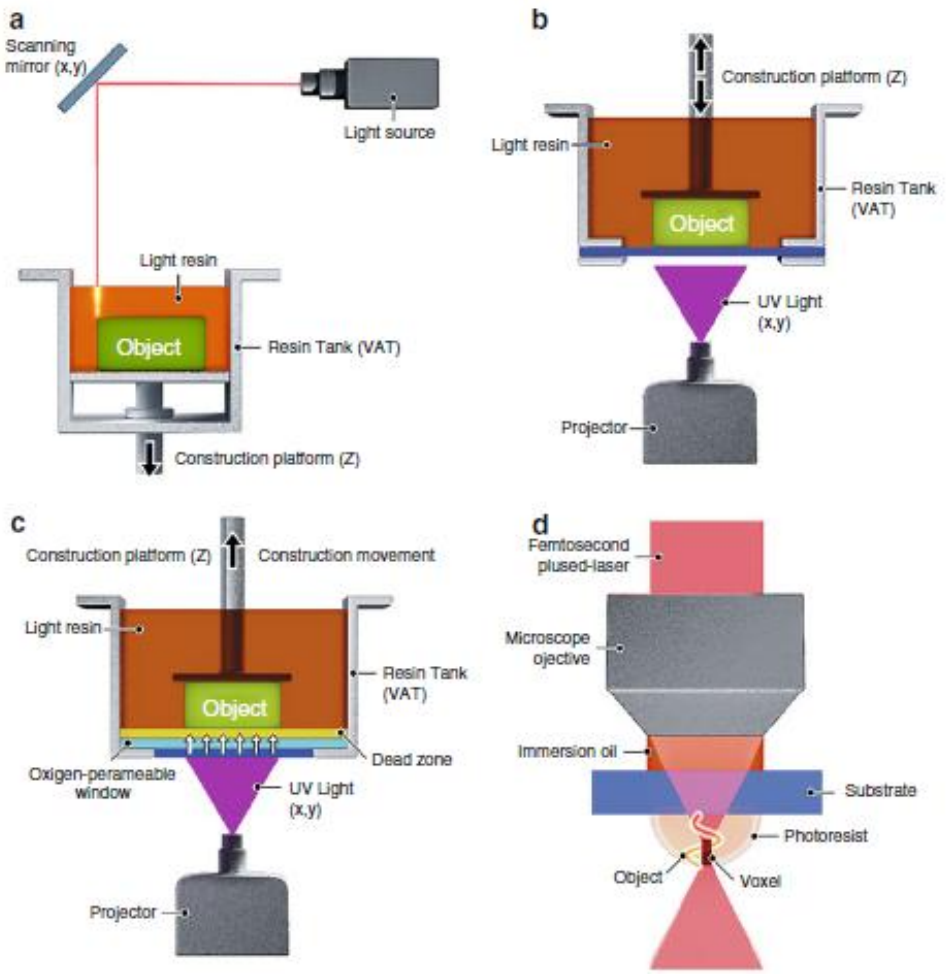

Figure 6. Vat photopolymerization subcategories: (a) SLA, (b) DLP, (c) CLIP and (d) TPP (reproduced from D'Ávila et al. [33]).

The liquid resins, employed with VPP 3D printing, are normally composed of photopolymers (monomers and oligomers) and photo-initiators. When the light source is activated, it triggers the photo-initiator to generate reactive species that catalyze chain formation between the photopolymers, resulting in the transition of the resin from a liquid to a solid state. Upon completion of the printing process, a post-processing step is typically performed in which the printed form is washed with solvents, such as isopropyl alcohol, to eliminate any unpolymerized resin. Subsequently, the object undergoes additional curing under UV light or sunlight to enhance its mechanical properties. Drugs can be either incorporated in the liquid resin before the printing, achieving a solution or a homogenous suspension, or soaked/loaded (es. dipping or spray coating) onto the printed form after the printing process. In the first case, photopolymers employed within the resin should protect the drug from UV degradation, which is avoided with the second

approach, involving an additional manufacturing process [34,35]. These 3D printing technologies offer several advantages, such as high surface resolution, short printing times, heat-free printing and relatively low material consuming and low-cost printers. Moreover, VPP printing enables the production of complex shapes that are not achievable with conventional manufacturing methods, allowing for controlled drug release by altering the geometry of drug tablets [33,36]. Despite all these unique characteristics and advantages, photopolymerization 3D printing brings with itself some concerns, primarily related to the safety of photocurable resins. These materials are typically composed of methacrylates or acrylic esters, materials not in the Generally Recognized As Safe (GRAS) list. Precisely, the residue uncured monomers could leach out from the printed forms, causing safety problems. The isopropyl alcohol washing step is mainly performed to remove the uncured residues, but careful must be taken, due to the nature of the washing solvent (highly volatile, flammable and central nervous system depressant). Moreover, the washing step could alter drug loading into the printed form, washing away drug particles entrapped on the surface during printing process. Then, another problem could be related to eventual reactions happening during drug incorporation into resin formulation. Drug must remain intact before, during and after printing process, without chemical reactions occurring with the photopolymer. Along with its high resolution and ability to print complex structures, it is important to note that, unlike BJP and SLS, VPP does not provide a self-supporting environment. As a result, there may be warping or collapsing of structures during printing if they are not reinforced by additional supports. Moreover, removing the temporary support could be labor-intensive and time-consuming, leaving marks and imperfections on the printed form surface. On the other hand, when fabricating objects with internal voids, the liquid resin inside cavities could unintentionally solidify, because the internal material could receive and absorb light during the printing process. Accordingly, it is essential to carefully calibrate the printing resolution for each resin, ensuring that a thorough washing process is performed immediately afterward, prior to proceeding to the curing stage. However, up until now no resins have been approved for use within medicinal products, lacking for regulatory specifications for the 3D printing technique [35]. Despite several dosage forms have been prepared with VPP, like immediate release oral solid forms, transdermal microneedles, porous scaffolds and printed molds, due to its safety concerns within the medicinal area, VPP is most widely used for medical devices (es. dental applications) or scaffolds to be further loaded with biologics [20].

1.4.5. Material extrusion (MEX)

The last category of 3D printing technologies employed within pharmaceutical area is material extrusion, described as a “process in which material is selectively dispensed through a nozzle or orifice” [17]. It is mainly divided into fused deposition modeling (FDM), semi-solid extrusion (SSE) and direct powder extrusion (DPE). Material extrusion is the most commercialized and employed in pharmaceutical area among all the 3D printing technologies, due to its low cost, flexibility of materials employed and ease of use [2, 25].

1.4.5.1. Fused Deposition Modeling (FDM)

FDM 3D printing technology was invented in 1988 by Scott Crump while trying to build a toy for his daughter with a simple glue gun. This gave him the idea of patenting the technology into an automated version, co-founding Stratasys, Ltd. to commercialize the equipment from 1992 [16]. It is one of the most popular among additive manufacturing categories due to its usefulness, low cost, ease of use, small size of printing equipment, accuracy and versatility of printed products [15]. Often referred also as Fused Filament Fabrication (FFF) [37], it is a process based on the deposition of successive layers of softened/fused material, according to the previously prepared and sliced CAD model, in order to reproduce the desired final object [16]. For the printing of solid dosage forms, usually a specific polymeric filament is employed, commercially available from the market or especially generated by Hot Melt Extrusion (HME) technique from thermoplastic polymers [37]. As graphically represented in Figure 7, the spooled filament is de-spooled and moved to the heating zone making use of rotating gear rollers. Once arrived towards the heated zone, the filament gets softened/melted and is extruded through the nozzle onto the printbed, where it cools down and hardens, ready to be bonded to successive layers [38].

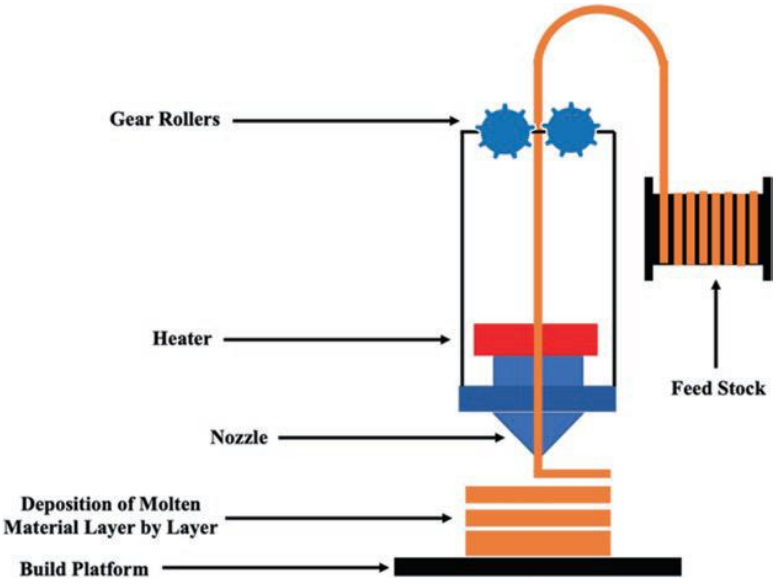

Figure 7. Schematic representation of FDM printing process (reproduced from Nyavanandi et al. [38]).

Fused deposition modeling is a useful 3D printing technique due to its characteristic to abstain printed forms from post fabrication treatments, such as solvent evaporation, washing or curing [49]. Its main complication is related to the filament fabrication and its required characteristics to enable an efficient printing process [16]. Another issue is represented by drug loading into printable formulations, which could be performed by filament impregnation into a saturated API solution or incorporation into polymeric blend prior to HME process [37]. Filament impregnation presents inherent challenges, primarily associated with the solvent removal process prior to printing. This step is time-intensive and typically results in drug particles remaining predominantly on the surface of the filament. Additionally, drug loading capacity is generally restricted to a maximum of 5% w/w [38]. Conversely, hot melt extrusion enables higher drug loadings but, as it is an additional formulation step, could be considered as the main challenge for FDM printing process, especially due to its high working temperatures [16]. FDM and HME are processes based on high temperatures, causing the softening or fusion of polymeric excipients. By that, the two processes are unsuitable for drugs that are affected by high temperature, causing degradation, lack of action or adverse effects [38]. Another important factor is the selection of polymers, often coupled with plasticizers, to improve their mechanical, rheological and thermal properties. First of all, polymers must be of pharmaceutical grade and, secondly, they should be compatible with the selected drug

[16,31]. Pharmaceutical grade available polymers are limited and, in addition, their frequent hydrophilic nature poses a challenge to the stability of solid forms, caused by the continuous absorption of moisture from the environment [38]. Adjusting the design of CAD model and the filament composition, various types of modified release formulations could be prepared using FDM. Solid dosage forms featuring early or delayed release, multicompartment and multilayer tablets, as well as fast-dissolving or extended-release formulations, can all be manufactured using this technology. Moreover, due to the generally good mechanical resistance of printed forms, is possible to print also systems to be assembled after fabrication or reservoir parts to be filled and closed in a second time [16,49]. Ultimately, FDM 3D printing technology may be considered more appropriate for research and rapid prototyping stages, rather than for industrial scale manufacturing or large volume production [2].

1.4.5.2. Direct Powder Extrusion (DPE)

Big part of pharmaceuticals works involving FDM 3D printing of solid dosage forms. A wide amount of effort is put on filament conceptualization and production, followed by drug loading testing into the selected excipients composition [39]. Direct powder extrusion (DPE) was developed as an improvement from FDM 3D printing technology. It is based on powder blends which are directly loaded into the printhead, heated and melted extruded from a hot nozzle onto the printbed following the CAD designed geometry and deleting the need for prior filament fabrication and/or modification [40]. DPE technology, introduced within pharmaceutical area in 2019, was ideated mainly to transform a two-step process like FDM into a one-step 3D printing process [31,37]. A schematic representation of the various DPE 3D printing technologies is reported in Figure 8.

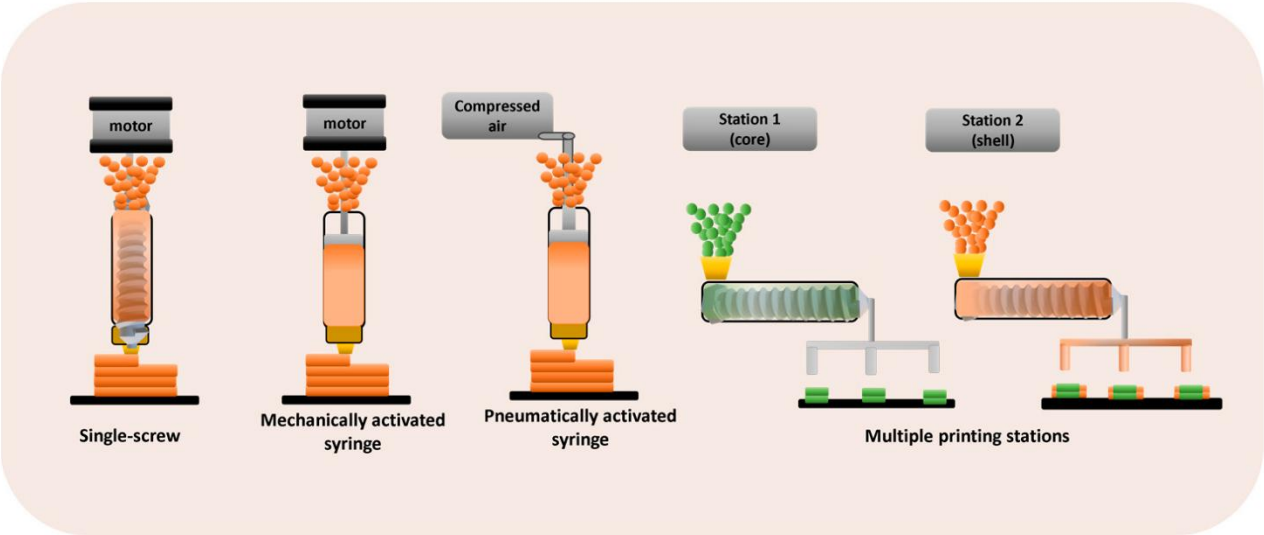

Figure 8. Schematic representation of DPE printers' technologies (reproduced from Aguilar-De-Leyva et al. [41]).

As already mentioned, DPE technology could pose solutions to the printing of formulations not adequate to FDM, due to unfavorable mechanical characteristics of the hot melt extruded filaments, such as too brittle or too flexible to be loaded into 3D printers [39]. Another big advantage of DPE regards small batch sized formulations. DPE printers do not need as much material as an hot melt extruder, making them especially tailored to formulative works in the preclinical research area, where usually amount of available drug is limited (see section 1.1) [9]. Moreover, DPE could help to improve amorphous solid dispersions' stability, avoiding the double heating of API included in FDM printing technology, which could lead to recrystallization of amorphous molecules [40].

DPE 3D printers are subdivided depending on the extrusion technique employed, as reported in Figure 8. Generally, extrusion is carried out using either a single-screw vertical extruder or pneumatically/piston-driven prefilled cartridges. Single-screw extruders normally are supported by a hopper and can accommodate a higher amount of material respect to prefilled cartridges. On the other hand, printers, incorporating a hot-end heating and a material extrusion procedure, can work with multiple printheads simultaneously to print complex or multi-compartment structures reducing printing times and increasing accuracy and efficacy of the printing process [41].

Nevertheless, it is important to emphasize that robust formulation development remains essential also for the 3D printing of solid dosage forms using DPE. Being especially suited for preclinical research phases, it must be noted that, on the other hand, the small amount

of drug available limits the batch size of dosage forms that can be printed for every printing process [41,42]. Another important factor to be taken into consideration is the rheological behavior of the powder blend or of the melted blend. Good flowability is requested by powder blends to be homogeneously and efficaciously extruded. If the flowability is not sufficient, rather than adding glidants or lubricants to the formulation, another solution could be represented by the use of pellets or granules, but the one-step characteristic of DPE would be loss. Flowability could be strongly influenced also by electrostatic forces, modifying the feeding amount of blend during the printing, interfering with homogeneity of the process and printed forms [42]. Moreover, the viscosity of the melt should be adequate to achieve satisfying extrusion, deposition and morphology retaining before solidification. Most often the molten polymers employed are non-Newtonian fluids with increasing or decreasing viscosity under pressures. As with HME processes, plasticizers could be used to modify the blend viscosity within the DPE 3D printing process [41]. Since DPE is essentially a modification of FDM, the main challenge to be faced is the high printing temperature employed. The materials used are required to be thermally stable at the processing temperatures, preventing thermolabile drugs to be processed with this 3D printing technology [40]. Normally, to enable sufficient adhesion to the printbed, a slight heating of the printing platform is required. Despite the printbed temperatures are usually lower than the ones utilized during extrusion, the API could be exposed to them for longer periods, therefore it is important to set the parameter adequately to avoid drug degradation [41].

DPE 3D printing technology could be employed to prepare both sustained or immediate release oral solid dosage forms, depending on polymers used during formulation preparation and dosage form density selected for the final printed form. Moreover, operating at high temperatures, drugs could be amorphized within polymeric melted matrix yielding to amorphous solid dispersion, helping to increase the drug solubility and dissolution rate, especially important for the preparation of immediate release solid formulations [40, 43].

1.4.5.3. Semi Solid Extrusion (SSE)

Semisolid extrusion (SSE), also known as Pressure Assisted Microsyringe (PAM), direct ink writing, micro-extrusion or many other names [44], is a 3D printing technology belonging to material extrusion category, extensively employed from the early 2000s to

prepare soft tissue implants and scaffolds [19,31]. As suggested by the name, the technology is based on the extrusion of semi-solid formulations, such as gels, pastes or melts, as deposited material. After deposition, the material starts to harden, allowing the subsequent layers to be sustained by the ones already deposited below [44]. The prepared formulation is loaded in advance into cartridges (or syringes), which could both be disposable or reusable, and extruded through the printhead nozzle with the help of pressurized air, mechanical forces or solenoid valves, following the path created during the slicing phase of the prepared 3D CAD model [31]. A representation of the different extrusion technologies usually employed in SSE 3D printing are reported in Figure 9 [44]. Another big difference from FDM or DPE 3D printing technologies is the lower temperature required by SSE to be carried out, making this technology more appropriate to print thermolabile drugs and bioprinting of living cell structures and organ-on-a-chip models [9,45].

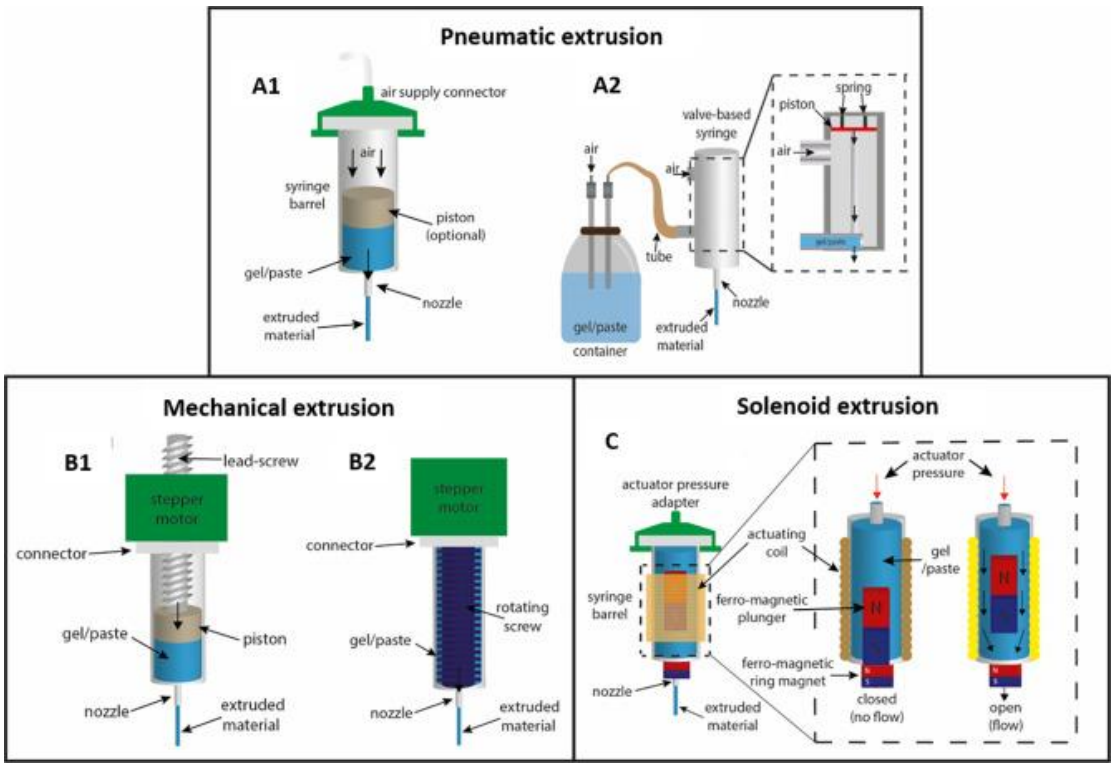

Figure 9. Schematic representation of various SSE technologies (reproduced from Rahman et al. [45]).

3D printed solid dosage forms and biostructures can be printed accommodating various widely known excipients during semi-solid formulation preparation. Moreover, it is possible to tailor release profiles and characteristics within a single step process in few

minutes, empowering this printing technology for its use in preclinical research fields. On the other hand, the scale up to industrial production is difficult due to low throughput, resolution of printed objects and post printing solidification processes required [44,45]. As shown in Figure 9-A1, pneumatic extrusion printers work with the help of pressurized air to obtain material extrusion. Plungers can also be inserted into reusable syringes before enabling the extrusion process, in order to seal off the formulation from solvent vapor escape and subsequent modifications. Pneumatic based printers are commonly referred as precise and fast responding, as the syringes could be efficiently pressurized [44,45]. Mechanical extrusion printers usually apply works with pistons or screws to apply a mechanical force to the material, as shown in Figure 9-B1 and 9-B2. Piston based printers can obtain greater control during extrusion, while screw-based printers can extrude higher viscous semi solid materials. Finally, with solenoid-based printers (Figure 9-C) the extrusion is obtained opening a valve with electrical pulses. These pulses act on ferromagnetic plungers to allow for dispensing of small volumes of low viscosity material (in the order of μL). This technique is usually employed to extrude bioink solutions, to be crosslinked with ionic or UV irradiation mechanisms [44]. These printing techniques embrace the use of different types of printheads, like temperature controlled, electrospinning, UV based or co-axials, quite often with disposable nozzles and single use or autoclavable syringes, trying to improve sterilization protocols during bioprinting. Moreover, with printers equipped with more than one printhead, there is the possibility to combine different printing techniques within a single process [45].

Semi-solid formulations are usually prepared mixing cross-linkable polymers, solvent, drug (even poorly soluble ones) and additives. Since the starting material is a viscous formulation, its rheological properties are fundamental to obtain a satisfactory printing process and may be considered as the main characteristics to be aware of when researching processes reproducibility [19]. First of all, the formulation should not be too viscous and guarantee to be extruded through the nozzle but, on the other hand, if the formulation is not viscous enough there could be leakage and the reproducibility of CAD model not obtained [31]. From these premises, the ideal rheological behavior of semi-solid formulations should be shear-thinning without thixotropy and, therefore, non-Newtonian. Generally, the formulation loaded into the cartridges must be extruded through the nozzle with a constant flow, to obtain continuous deposition of a homogeneous filament. By that, material flow is required only with application of air or mechanical pressure, not before. This behavior is described by the relationship between

elastic and viscous modulus of hydrogels (G' and G'', respectively). Initially, extrusion elastic (or storage) modulus results to be higher than viscous (or loss) modulus but, during extrusion, the situation is flipped over and G'' modulus results to be higher than G' modulus. This overturning moment is defined as the cross-over point (or yield point) and is the moment at which the material flow is initiated for the first time. After that, once the applied force is stopped, further material extrusion should be avoided showing a fast recovery of initial viscosity, to ensure maximum shape fidelity of printed material [44,45]. This fast restoration of hydrogel network, achieved with a good balance of elastic and viscous properties, is also of great importance in maintaining the cylindrical shape of the extruded material through the nozzle. Swelling of the extruded strand at the exit point or shrinking caused by excessive viscosity recovery are directly linked to unsatisfactory printed form resolution. By the way, the rheological prediction of nozzle extrudate characteristics is still a challenging task to be carried out [44].

Within this 3D printing technology other factors are important to be considered, such as nozzle dimension, printing and printbed temperature, drying and solidification. The nozzle diameter considerably influences printing resolution. A lower diameter is directly linked with a higher resolution of the printed object but, on the other hand, with smaller nozzles the force required to extrude the formulation turned out to be much higher and attention must be paid to eventual insoluble excipients. As a general rule, any insoluble or crystalline material should be at least ten times smaller than the nozzle diameter to avoid obstructions which could lead to imperfections and stability problems or incomplete printing process. Moreover, when a larger nozzle is employed, the risk of structural collapse is lower, due to less contact points which give more rigidity to the printed structure [44]. Another important parameter to be precisely set is the printing temperature. The viscosity of starting material could be influenced by variation in printhead temperature, enabling a better material extrusion or causing printing problems if not carefully controlled. The printbed temperature should be adjusted as well. It could be raised to improve extruded material adhesion or speed up the solidification process for the printed forms. Adhesion to the printing platform should not be excessive, since the printed object must be easily removed at the end of the printing process. In addition, printbed temperature could be fine-tuned to reduce warping or curling of printed material during drying [45]. The most important parameter to be taken into account with semi-solid extrusion 3D printing technology in the post-printing phase is the printed object solidification step. If the extruded structure lacks sufficient strength, collapse may occur

due to the inability of the lower layers to support the weight of the upper layers. As a consequence, the extruded material could change shape and sized over time, resulting in shrinking or deformation of the built structure. Usually, solidification procedures include drying, cooling, crosslinking or crystallization [19,45]. Crosslinking of polymers could be induced in several ways. One of the most common methodologies is represented by the ionic crosslinking, usually performed with the help of bi- or trivalent cations added both initially within the formulation or after ending the material deposition, as external solution. Another approach to obtain crosslinking includes the exposure of printed objects to a light source (commonly UV light), obtaining photopolymerization of monomers/oligomers included in the printed formulation. A more alternative approach regards the use of chemical reactions between materials, once they come in contact with each other. These reactions could happen for example between an embedding matrix and the supported material or in the case of coordinated printing processes. Finally, since this printing technology is based on formulations prepared with the aid of solvents, the most common solidification process is represented by drying, cooling and solvent removal. When the extrusion is carried out using heat, the solidification is determined by the cooling of the material. On the other hand, for a major part of low temperature printing processes, solvent (or combination of solvents) must be removed employing high temperatures, controlled conditions, freeze drying or vacuum-drying. Temperature drying must be carefully monitored, to avoid drug degradation, warping or collapsing of extruded structures. Moreover, controlled drying could be also used to functionalize the printed object, introducing surface modifications or required porosities [19,44,45]. Lastly, the solvent removal from the semi-solid formulation is important also to avoid eventual residuals in the printed solid form which could be harmful or lead to stability issues regarding the included API, like promoting re-crystallization or Ostwald ripening [19,45].
Due to its unique characteristics, SSE 3D printing has the possibility to produce small batches in short times, adapting the final drug dosage with flexibility, together with the use of biocompatible excipients, making it the perfect choice for preclinical areas applications, overcoming eventual problematics derived from the lack of designed equipment to prepare formulations specifically for animal testing [44]. More than that, SSE is probably the most suitable 3D printing technology to produce personalized medicines (together with FDM and DPE) due to the variety of dosage forms that can be prepared and the amount of excipients listed as GRAS, to be employed within semi-solid formulations in a simple, fast and reproducible way [44]. In addition to oral solid forms, other dosage forms

could be prepared, like suppositories, films, implants, scaffolds and patches. Regarding solid oral dosage forms, both sustained and fast release could be obtained, tailoring formulations and 3D model design (infill density or infill pattern). Gastric floating forms are mainly produced, due to low density of semi-solid material. In addition, attention must be paid to disintegrants employed for immediate release, since their enhancing release ability could be altered by the interaction with polymeric matrix and, by that, must be further investigated. Also targeted drug delivery could be obtained together with the inclusion of specific excipients and specifically adapting 3D structures [31,45]. To conclude, another aspect that could be further explored is formulation stability and how prolonged storage could affect semi-solid material properties. Although the printlets could be prepared right before the administration, it could be useful to store pre-filled cartridges with an already prepared formulation, ready to be printed when necessary [44].

2. Aim of the research

The research project investigated the application of 3D printing technology for the preparation of oral solid formulations for preclinical purposes. Considering the intrinsic limitations arising from an early stage of preclinical research area, the formulation prototypes were conceived and designed to improve key properties of active pharmaceutical ingredients, essential for drug administration and activity. Caffeine and naproxen, belonging to classes I and II of the Biopharmaceutical Classification System (BCS) respectively, were selected as model drugs. The main goal of the project was to enhance the prolonged release of caffeine and fast release of naproxen in simulated gastric environment by means of formulations produced with 3D printing technologies.

The 3D printing techniques employed in this thesis, semi-solid extrusion (SSE) and direct powder extrusion (DPE), are classified under material extrusion processes. These technologies were chosen for their simplicity, versatility, resolution, low consumption of starting materials, and the possibility to be investigated using a single 3D printer equipped with interchangeable printheads.

The 3D-printed dosage forms were manufactured to match the dimensions of the size 9 capsules, typically used at preclinical stage to administer *in vivo* the drugs to rodent animal models. Small dimensional constraints of rodent's administration pose a great challenge for the formulation technologies, also in relation to the target dose of drugs, which was set to 1.65 mg/dosage form.

Formulations containing caffeine (BCS class I: high solubility and high permeability) aimed to achieve sustained release, whereas naproxen formulations (BCS class II: low solubility and high permeability) were intended to increase the drug release in simulated gastric environment. For all formulations, excipients approved for oral administration and listed as GRAS were selected supporting the potential for *in vivo* administration.

The printed solid formulations were fully characterized. The API solid state was investigated before and after the printing process, to evaluate potential physico-chemical modifications. Rheologic evaluations of caffeine hydrogels were performed, as general comparison between several different formulations. Imaging involving SEM and Micro-CT was carried out on all the printed formulations. Release test and drug loading were performed on selected 3D printed structures in order to evaluate the project objective's achievement and to enable the selection of solid formulations exhibiting the most promising *in vitro* release profiles. The optimized prototypes were subsequently moved

to *in vivo* administration studies. The primary objective of this activity was to assess the performance and suitability of different formulation platforms for their potential application in future proprietary projects. By evaluating the *in vivo* efficacy and adaptability of each platform, this approach aimed to support the strategic development of novel chemical entities, ensuring that only the most effective and reliable of them are considered for advancement within the company's research pipeline.

3. 3D printlets for sustained release of caffeine

3.1. Semisolid Extrusion

3.1.1. Materials

Model drug caffeine was purchased from Merck Life Sciences (Darmstadt, Germany). The following excipients were employed to formulate the printlets. Calcium chloride, carboxymethylcellulose sodium salt (NaCMC, viscosity 50-200 cP, c=4% H_2O at 25°C), cellulose acetate phthalate, chitosan, citric acid, glycerol, mannitol, sodium alginate and sorbitol were purchased from Merck Life Sciences (Darmstadt, Germany), while hydroxy propyl cellulose (-H MW 1.000.000 kDa) was kindly donated by Nippon Soda (Tokyo, Japan).

Hydroxy propyl methyl celluloses (HPMCs: Methocel K4M, K15M and K100M) were obtained from Colorcon (Gallarate, Italy). Kollidon® CL (crospovidone) was provided by BASF (Ludwigshafen, Germany). Polyvinyl alcohol (PVA, GOHSENOL™ EG-03P, 27-33 mPas) was obtained from Harke (Milan, Italy). Simulated gastric fluid (FaSSGF) prepared for dissolution studies in acidic media was obtained from Biorelevant (London, UK). Deionized and purified water was obtained with MilliQ® systems (Merck Life Sciences, Darmstadt, Germany). All the solvents used were analytical grade.

3.1.2. Methods

3.1.2.1. Hydrogel preparation

Hydrogel formulations were all prepared following a procedure shown in Figure 10 and adapted from the work published by Khaled et al. [46] and Moroni et al. [47]. Briefly, deionized water was heated up to 80°C; then, excipients and API were added under magnetic stirring until complete dispersion. After that, the appropriate amounts of polymer and chemical crosslinker were added to the hot solution still under magnetic stirring and left until complete homogenization. Heating was switched off and the obtained suspension was left to cool down until room temperature enabling the hydrogel formation. The mixtures were then left to rest overnight at 5°C. To remove air bubbles eventually trapped inside the hydrogel network, a centrifugation process was carried out for 1h at 5000 rpm and 23°C. Air bubbles should be avoided, because during the printing process could create holes or defects into the printed forms.

For interesting formulations the extrudability was evaluated, considering formulations “extrudable” when a good flowability and a uniformity of material coming out from the nozzle were observed. Subsequently, the extrudable formulations were considered “printable” when the layer-by-layer deposition of the hydrogel led to the production of the desired design.

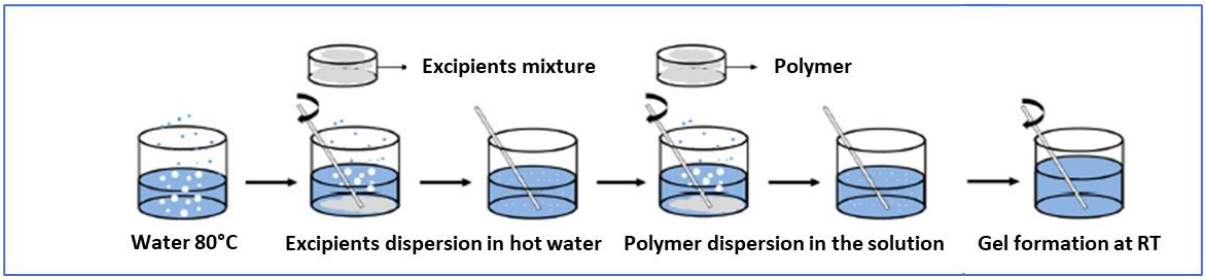

Figure 10. Hydrogels formulation process flow (adapted from Moroni et al. [46]).

3.1.2.2. 3D printing process

The printing process was carried out with a Cellink BIOX (Cellink Life Sciences, Gothenburg, Sweden), which gave us the possibility to interchange printheads in relation to the type of 3D printing technology to be employed. The uploaded G-Code of the design was generated in accordance with the predesigned CAD model (prepared with free software Tinkercad, Autodesk). Printing heads (4-250°C depending on mounted printhead) and printing bed (4-65°C) temperatures were adjusted according to material necessities. Extrusion pressures ranged from 0 to 200 kPa (with internal pump of the machine). Printheads employed were pneumatic, temperature controlled or thermoplastic, in relation to material properties and formulation type. Pneumatic and temperature-controlled printheads were employed with hydrogels or pastes (SSE) while thermoplastic printhead with powder blends (DPE).

3.1.2.3. Rheology investigation

Hydrogels rheological behavior was studied using a TA Instrument Discovery HR20 5343-1204 rheometer (New Castle, US), equipped with a 20 mm diameter plate geometry. Analyses were performed by placing an amount of gel (approximately 0.3 mL) onto the rheometer's plate with a stainless-steel spatula, ensuring full coverage of the geometry plate positioned on the rotor. The lowering of the rotor onto the stator (plate) was

automatically calibrated by the instrument. The gels were immediately analyzed to prevent dehydration. Each gel was subjected, under the same experimental conditions, to the following tests: amplitude sweep test, flow test, yield stress, peak hold.

- Amplitude sweep test: the test was conducted at 25°C or 50°C (for specific formulations). During the analysis, the oscillation strain, expressed as a percentage, was increased from 0.01 to 100% (from 0.001 to 100% for specific formulations), while the frequency, representing the number of oscillations per second, was set at 10 Hz and kept constant throughout the test.
- Flow test: the analysis was carried out using a Control Rate method (with controlled shear rate). The sample was placed on the plate which was automatically lowered by the instrument. Analyses were performed at 25°C or 50°C (for specific formulations), increasing the shear rate from 0.001 to 1 s^{-1} (60 rpm) over 300 seconds; immediately afterwards (without allowing the sample to rest), the shear rate was decreased from 1 to 0.001 s^{-1} (0.06 rpm) over another 300 seconds.
- Peak hold: the analysis was performed at 25°C, maintaining a constant shear rate of 0.1 s^{-1}. The duration of the analysis was set at 30 seconds, required to stabilize the viscosity values.
- Yield stress: the analysis was conducted by applying an increasing shear stress from 0.1 to 2000 Pa or to 4000 Pa in 60 seconds.

3.1.2.4. Solid state characterization

3.1.2.4.1. X-Ray Diffraction (XRD)

The solid state of 3D printed forms was investigated by X-ray Powder Diffraction with Empyrean V2.0 (Malvern Panalytical, Almelo, Nederlands), equipped with Cu radiation source (Cu Kα 1.5406 Å), generator voltage set to 40 kV and the current to 40 mA. Samples were acquired under transmission mode spinning with revolution time 0.5 s. The measurements were scanned over 2θ range from 2 to 45°, step size 0.02°, soller slit 0.02 rad, divergence slit 1/2°, antiscatter slit 1/2°. The analyses were conducted in duplicate on different printed forms.

3.1.2.4.2. Differential Scanning calorimetry (DSC)

DSC analyses of caffeine printed forms were performed to detect drug crystallization or thermal phases that occurred during the printing process. TA Instruments Discovery (Waters, New Castle, US) was used to conduct the DSC analysis. First, the instrument was calibrated for energy and temperature using certified Indium. Typically, one third or half of each printlet was placed into an aluminium pan. The pan was covered with a lid but not sealed. The sample was equilibrated at 0°C and heated up to 250°C at a rate of 10°C/min under a nitrogen flow of 50 mL/min. The instrument control and data analysis software used was Trios. The analyses were conducted at least in duplicate.

3.1.2.4.3. Scanning Electron Microscopy (SEM)

Images of the surface of printed forms were acquired, under high-vacuum environment at various magnifications, using an EVO HD Scanning Electron Microscope (Zeiss, Oberkochen, Germany). The voltages, used to acquire images, are embedded in the image itself. The chemical map was carried out in energy dispersion spectroscopy (EDS) with X-MAXN detector (Oxford Instruments, Abingdon-on-Thames, UK). Samples were analysed as they are or coated in Gold for three minutes using an Agar Sputter coater at 30 mA.

3.1.2.5. Drug content assay

3.1.2.5.1. Method developed in Chiesi Farmaceutici

The amount of caffeine loaded and released from the printed forms was determined by UHPLC Waters Acquity (Milford, US) and analysed using DAD Water software. Samples (5 µL) were injected into a C8 column (Kinetex C8 100 x 2.1 mm, 1.7 µm, Phenomenex, Torrance, US) and eluted with a gradient: ammonium formate 0.0025M pH 3 (phase A) and acetonitrile with 0.1% v/v formic acid (phase B). The gradient timetable is shown in Table 2.

Table 2. Gradient timetable for caffeine quantification method.

Time (min)	A (%)	B (%)
0.00	99.0	1.0
0.50	99.0	1.0
3.00	70.0	30.0
6.50	50.0	50.0
7.50	20.0	80.0
8.00	20.0	80.0
8.10	99.0	1.0
10.00	99.0	1.0

The column temperature was set at 55°C. The flow rate was 0.5 mL/min and the detection wavelength was set at 254 nm. The samples were prepared using pure water (by Milli-Q system) and the retention time was 1.24 minute. The data are presented as mean ± standard deviation, n = 3.

3.1.2.5.2. Method developed at University of Parma

The determination of caffeine in the samples was carried out using a Shimadzu Nexera LC-40DXS UHPLC chromatographic system (Shimadzu Corporation, Kyoto, Japan), equipped with a UV photodiode array detector SPD-M40, an autosampler SIL-40CXS, and an oven CTO-40C. A Symmetry column (250 x 4.6 mm, 5 µm; Waters, Wexford, Ireland), heated to 30°C, was used as the stationary phase. The mobile phase consisted of a mixture of methanol:water in a 30:70 ratio (%, v/v), with a flow rate of 1 ml/min and an injection volume of 10 µL. The wavelength was set at 274 nm. The chromatographic analysis lasted 9 minutes, and the retention time for caffeine was 6.5 minutes. The analytical method was validated in terms of linearity in the range 0.25 - 100 µg/mL (R^2 = 0.999), precision (RSD < 1%), and sensitivity (LOD 0.005 µg/mL, LOQ 0.016 µg/mL).

3.1.2.6. In vitro dissolution

3.1.2.6.1. Method developed in Chiesi Farmaceutici

Preliminary *in vitro* dissolution test of caffeine semi solid printed forms was performed in 15ml of FaSSGF fluid (Biorelevant, London, UK). The mixing of simulated gastric media

was guaranteed by magnetic stirring fixed at 75 rpm and the temperature kept controlled at 37 ± 0.5°C. A customized 3D printed plastic support, designed and printed within Chiesi Farmaceutici S.p.A, was inserted to avoid the floating of the printlets and the contact between them and the magnetic stirrer. Commercial capsules size 9 (Torpac®, Fairfield, US) filled with pure drug were taken as reference. The dissolution release was monitored for two hours using a UV probe (Pion Rainbow system, North Carolina, US) which allowed a continuous measurement of the concentration of caffeine in solution (acquisition range 200-710 nm, processing range 290-305 nm).

3.1.2.6.2. Method developed at University of Parma

According to the *in vitro* dissolution profiles obtained with the method described in section 3.1.2.6.1, selected printed forms were further characterized in terms of *in vitro* dissolution studies using the USP II apparatus (Varian 705 DS, Agilent Technologies Inc, Santa Clara, US). Analyses were performed at pH 1.2 for two hours. Dissolution media were prepared according to specifics reported in Ph. Eur. Ph. last edition, monography 5.17 *"Recommendations on methods for dosage forms testing"*. For pH 1.2, 250 mL of KCl 0.2 M solution were mixed with 425 mL of 0.2 M HCl solution and made up to 1 L volume with MilliQ water. The pH was adjusted, if necessary, with HCl 37%.

In each vessel, equipped with paddle, three printlets were added to 300 mL of acidic media. Temperature was set to 37 ± 0.5°C and paddle rotation was kept at 100 rpm. During dissolution test, samples of 5 mL were withdrawn at prefixed timepoints, filtered with 0.45 µm regenerated cellulose syringe filters (Sartorius, Göttingen, Germany). After every sampling the dissolution media volume was restored with 5 mL of fresh one, kept at 37°C.

During the 2h at pH 1.2 dissolution test, sampling was performed every 10 minutes.

3.1.2.7. X-Ray micro-computed tomography

X-Ray micro-computed tomography (µTC) was conducted using the Skyscan 1276 high-resolution microCT system (Bruker, Kontich, Belgium) equipped with a tungsten anode, controlled by the software Skyscan 1276 control program (Bruker, version 1.8). Samples underwent scanning with filter, employing a pixel size of 4.49 µm, a source voltage of 50 kV, and a current of 72 µA, rotating through 360° at increments of 0.2°. Projections were

reconstructed using NRecon software (Bruker, version 2.1.0.1). The resulting three-dimensional reconstructions were analyzed both in three-dimensional and two-dimensional perspectives using CT Analyzer (Bruker, Version 1.20.8.0). A fixed threshold range of 67–256 grey levels was chosen for all analyses. The threshold range selected allowed the identification of voids in the material, avoiding the inclusion of artefacts in the analysis.

3.1.2.8. In vivo administration in rats

3.1.2.8.1. In vivo administration protocol

A total number of 12 male Sprague-Dawley rats, with a body weight (BW) of 367-467 g at the day of experiment, were used in this study. Animals were catheterized at the femoral vein by the supplier (Charles River Labs, Lyon, France), to enable serial blood sampling from each rat. The vascular catheter was externalized in the scapular region and connected to a Vascular Access Harness (VAH). After the arrival at the test site, an acclimatization period of one week was given to the animal. Animals were not fasted before the experiment. The experimental procedures involving animals, carried out at Chiesi Farmaceutici S.p.A, Parma (Italy), were approved by Italian Ministry of Health (Aut. N. 113/2024-PR) and complied with the European and Italian regulations for animal care and use of laboratory animals. Animal studies were performed in accordance with the recommendations of the Association for Assessment and Accreditation of Laboratory Animal Care (AALAC) of which the accreditation was granted in July 2024 and with efforts to minimize the number of animals used and their suffering.

3.1.2.8.2. In vivo oral PK in rat

Different selected solid oral 3D printed formulations of caffeine were administered to catheterized rats (n=4 rats for each formulation) using a suitable device (stainless steel capsule dosing syringe, for size 9 capsules, provided by 2 Biological Instruments, Besozzo, Italy). After administration, rats were kept for one minute on the bench to be sure that the capsule was not expelled and then returned to their cage. The final dose (in mg/kg) was calculated according to the capsule loading and rat body weight and reported in the results section. After administration, at fixed time points, 300 µL blood samples were withdrawn from the femoral vein catheter, added with sodium heparin anticoagulant,

and centrifuged within 30 min from the collection at 1400 G, 4°C, 10 min, to obtain plasma samples. All the available plasma volume was transferred in labelled plastic tube and immediately stored at -80°C until the analysis. Plasma aliquots were analyzed for caffeine quantitation using HPLC-MS/MS equipment.

3.1.2.8.3. HPLC-MS/MS analysis for caffeine quantification

Sample analysis was performed on a Triple Quad 5500 mass spectrometer (AB Sciex, Milan, Italy) in ESI positive MRM mode, coupled to UPLC I Class (Agilent Technologies, Santa Clara, US). Separation was done through a Gemini 5µm C18 110A column 50 x 2.00 µm (Phenomenex Inc., Torrance, US). Analyte separation was achieved with 1% v/v formic acid in water (eluent A) in gradient with methanol 100% (eluent B), at a flow rate of 300 µL/min. The gradient timetable is shown in Table 3.

Table 3. Gradient timetable for caffeine quantification method from in vivo samples.

Time (min)	A (%)	B (%)
0	90	10
0.8	90	10
1.8	30	70
3.5	30	70
4.5	90	10
5.5	90	10

Theophylline was included as a suitable internal standard (IS) to reduce the impact of variability of sample preparation and analysis on the bioanalytical result. The detection of the ions was performed in the multiple reaction monitoring (MRM) mode, monitoring the transition of m/z 194.905 precursor ion $[M+H]^+$ to the m/z 138.0 product ion for caffeine and m/z 180.895 precursor ion $[M+H]^+$ to the m/z 124.00 for IS, respectively. The MS caffeine parameters were set as follows: CUR: 35; CAD:7; TEM: 500; IS: 5500; CE:25; CXP:8; EP:7; GS1:40; GS2:40. The linearity range for caffeine in rat plasma was 0.1 – 400 ng/mL.

Calibration standards and quality control samples were prepared by adding 10 µL of caffeine calibration standard or quality control (QC) solutions to 25 µL of blank heparinized rat plasma, stored at -80°C in polypropylene tubes until use. Then, 10 µL of IS solution

and 150 µL of ACN were added before the agitation, filtration and extraction process. For the analysis of blank samples and analyte unknown samples, 10 µL analyte were replaced by 10 µL ACN/H20 50/50. The extraction from matrix was performed by protein precipitation method using Whatman syringless Uniprep devices. After filtration and addiction of 50 µL water + 1% formic acid, the Mini-Unipreps were placed directly into the auto-sampler and 5 µL of the filtrated sample were injected into the LC-MS/MS system.

3.1.2.8.4. Pharmacokinetic analysis

Plasma data were used for the calculation of the relevant PK parameters C_{max}, T_{max}, AUC_{0-24}, $t_{1/2}$, and Mean Residence Time, used for the comparison of the different formulations, by Winnonlin non-compartmental analysis of Phoenix 64 software (Certara, USA).

3.1.3. Results

Caffeine is an oral BCS Class I drug, characterized by a high water solubility (around 20 g/L) and permeability [48]. Due to its intrinsic characteristics, formulation activities object of this work was intended to prolong its release kinetics in simulated gastric media, obtaining a sustained release. To do so, the 3D printing technology selected to start with was semisolid extrusion, which includes the extrusion at low temperatures of polymer-based gels or pastes. In polymer-based drug delivery system, a polymer is used to reach the desired sustained release (first order) maintaining persistent levels of drug. Diffusion and swelling are two of the most common release mechanisms from polymeric systems, achieved with polymers like cellulosic ones. Due to their hydrophilic nature HPMC and NaCMC were the first polymers to be investigated within polymeric formulations with caffeine employed as model drug [32, 45, 49-52].

3.1.3.1. Matrixial formulations

To obtain the sustained release of caffeine [53,54], from the various polymer-based drug delivery systems available, the one chosen to begin with was the matrix one. Matrix systems are one of the largest explored in 3D printing formulations. Within these systems, the drug can be dissolved or in a dispersed phase, depending on the polymer-drug solubility and drug concentration, very often with the addition of soluble or insoluble fillers [49,55]. During early release phases from matrix hydrogels, the first phenomenon observed is polymer solvation and swelling, followed by its dissolution in the surrounding media. They continue to act concomitantly and are coupled with diffusion and dissolution of the drug through the expanded polymer in the release media. The successive polymeric chain disentanglement (true polymer dissolution) and the dissolution of the drug or fillers used counteracts this increase in thickness, producing a diminution of the volume of the matrix. In the end, if the media solvation activity leads to a complete dissolution of the swollen matrix, these are called swellable-soluble matrices. Using a combination of glassy polymers, additives and incorporation of crosslinks, dynamic swelling and drug release from a system can be appropriately modulated [49,55].
For the scope of this project, first a 3D CAD model was prepared (see section 3.1.2.2), reproducing the aspect and dimensions of Torpac® commercial capsules size 9 (Table 4). Since it could be difficult to reproduce the rounded shape of a commercial capsule, it was decided to modify the 3D CAD model into a shape more similar to an elongated tablet.

The edges were rounded while the upper and lower surfaces were flattened in order to achieve better adhesion to the printing bed and a better resolution of the process. The CAD model is reported in Figure 11.

Table 4. Dimensional requirements of capsule size 9.

Description	Capsule size 9
Capsule body capacity	0.025 ml
Maximum external diameter	2.65 mm
Maximum lenght	8.6 mm
Weight empty average	9 mg

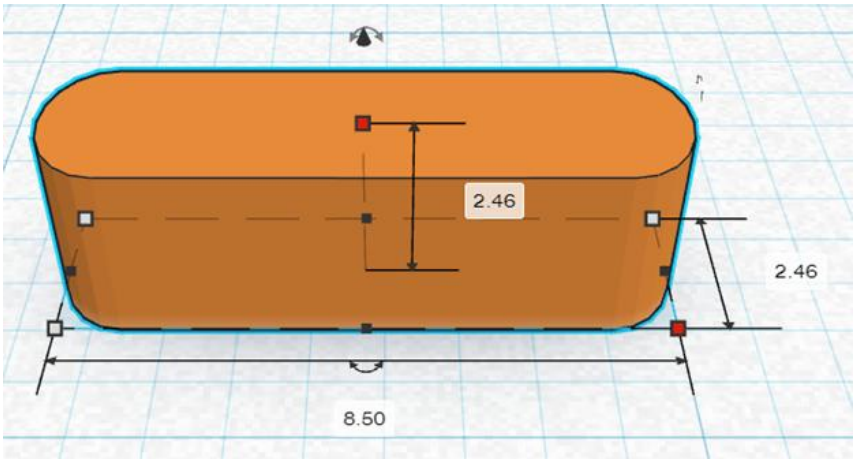

Figure 11. CAD model of printlets reproducing dimensions of size 9 capsule.

Preliminary formulation trials on the effectiveness of the 3D printing process, applied to the CAD model previously designed, started with gelation studies of cellulosic polymers. Following the formulation process reported in section 3.1.2.1, placebo hydrogels of HPMC K4 and NaCMC were prepared, obtaining concentrations of 12% w/v and 20% w/v, respectively. As reported in the work of Moroni et al. [47], citric acid was employed together with NaCMC as chemical crosslinker at 2% w/v concentration. Both placebo hydrogels resulted to be extrudable within manual extrusion trials from the 3D printer. As a result, new formulations, including caffeine, were prepared (composition reported in Table 5) in order to investigate how the caffeine addition could affect extrudability of hydrogels.

Table 5. Composition of caffeine loaded A/B formulations. All concentrations are reported as % w/v respect to water.

Formulation	HPMC K4M	NaCMC	Citric acid	Caffeine
A	12	-	-	15
B	-	20	2	15

The starting concentration of caffeine to be added to cellulosic hydrogels was set at 15% w/v, taking into account the 5 mg/kg dose for eventual *in vivo* administration in rodents. The caffeine loaded hydrogels resulted extrudable and were loaded in the printer to perform a complete printing process, following the CAD model reported in Figure 11. The printing parameters employed for formulations A and B are reported in Table 6.

Table 6. Printing parameters of formulations A and B.

Formulation	Extrusion Pressure (kPa)	Printing Speed (mm/s)	Printing Temperature (°C)	Layer height (mm)	Preflow (ms)	Postflow (ms)
A	170	1	60	0.4	-200	200
B	110	1	-	0.4	-200	300

Formulations were printed with a 100% infill density and a concentric infill pattern, generated by the printer's software. The obtained printed forms were then left to dry overnight at standard laboratory conditions (24°C, 60%rh, open air) and collected after complete drying. The first analysis to be performed on the dried printlets was the quantification of caffeine, in order to adjust caffeine amount in future formulations. The printlets were then analyzed following the method reported in section 3.1.2.5, revealing a caffeine loading of 7.64 mg/printlet and 7.51 mg/printlet in formulation A and B, respectively, much higher than the target dose of 1.65 mg/printlet. For this reason, it was decided to prepare new formulations, reducing the loaded amount of caffeine from 15% to 3.5% w/v. Moreover, a dimensional reduction of dried formulations A and B was observed, common with hydrogels formulation, due to water evaporation in the drying process [56-58].

Due to the size reduction, the dried formulations were too small for an eventual *in vivo* administration, as it was not possible to place them in the Torpac® dosing syringe (shown in Figure 12).

Figure 12. Torpac® dosing syringe employed to administer capsules size 9 in rodents.

It was then decided to rearrange the CAD model, increasing the height and width of the printlet design, trying to overcome the reduction in size from water evaporation during drying process (Figure 13).

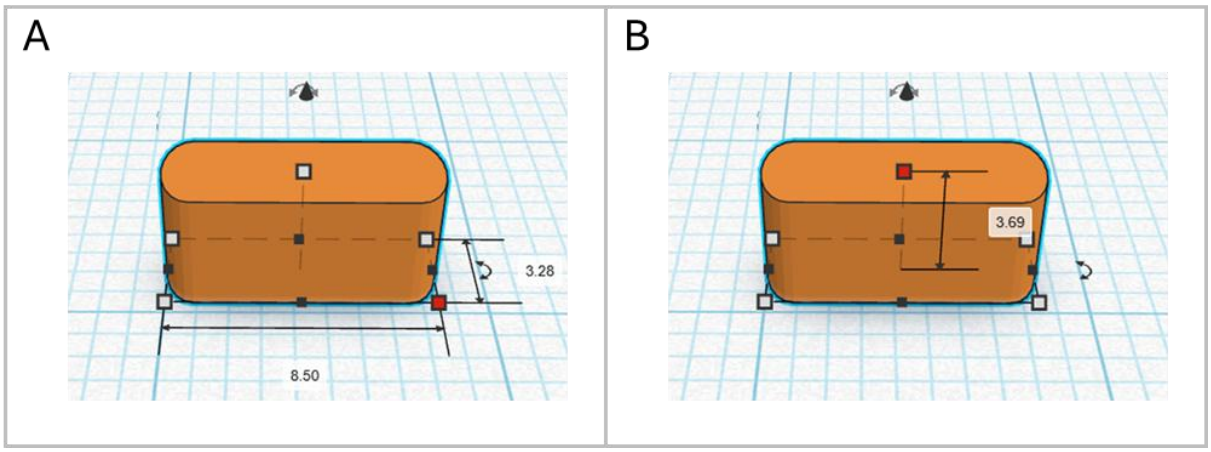

Figure 13. Modified CAD model of printlets with larger dimensions than size 9 capsules.

Moreover, viscosity enhancing excipients were added to the formulations to be printed. The composition of the new set of formulations is reported in Table 7.

Table 7. C/F formulation composition. All concentrations are reported as % w/v respect to water.

Formulation	HPMC K4M	NaCMC	Kollidon CL	Citric acid	Caffeine	HPC-H
C	12	-	1.8	-	3.5	10
D	12	-	-	1.8	3.5	10
E	-	20	2	-	3.5	10
F	-	20	-	2	3.5	10

HPC-H was introduced (10% w/v) as an additive excipient with a double role. Since it is an HPC high viscosity grade it could retard the drug dissolution, contributing to sustain the caffeine release. In addition, viscous solutions at low temperatures are obtained, which could help to better maintain the printlet morphology and dimension, once dried [31]. In parallel, a comparison in terms of crosslinking ability was made between citric acid and Kollidon® CL, together with HPMC K4. As a result, formulations C and D were prepared following the procedure detailed in section 3.1.2.1 and resulted to be not extrudable, as too viscous and not homogeneous. On the other hand, formulations E and F resulted easily extrudable and were then subjected to a complete printing process to obtain final printed forms for caffeine quantification and dissolution test. The printing process was successfully completed, employing the parameters reported in Table 8, and the resulting printlets, renamed CC1 and CC2 respectively, were dried overnight at standard laboratory conditions. An image of the dried formulations obtained is reported in Figure 14.

Table 8. Printing parameters employed with formulations CC1 and CC2.

Formulation	Extrusion pressure (kPa)	Printing speed (mm/s)	Printing temperature (°C)	Layer height (mm)	Preflow (ms)	Postflow (ms)
E (CC1)	90	1	-	0.4	-300	-
F (CC2)	85	1	-	0.4	-200	-

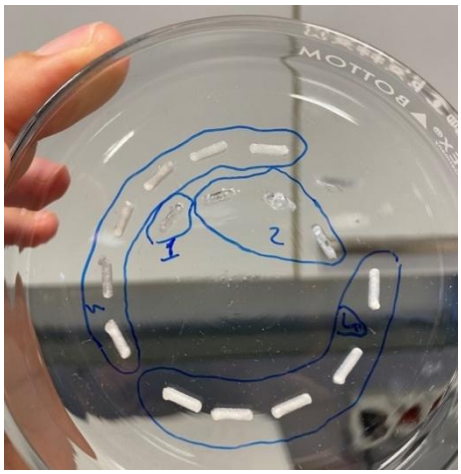

Figure 14. Results of the printing process performed on Formulations C/F. The printed forms coded with numbers 3 and 4 correspond to CC1 and CC2, respectively.

Before caffeine quantification and dissolution trials of formulation CC1 and CC2, other formulations with HPMC were evaluated, to compare drug release kinetics from different polymeric systems. The new HPMC formulations are reported in Table 9.

Table 9. G/J formulations based on HPMC K4M. All concentrations are reported as %w/v respect to water.

Formulation	HPMC K4M	Kollidon CL	Citric acid	Caffeine	HPC-H	PVA
G	12	-	-	3.5	12	-
H	12	-	1.5	3.5	-	-
I	12	1.5	-	3.5	-	-
J	12	-	-	3.5	-	12

Since formulations C and D (see Table 7) resulted not extrudable, the viscosity of hydrogel was reduced in formulations G – J: the crosslinker was removed, while the amount of secondary polymer, HPC-H or PVA, was increased from 10 to 12% w/v. Results obtained were not satisfactory, since the hydrogel of the formulation G was still too viscous with an excessive elastic return after extrusion, while the hydrogel of formulation J was not homogeneous. It was not possible to continue the printing process, encountering water dripping followed by unexpected nozzle blockages.

In the case of formulations H and I the crosslinking effect of Kollidon® CL or citric acid was evaluated at a concentration of 1.5% w/v. The hydrogels obtained turned out to be correctly extrudable but not printable, because a loss of printlet morphology during the printing process was observed, obtaining an undefined mass difference compared to the CAD model to be printed. This result showed that the crosslinkers used may not be sufficient to work only with HPMC and that there could be the need for a second polymer to better sustain the extruded morphology during printing and drying process. Moving on with the investigation of HPMC K4 based hydrogels, more formulations were prepared and are reported in Table 10.

Table 10. K/O hydrogel formulations HPMC K4M based. All concentrations are reported as %w/v respect to water.

Formulation	HPMC K4M	Kollidon CL	Citric acid	Caffeine	HPC-H	Sodium alginate	PVA
K	12	-	3	3.5	-	-	-
L	12	3	-	3.5	-	-	-
M	12	-	1.5	3.5	-	12	-
N	12	1.5	-	3.5	-	24	-
O	5	-	1.5	3.5	5	-	5

First, crosslinking ability of Kollidon CL or citric acid was evaluated, preparing hydrogels (formulations K and L) with a double concentration respect to previous trials (3% w/v instead of 1.5% w/v, see Table 9). This change showed an unsuitable printing process for formulation K, with elastic return of extruded material during printing and loss of morphology after the completion of the process. On the other hand, Formulation L showed good extrudability and printability but a loss of morphology during drying was observed as well. Both formulations were discarded and no further investigated. Since no improvements were observed increasing the amount of crosslinker, successive formulations were prepared returning to 1.5% w/v of crosslinker coupled with the addition of other polymers. Sodium alginate was evaluated for the scope, due to its properties in hydrogels formation as previously studied by Rony et al. [59]. In the formulation M, sodium alginate was added in a 1:1 ratio with HPMC K4 (12% w/v, see Table 10). This addition contributed to better maintaining the printed morphology of extruded material, both during printing and drying steps, and the obtained printed formulation, renamed CH1, was left to

dry at standard laboratory conditions. On the other hand, a similar composition was explored with formulation N, where the crosslinker selected was Kollidon® CL.
The main difference from previous formulation was the ratio between HPMC and sodium alginate, since the second component was doubled respect to the first one (ratio 1:2). Since Kollidon® CL showed less crosslinking ability than citric acid, the amount of additive polymer was increased to improve the formulation ability to maintain the printed morphology. As a result, the prepared formulation proved to be too viscous to be printed at room temperature, so the printhead temperature was raised up to 45°C. Then, also formulation N turned out to be printable and it was dried at room temperature overnight. The formulation N was renamed as CH2. Printing parameters employed with formulations CH1 and CH2 are reported in Table 11.

Table 11. Printing parameters employed with formulations CH1 and CH2.

Formulation	Extrusion pressure (kPa)	Printing speed (mm/s)	Printing temperature (°C)	Layer height (mm)	Preflow (ms)	Postflow (ms)
M (CH1)	195	1	-	0.4	-300	300
N (CH2)	195	1	45°C	0.4	-300	300

After the successful introduction of sodium alginate in formulations CH1 and CH2, in the formulation O a polymeric system based on three polymers in a ratio 1:1:1 was examined. Crosslinker amount was left at 1.5% w/v concentration while the amount of the three polymers was set to 5% w/v each (see Table 10), to avoid an excessive increase in hydrogel viscosity. As a result, obtained viscosity was very low and the printed formulation showed loss of morphology during and after conclusion of printing process. For that reason, formulation O was discharged and no further investigated. Based on the latest results obtained, one last formulation was attempted, prepared with the composition reported in Table 12.

Table 12. P formulation prepared with both HPMC and NaCMC. Concentrations are reported as %w/v respect to water.

Formulation	HPMC K4M	NaCMC	Citric acid	Caffeine	Sodium alginate
P (CHC1)	10	20	1	3.5	10

Formulation P was prepared using HPMC K4:sodium alginate 1:1 ratio, differently from formulation M (see Table 10). The concentration of HPMC K4 and sodium alginate was lowered to 10% w/v to reduce viscosity, considered also the addition of NaCMC (20% w/v). In this formulation the possible synergistic effect between the two cellulosic polymers employed so far, to reach a sustained release of caffeine, was explored. The formulation was successfully extruded and the printhead temperature was up to 50°C, with parameters reported in Table 13. Formulation P was renamed CHC1 and dried overnight at laboratory room temperature (about 20-22°C).

Table 13. Printing parameters employed with formulation CHC1.

Formulation	Extrusion pressure (kPa)	Printing speed (mm/s)	Printing temperature (°C)	Layer height (mm)	Preflow (ms)	Postflow (ms)
P (CHC1)	195	1	50°C	0.4	-300	100

3D printed matrix formulations, based on HPMC K4 as polymeric system, were prepared. All the formulations, printed so far, are reported in Figure 15. Drug quantification and dissolution studies (see section 3.1.3.3), together with CC1 and CC2, were carried out.

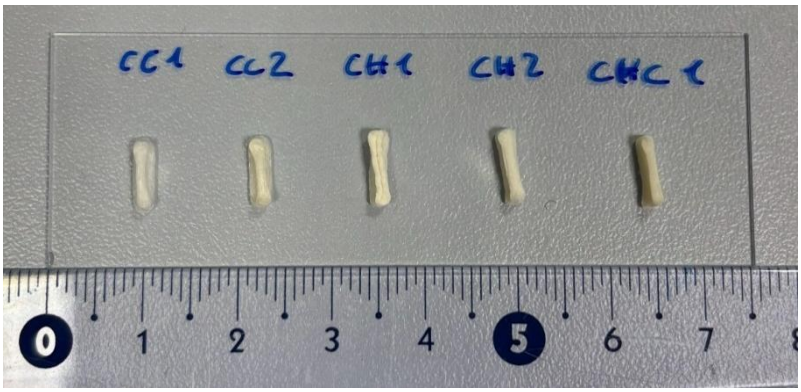

Figure 15. 3D printed matrixial formulations.

3.1.3.2. Drug content

Printed caffeine matrixial formulations were analyzed in terms of drug content and reproducibility, with the method reported in section 3.1.2.5. The results are reported in Table 14.

Table 14. Caffeine content in the printed matrixial formulations (mean value ± deviation standard, n = 3).

Formulation	Drug content (mg/cpr)
CC1	1.70 ± 0.25
CC2	1.60 ± 0.19
CH1	2.91 ± 0.22
CH2	2.05 ± 0.06
CHC1	1.46 ± 0.10

Considering the theoretical target dose of 1.65 mg/printlet, is worth noting as CC1 and CC2 are perfectly on target, despite an unacceptable SD, which means that the printing process must be optimized to obtain more reproducible printlet. On the other hand, CH1 and CH2 showed an excess of caffeine in the printed forms, meaning that caffeine amount has be reduced in the semisolid formulation, before starting the 3D printing process, which turns out anyway more reproducible, accordingly the standard deviation obtained. Finally, CHC1 shows a slightly low amount of caffeine, which could still be acceptable, and a good standard deviation, showing to be nearly optimized in terms of formulation preparation and printing process.

3.1.3.3. Dissolution test on matrix formulations

Preliminary dissolution test was performed in simulated gastric fluid on printed caffeine matrix formulations following the methodology reported in section 3.1.2.6.1. Figure 16 shows the released amount (%) of caffeine from matrix formulations, compared to a commercial Torpac® capsule size 9 filled with pure caffeine.

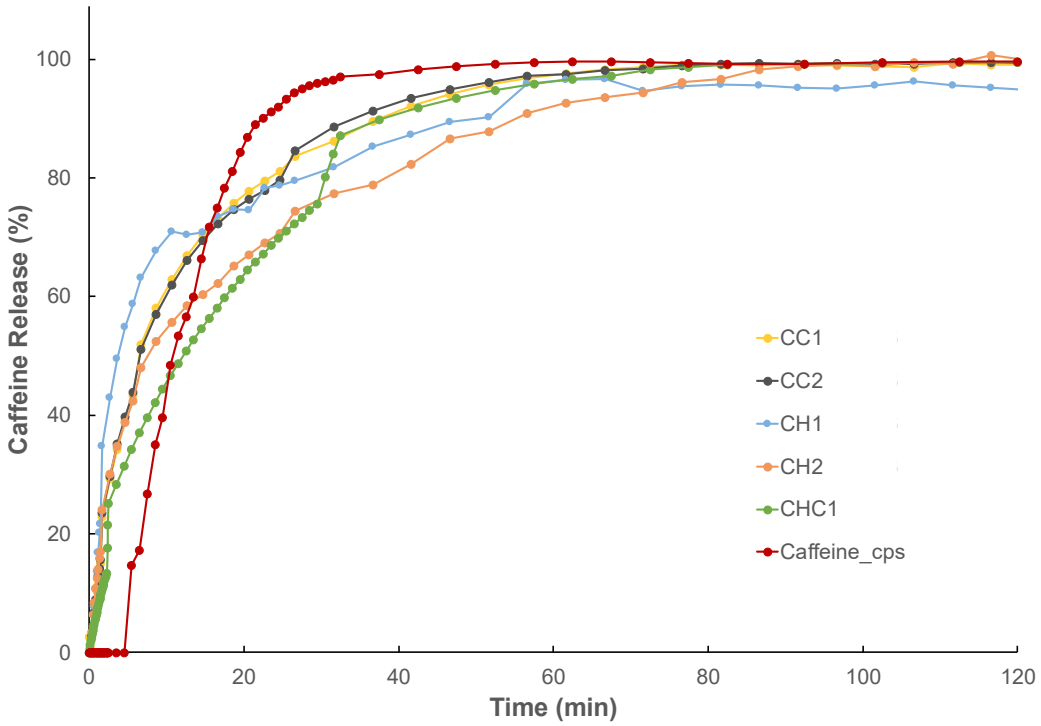

Figure 16. In vitro dissolution profiles in FaSSGF of formulations CC1 (yellow), CC2 (dark grey), CH1 (light blue), CH2 (orange), CHC1 (green) and caffeine in Torpac® capsules (red).

The release of caffeine from the commercial capsule starts after 7 minutes, which is the time needed for capsule's gelatin shell dissolution. The release rate of drug immediately increases and, due to the high solubility value of caffeine in simulated gastric fluid [60], reaches 94% within 16 minutes from the start of the dissolution test.

All the matrix formulations analyzed showed a similar behavior in the release profile. From all of them, caffeine starts to release from the beginning of the dissolution, displaying a burst effect probably caused by the dissolution of caffeine particles already exposed to the medium before hydration and swelling of the polymer chains as suggested by Cerea et al. [61]. Then, the release of caffeine starts to decrease because hydration and swelling of polymeric matrix which starts to govern drug release kinetics [55]. Anyway, the release kinetics from the formulations failed to become constant during the time, probably due to high solubility of drug which acts as pore former, speeding up diffusion of external medium through the inner layers of the printlet. As a result, all the formulations showed more than 64% of caffeine released within 20 minutes. CC2 displayed the faster release, reaching nearly 95% of released caffeine in 35 minutes, while CC1 and CHC1 reached 88% of the release in the same time range. On the contrary, CH1 and CH2 needed, respectively, 50

and 55 minutes to reach 90% of released caffeine and showed a slower release compared to the other formulations. However, none of them met the requirements to obtain a sustained release of caffeine in acidic environment [53,54], since 100% of drug was released within 60 minutes and for that reason, these printlets were discarded and not further characterized.

3.1.3.4. Reservoir formulations

Based on the observations from the latter matrix-based 3D trials, it became evident that a different formulation approach was necessary to achieve the desired sustained release. Therefore, it was decided to investigate polymeric reservoir-based systems. Reservoir systems differ from matrix systems in their basic design, containing drug (dispersed or dissolved phase) as a solid core enclosed by a polymeric membrane. The drug diffusion rate across the membrane governs the release profile, providing almost zero-order constant release. Within the polymeric reservoir systems studied, the drug was dispersed in matrix formulation, starting from the work described in section 3.1.3.1, and enclosed by crosslinked hydrogel layers. Using a combination of glassy polymers, additives and incorporation of crosslinkers, dynamic swelling and drug release from the system could be appropriately modulated. During the release test, dissolution media would cause swelling of polymeric external layers, creating a constant concentration gradient through them, until the internal reservoir gets depleted, reaching zero order release kinetics. Moreover, with these systems undesired damage of reservoir external membrane should be avoided, reducing risks of eventual dose dumping during release tests [49].
In order to successfully print reservoir formulations, a coordinated printing approach, as suggested by the work described by Okwuosa et al. [62], must be followed, preparing an appropriate CAD model and setting the 3D printer alternating two printheads. The newly prepared CAD model was comprehensive of the two components of reservoir drug delivery systems, the internal core and the external shell. The new CAD model is schematically described in Figure 17.

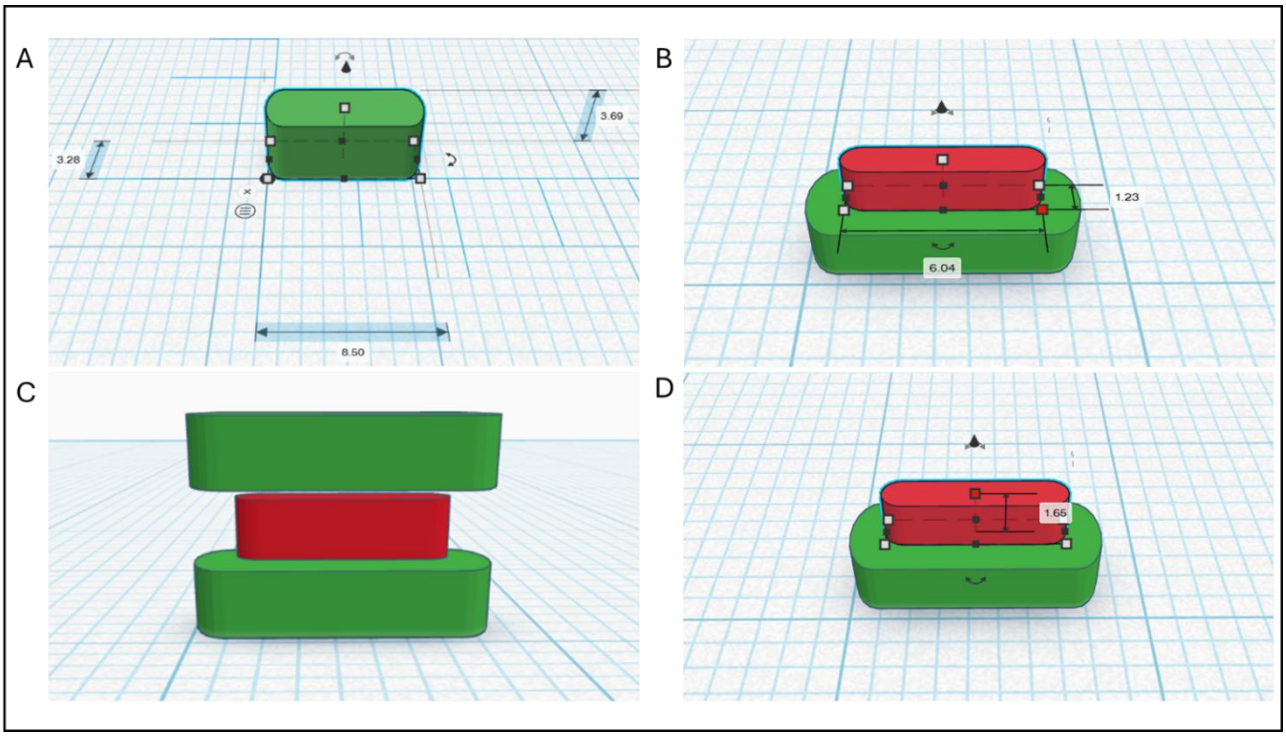

Figure 17. New CAD model of the reservoir structure. (A) measures of resulting final model, (B) length and width of core, (C) exploded structures, (D) height of core.

Since the internal part, or core, includes all the amount of API and the total capacity of the core is smaller than the one of matrix formulation, the resulting hydrogels were more concentrated than matrix formulations, in order to reach the target drug dose of 1.65 mg/printlet. First, two different hydrogels for the core composition were prepared, one based on HPMC K4M and the other based on NaCMC. The two polymers' ability to reach the sustain release of caffeine was compared. It was used the composition, already studied in the first set of matrix hydrogels (see Table 5), since they could incorporate higher amount of drug. Their composition was slightly adapted to the small dimensions given by the core structure and the concentration of drug was raised up. The formulations composition is reported in Table 15 and the preparation method was the same of the matrixial experiments reported in section 3.1.2.1. The final hydrogel exhibited a paste-like appearance, which was likely attributable to the elevated concentration of incorporated caffeine, rather than displaying the characteristics of a conventional hydrogel.

Table 15. Reservoir's core formulations composition. All concentrations are reported as %w/v respect to water.

Polymer based core	Formulation	HPMC K4M	NaCMC	Citric acid	Caffeine
NaCMC	Core A	-	20	2	20
HPMC K4	Core B	12	-	-	

In parallel, regarding the polymeric formulations employed for the external shell, it was decided to prepare four different compositions starting from previous matrixial experiments (see Table 7, Table 10 and Table 12). Formulations selected and their compositions are reported in Table 16.

Table 16. Shell formulations composition. All concentrations are reported as %w/v respect to water.

Formulation	HPMC K4M	HPMC K15M	NaCMC	Calcium chloride	Citric acid	Sodium alginate	HPC-H
Shell 1	-	-	20	2	-	-	10
Shell 2	10	-	20	-	2	10	-
Shell 3	10	-	-	-	1.5	10	-
Shell 4	-	15	-	-	2.25	10	-

Regarding Shell 1, hydrogel was obtained from NaCMC and HPC-H in a ratio 2:1, using $CaCl_2$ as crosslinker to improve the printed morphology retaining after drying process. In the case of Shell 2, the same formulation composition of CHC1 (reported in Table 12) was replicated, without caffeine. A comparable approach was employed in the preparation of Shell 3, wherein formulation CH1 (refer to Table 7) was modified by preserving the HPMC K4:sodium alginate 1:1 ratio, while decreasing their concentration to 10% w/v to facilitate improved extrusion. In the case of Shell 4, a different grade of HPMC, namely K15, was utilized to enable a comparative analysis of its release compared to that with HPMC K4 grade. Due to its different molecular weight and gelification properties [31] its concentration was raised up to 15% w/v, but the ratio with crosslinker (citric acid) was maintained. All formulations reported proved to be extrudable and were moved to the printing process, together with core formulations reported in Table 15.

An important feature of this new reservoir formulation regarded the printing process. Since it was approached a final printed form composed of two different formulations, the print must be carried out using two different printheads. To achieve this, it was necessary to configure an alternating dual-head printing G-code during the slicing process. The printing instructions were set in order to print the lower part of the external shell at the beginning with the first printhead, leaving aside the cavity in which the internal core would be printed. Then, the real alternate printing process started with the second printhead, filling the empty space with the core formulation alone which will be then surrounded again with outermost shell formulation. The alternate printing continued until the internal core was fully printed, allowing the first printhead to complete the process by printing the final upper section. In Figure 18 images of the alternate printing process, described above, are reported.

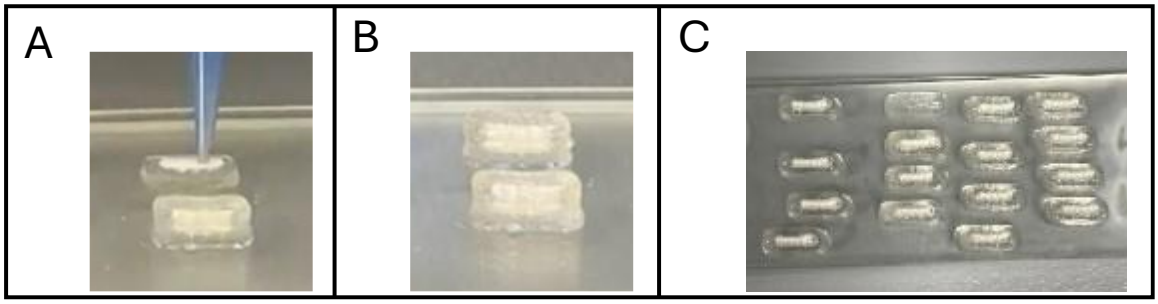

Figure 18. (A) Snapshot of a moment of the alternate printing process. (B) Final printed form where is clearly visible the API located reservoir surrounded by polymeric hydrogel. (C) Upper vision of a set of freshly printed formulations.

To better evaluate the difference in release kinetics between HPMC and NaCMC as swellable polymers, the final reservoir formulations were prepared coupling core and shell formulations by cellulosic polymers (Table 17). Core formulation A, containing NaCMC, was printed together with shell formulations containing NaCMC. The same principle was applied to core formulation containing HPMC, where core formulation B was printed together with shell formulations containing HPMC. Within CC4, core A was printed together with shell 2, because in shell 2 formulation NaCMC was the polymer more concentrated (see Table 16).

Table 17. Reservoir printed forms composition.

Printlet	Core	Shell
CC3	A	1
CC4	A	2
CH3	B	3
CH4	B	4

The printing parameters, employed to carry out the 3D printing process of the formulations listed above, are reported in Table 18.

Table 18. Printing parameters employed to print the core and shell formulations.

Formulation	Extrusion pressure (kPa)	Printing speed (mm/s)	Printing temperature (°C)	Layer height (mm)	Preflow (ms)	Postflow (ms)
Core A	140	1	-	0.4	-300	100
Core B	115	1	60°C	0.4	-300	100
Shell 1	140	1	-	0.4	-200	100
Shell 2	190	1	50°C	0.4	-300	100
Shell 3	120	1	-	0.4	-200	100
Shell 4	100	1	-	0.4	-200	200

All the formulations were successfully printed and dried overnight at ambient conditions. An example is shown in Figure 18.

Formulations CC3 and CC4 were printed without significant issues, while CH3 and CH4 presented some minor concerns, related to the exterior aspect of the dried printlets. It was noticed that there was an excessive shrinking of the printed form, with pronounced loss of adherence compared to CAD model aspect showed in Figure 17-A.

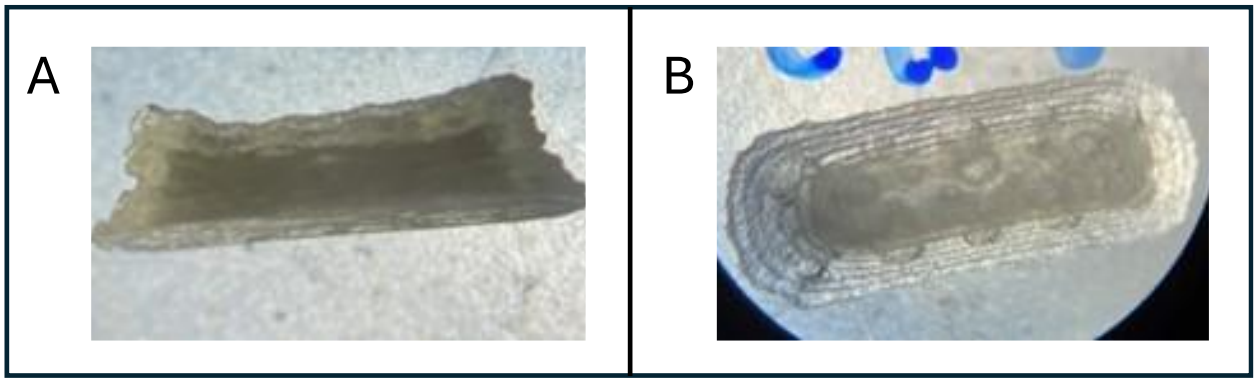

Figure 19. Optical microscopy at 4x magnification, lateral (A) and top (B) view of dried reservoir formulations, highlighting the inward shrinkage of the upper surface.

As can be noted in Figure 19, an inward shrinking towards the top center of the printed form was observed. This structural modification occurred when the total printing process required a prolonged time of printing, such as when the number of printed forms is relevant. A possible explanation of this undesired effect is that water was not enough entrapped in the expanded polymer chains and escaped too fast leaving an imperfect dried printed form. To enhance the shape retention during the printing process, some modifications to shell 3 and shell 4 compositions were investigated.

New formulations were evaluated and are reported in Table 19. The performed attempts were focused on improving shape retention during printing process, with the addition of excipients or substituting citric acid with a stronger crosslinker, as calcium chloride.

Table 19. HPMC K4 shell formulations composition. All concentrations are reported as %w/v respect to water.

Formulation	HPMC K4M	$CaCl_2$	CA	SA	Glycerol	Chitosan	HPC-H
Shell 5	10	1.5	-	10	-	-	-
Shell 6	10	1.2	-	10	-	-	-
Shell 7	10	-	1.5	10	20	-	-
Shell 8	10	-	1.5	20	20	-	-
Shell 9	10	-	1.5	10	-	10	-
Shell 10	10	-	1.5	10	-	-	5

The extrudability of the new formulations was evaluated. In shells 5 and 6 the evaluation focused on employing a stronger crosslinker, selecting calcium chloride for the scope,

since it is always coupled with sodium alginate [63,64]. First of all, concentration of 1.5% w/v was evaluated but the obtained hydrogel resulted not extrudable. Then, the concentration was reduced to 1.2% w/v in the shell formulation 6, but still the hydrogel obtained resulted to be not extrudable and the crosslinker changing was abandoned. Returning to formulations crosslinked with citric acid, the addition of glycerol was investigated. In the case of shell 7 formulation, a hydrogel with 20% w/v of glycerol was tested but, after performing a complete printing process, the formulation was discarded due to loss of morphology of the printed form. In shell 8 composition glycerol was employed as well, but coupled with sodium alginate in a 1:1 ratio (20% w/v). The prepared formulation was too viscous and not extrudable. For that reason, this formulation was discarded and the investigation of glycerol as an additive was no further investigated. Then, a new formulation including chitosan as viscosity enhancer [65] was prepared (shell 9 composition) but, also in this case, the viscosity obtained was too high and the hydrogel resulted to be not extrudable. With the same principle of increasing viscosity, one last formulation was attempted and consisted of adding 5% w/v of HPC-H to shell 3 composition previously formulated (see Table 16). The hydrogel demonstrated favorable extrudability and was employed throughout the printing process alongside the core B formulation as reported in Table 12. The printing process was completed successfully with the conditions reported in Table 20. The modified printed formulation was renamed CH5. Immediately after printing, the printed forms CH5 were dried overnight at 4°C in a fridge, placed in a Petri dish covered with parafilm, rather than at room temperature as previously used. Then, the whole plate was moved to a climatic chamber previously set at 45°C and 75%RH for controlled drying.

Table 20. Printing parameters employed for CH5, composed by formulations core B and shell 10 (see table 12 and 16).

Formulation		Extrusion pressure (kPa)	Printing speed (mm/s)	Printing temperature (°C)	Layer height (mm)	Preflow (ms)	Postflow (ms)
CH5	Core B	115	1	60°C	0.4	-300	100
	Shell 10	180	1	-	0.4	-200	200

Figure 20 displays images of the placebo printlet batch made only with hydrogel shell 10. The pictures show the placebo printlet, after stored at 4°C (Figure 20-A and B) and after

the addition of new drying steps (Figure 20-C and D). All the images were acquired at 4X magnification utilizing optical microscopy.

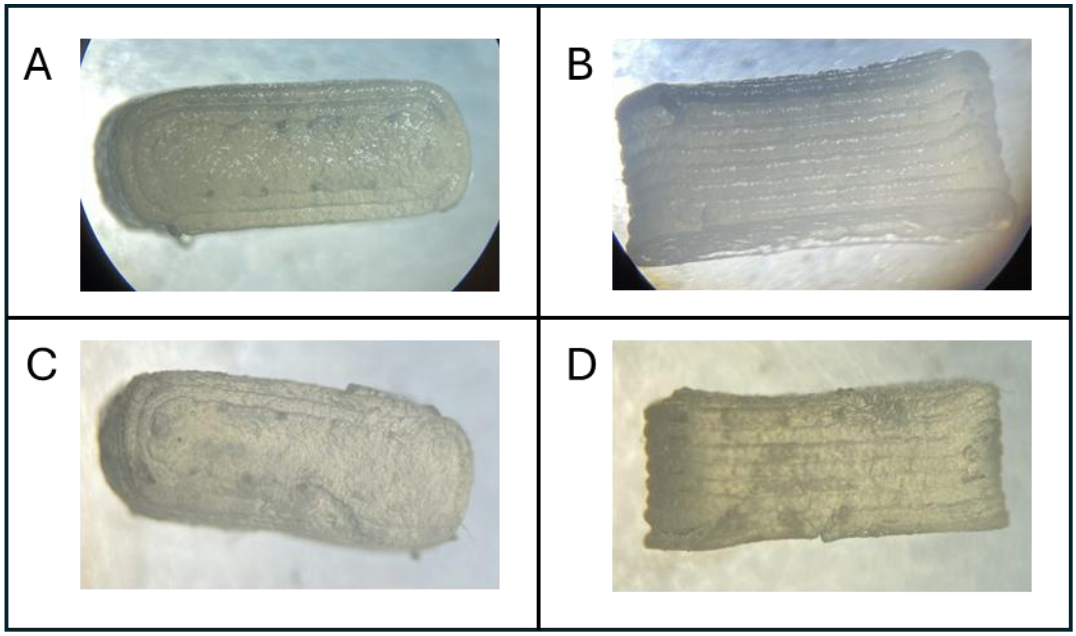

Figure 20. Comparison of shell 10 placebo printlets after overnight rest at 4°C (A – top view, B – side view) and after complete drying (C – top view, D – side view).

The newly set up drying process was then applied to all the subsequently printed formulations.

Taking into account the satisfactory results obtained with the addition of 5% HPC-H in terms of retained morphology during printing process, it was also added to formulation shell 4 (see Table 16). Then, a new formulation was prepared, with the composition reported in Table 21.

Table 21. Shell 11 formulation composition. All concentrations are reported as %w/v respect to water.

Formulation	HPMC K15M	Citric acid	Sodium alginate	HPC-H
Shell 11	15	2.25	10	5

Coupling this last formulation with core B (see Table 15) in a complete printing process, the printlet CH6 was obtained and the printing parameters employed are reported in Table 22.

Table 22. Printing parameters employed for CH6, composed of formulations core B and shell 11 (see table 12 and 18).

Formulation		Extrusion pressure (kPa)	Printing speed (mm/s)	Printing temperature (°C)	Layer height (mm)	Preflow (ms)	Postflow (ms)
CH6	Core B	115	1	60°C	0.4	-300	100
	Shell 11	120	1	-	0.4	-200	100

From reservoir formulation experiments four different printed formulations (CC3, CC4, CH5 and CH6) were obtained (Figure 21) and all of them met the dimensional requirements given by dosing syringe for rodents administration, reproducing capsule size 9 measures as reported in Table 4. These reservoir formulations were further characterized in terms of caffeine content, drug homogenicity and *in vitro* dissolution studies in acid environment.

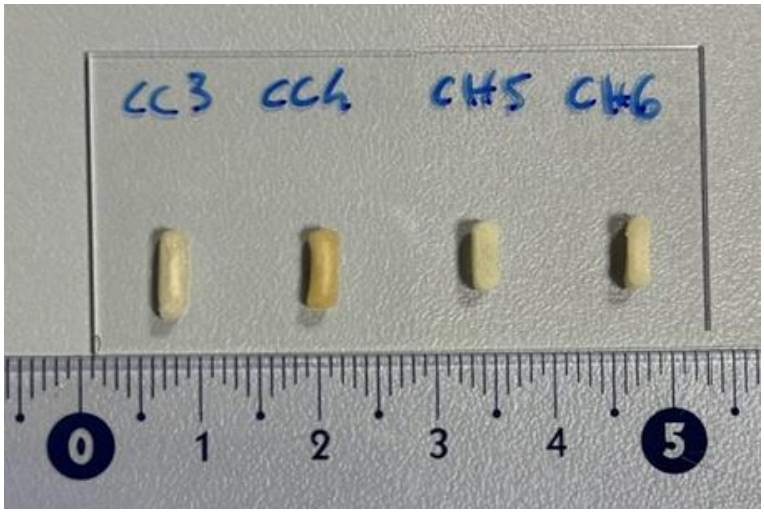

Figure 21. 3D printed reservoir formulations.

3.1.3.5. Drug content in reservoir formulations

Printed caffeine reservoir formulations were analyzed in terms of drug content, with the method reported in section 3.1.2.5. The results are reported in Table 23.

Table 23. Caffeine quantification and content uniformity analysis performed on printed reservoir formulations (mean value ± deviation standard, n = 3).

Formulation	Drug content (mg/cpr)
CC3	1.29 ± 0.26
CC4	1.26 ± 0.25
CH5	1.46 ± 0.09
CH6	1.80 ± 0.10

The first two analyzed formulations (CC3 and CC4) contained less caffeine than the desired target dose of 1.65 mg/printlet, indicating the requirement for further improvement in drug content uniformity and target dose. Moreover, the high standard deviation could be due to variability of caffeine distribution across different batches, suggesting also inconsistencies in the mixing or printing process. Therefore, in the subsequent core formulation the loading of API was set at 25% w/v, to increase the final amount of caffeine in printlets, as reported in formulation CH6 (see Table 23).
Caffeine content in the printlets was in parallel evaluated at the Department of Food and Drug, University of Parma, using the method described in section 3.1.2.5.2, before performing dissolution tests in dissolution media. Results were in line with the ones obtained in Chiesi laboratories.

3.1.3.6. Dissolution test on reservoir formulations

Preliminary dissolution test in simulated gastric fluid was performed on printed caffeine reservoir formulations following the methodology reported in section 3.1.2.6. Figure 22 shows the caffeine released (%) from reservoir formulations, compared to a commercial Torpac® capsule size 9 filled with caffeine powder.

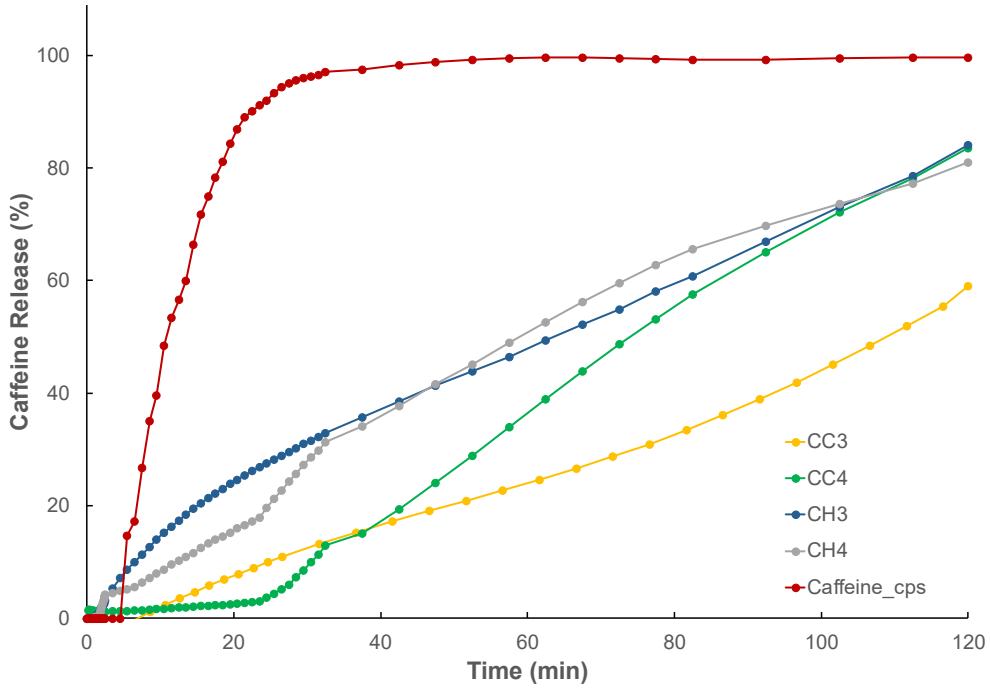

Figure 22. Dissolution curves in FaSSGF media obtained in Chiesi laboratories with formulations CC3 (yellow), CC4 (green), CH3 (blue), CH4 (grey), compared with caffeine in Torpac® capsules (red).

As shown in Figure 22, the release curves of the reservoir formulations are different from matrix formulations. The burst effect is absent; after 20 minutes, all tested formulations released less than 25% of the API. CC3 and CC4 hydrate their external polymer layers more slowly than CH3 and CH4, resulting in delayed drug release (CC3 released 8% and CC4 only 2% after 20 minutes). After 60 minutes of dissolution study all the formulations released less than 55% of drug, meaning that diffusion gradient created through the polymeric swelled layers was effective in sustaining the release of caffeine [49, 55]. After two hours of dissolution test, CC4, CH3 and CH4 reached around 85% of caffeine release, while CC3 exhibited a 60% of drug release. The results obtained with in house preliminary dissolution test enable the scale up moving towards Pharmacopoeia regulations release test to confirm the sustained release generated by 3D printed reservoir formulations. The dissolution test was conducted by the Department of Food and Drug, University of Parma with methodology reported in section 3.1.2.6.2. Results obtained are reported in Figure 23 below.

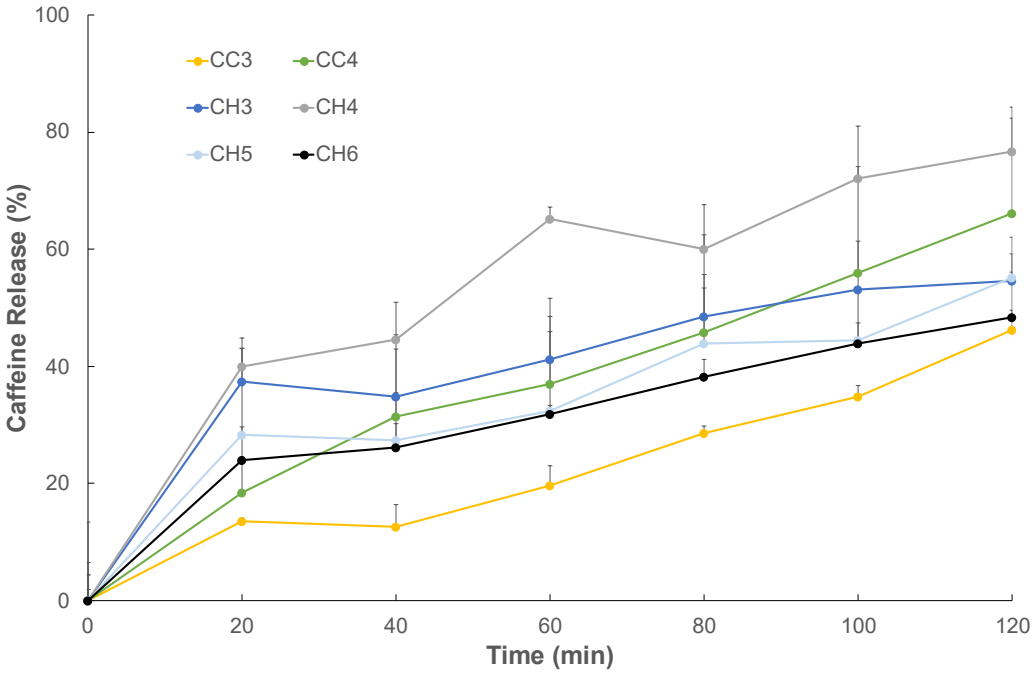

Figure 23. Dissolution curves in acidic media obtained at University of Parma with formulations CC3 (yellow), CC4 (green), CH3 (blue), CH4 (grey), CH5 (light blue) and CH6 (black).

All the formulations achieved a sustained caffeine release, with less than 76% of drug release at 120 minutes. In particular, CH4 showed the fastest release, reaching nearly 40% in 20 minutes and a 76% of the drug release in 120 minutes, aligning with the preliminary tests. CC3 released caffeine most slowly, with only 14% in the first 20 minutes and less than 50% after two hours. Chiesi and University of Parma dissolution tests gave in some cases different results. In general, Chiesi tests showed slower initial release of caffeine but higher overall drug release compared to USP II apparatus. Variations likely result from differences in test conditions, but all tested printlets demonstrated sustained release.

3.1.3.7. X-Ray micro-computed tomography

Caffeine 3D printed solid formulations were analyzed also with Micro-CT imaging, following the methodology reported in section 3.1.2.7. The images acquired are reported in Figure 24, where circular sections were cut out from the whole layer scanned.

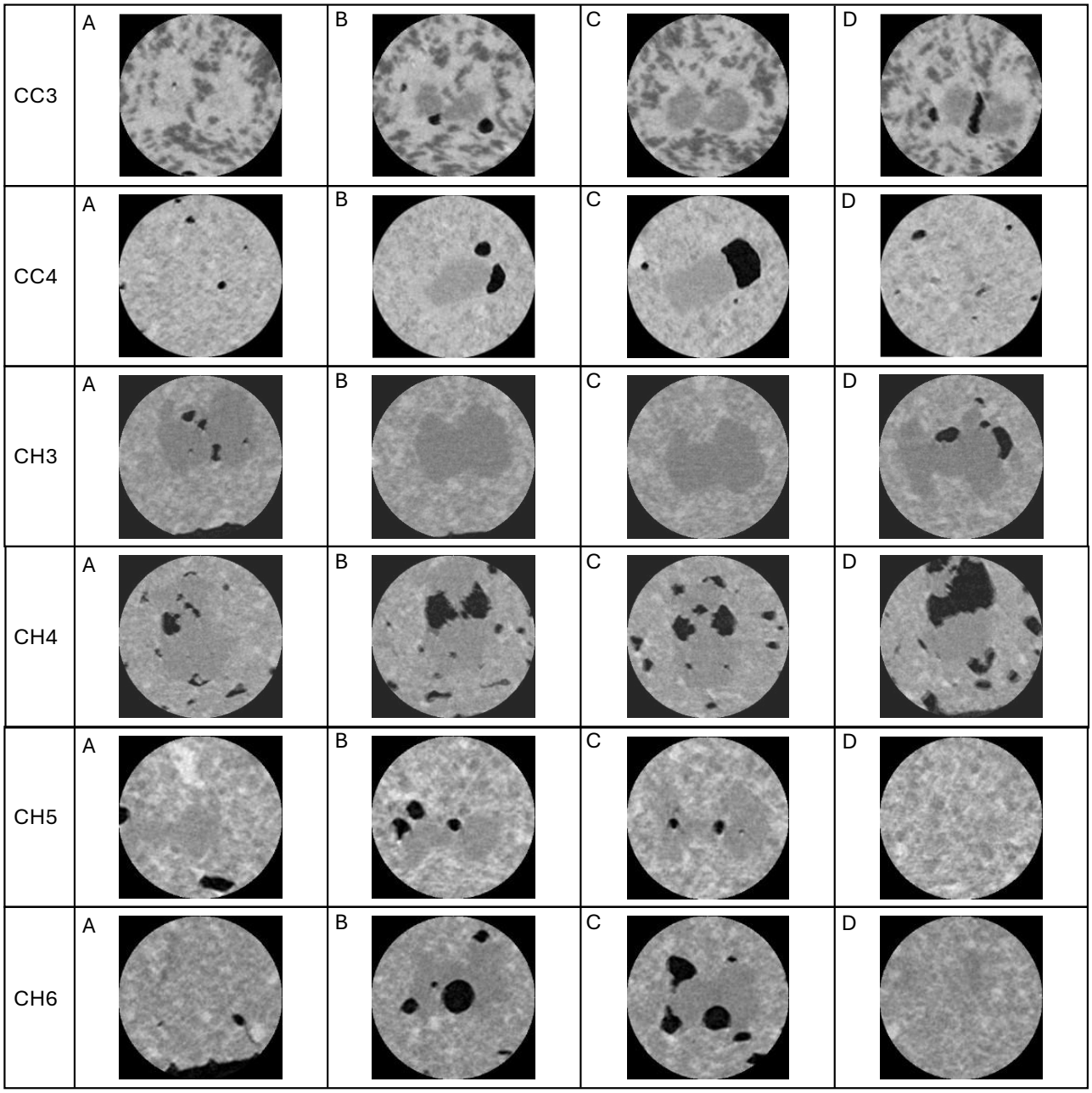

Figure 24. Micro-CT images obtained with 3D printed reservoir formulations (different section views).

From the images reported in Figure 24 some affinities between formulations are visible. First of all, in all the formulations analyzed, the zone in which the API is located (cores formulation) is recognizable as a darker central area. The different density of the drug matrixial formulation enclosed in the core of the printlet make it detectable and visible. Especially in all the figures B and C, sections of the reservoir system are reported. Sometimes black zones are present, probably air voids generated during the drying process of the printlets. The water removal from hydrogel formulation yielded contraction

of the polymeric chains, leaving voids during the retraction of the printed layers. These voids are more present within CH4 and CH6, probably due to the type of HMPC employed, the K15. Looking at CC3 reported pictures is clearly visible how the different external layers' hydrogel composition affects its density. The polymeric layers composed by NaCMC and HPC-H are less homogeneous than all the other formulation ones, probably due to the higher amount of HPC-H present, which yields a more porous structure (dark grey dots) after water removal [66]. The low density zones are more localized in CC3, while more homogeneously distributed within all the other formulations. All the CH formulations, mainly composed of HPMC and sodium alginate, resulted to have a more homogeneous density distribution, suggested by the smaller and more distributed dark grey zones. CC4, similarly to all the CH formulations, showed homogeneous distribution between less dense and more dense zones. Its polymeric composition, based on NaCMC, HPMC and sodium alginate, resulted in less porosity than CC3, suggesting that HPC-H plays and important role in defining the density distribution during hydrogels preparation. The differences in terms of hydrogel density apported by HPC-H are less evident between formulations CH. CH5 and CH6 were prepared with the same composition of CH3 and CH4 respectively, with the only difference of a 5% w/v added of HPC-H (see section 3.1.3.4). This difference is slightly perceivable within the acquired micro-CT images, but CH5 and CH6 showed more defined variations in lower density spots, resulting in a less homogeneous general distribution.

Probably, the low amount of HPC-H dispersed in an homogeneous system like the one obtained with HPMC-sodium alginate would not generate high presence of low density sites like with CC3 printed formulation, impacting less with the water bounding ability of the other polymers [66]. In order to better define polymers interactions and their correlation with dissolution behavior in simulated gastric fluids, further investigations will be performed.

3.1.3.8. Rheologic investigation

This section provides a comprehensive and detailed insight into the rheological characterization of the various hydrogel of reservoir formulations used for 3D printing process. The method was reported in section 3.1.2.3. The formulations analyzed are reported in Table 24. The systematic approach, beginning with amplitude sweep tests and moving through yield stress, peak hold, and flow tests, demonstrates careful attention to

how each formulation behaves under mechanical stress. The inclusion of thixotropic and shear-thinning properties is especially relevant for extrusion-based 3D printing, as these characteristics directly impact the printability of the final forms.

Table 24. Composition of hydrogels analyzed with rheology tests. All concentrations are reported as %w/v respect to water.

Formulation	HPMC K4M	HPMC K15M	NaCMC	$CaCl_2$	CA	Caffeine	SA	HPC-H
Core A	-	-	20	2	-	20	-	-
Core B	12	-	-	-	-	20	-	-
Shell 1	-	-	20	2	-	-	-	10
Shell 2	10	-	20	-	2	-	10	-
Shell 3	10	-	-	-	1.5	-	10	-
Shell 4	-	15	-	-	2.25	-	10	-
Shell 10	10	-	-	-	1.5	-	10	5
Shell 11	-	15	-	-	2.25	-	10	5

The first formulation tested was core A. The results obtained are reported Figure 25.

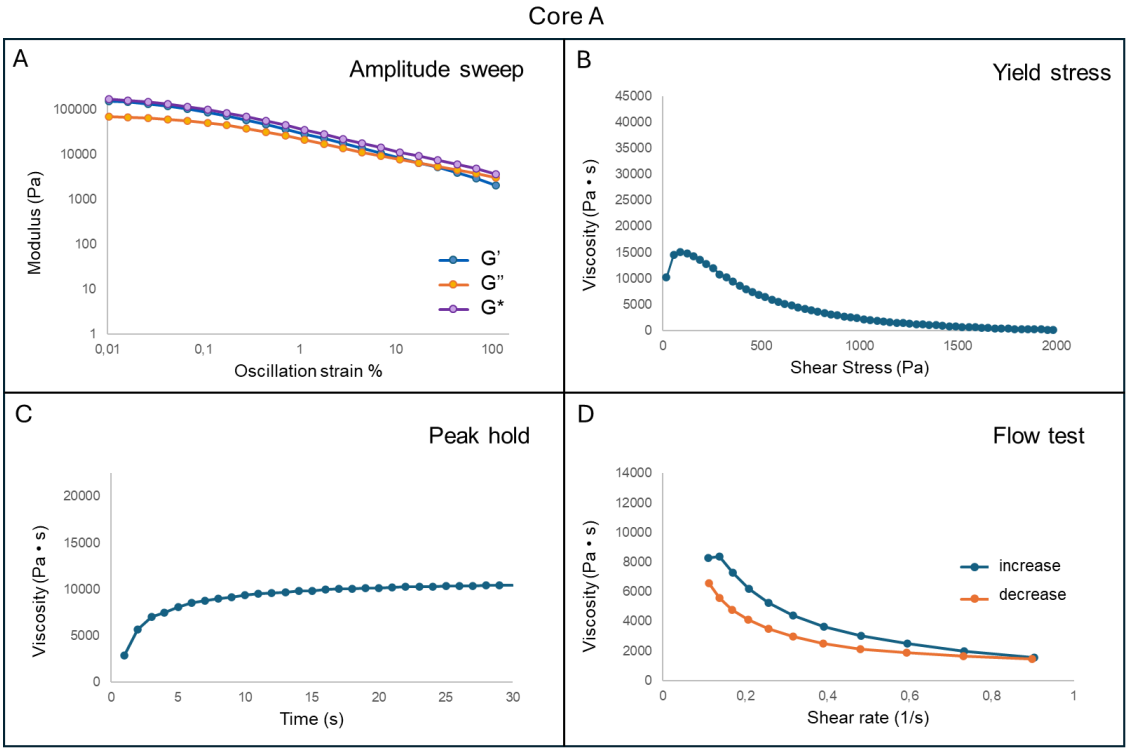

Figure 25. Rheological tests conducted on core A hydrogel.

With amplitude sweep test, curves relative to storage modulus G' and loss modulus G'' were obtained (Figure 25-A, blue and orange curves, respectively). The profiles of the modules are reported as a function of oscillation strain, both expressed in logarithmic scale. The curves are running nearly parallel and cross at 21% oscillation strain, representing the flow point where viscous component reaches higher values respect to elastic component. The Linear Viscoelastic Region (LVER) is delimited between the two modules, here the hydrogel structure is stable and resistant. This region is very limited in the case of core A formulation. Initially, elastic component (G') results to be higher than viscous component (G'') giving a "solid-like" behavior of the hydrogel. Passing over yield point, core A acquires flowing characteristics "liquid-like" [67]. Looking at the yield stress test (Figure 25-B), which analyze the formulation looking at viscosity modifications with increasing shear stress, the viscosity peak was reached at 15122.7 Pa·s, corresponding to 87.38 Pa of shear stress and 0.006 s^{-1} shear rate. Given that, subsequent peak hold and flow test analysis were conducted at a shear rate higher than the yield point's one.

Peak hold analysis allowed the determination of viscosity value at a fixed shear rate. Analysis was conducted at 25°C, stabilizing the shear rate at 0.1 s^{-1} for 30 seconds, essential to let viscosity stabilize. Profile is reported in Figure 25-C, showing a stabilization of viscosity values around 10382.62 Pa·s, calculated as a media from last six points of the curve. Finally, flow test (Figure 25-D) permitted the evaluation of viscosity and shear stress variation as a function of applied shear rate. Analysis was conducted at 25°C, increasing the shear rate from 0.1 to 1 s^{-1} (60 rpm maximum) within 300 seconds and immediately (without pause) lowering back down from 1 to 0.1 s^{-1} within 300 seconds. In Figure 25-D the curve viscosity vs shear rate is reported on a linear scale. The curves allowed us to obtain viscosity values at different shear rates, describing the non-Newtonian behavior of the hydrogel, since the return to initial viscosity values was nearly complete [58].

In Figure 26 rheological results obtained from analysis of core B formulation are reported.

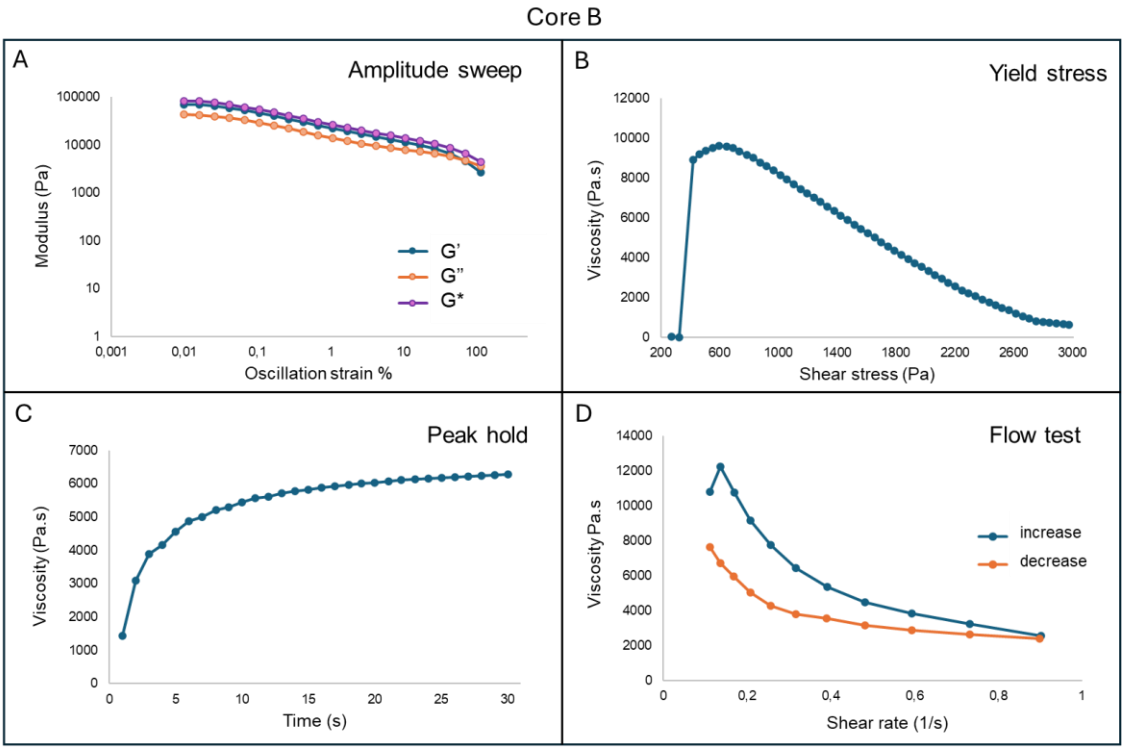

Figure 26. Rheological tests conducted on core B hydrogel.

From the amplitude sweep test (Figure 26-A) it was observed that the curves, which follow a decreasing tendency, run parallel until the crossover point at 65% oscillation strain. LVER region was limited like with core A formulation, with hydrogel structure starting breaking at low strain values, probably showing a gradual structural decline. From yield stress analysis (Figure 26-B), viscosity at increasing shear stress was obtained and the viscosity peak was reached at 9609.1 Pa·s, corresponding to 598.4 Pa shear stress and 0.062 s^{-1} shear rate. An increase in temperature to 60°C was necessary to obtain the core B formulation suitable for extrusion. Peak hold analysis (Figure 26-C) shows stabilization of viscosity values at 6226.8 Pa·s, obtained after 30 seconds at 0.1 s^{-1} shear rate. Stabilized viscosity was calculated as a media from the last six points of the curve. From flow test analysis (Figure 26-D), viscosity and shear stress were evaluated as a function of applied shear rate. The viscosity tended to decrease with increasing shear rate, showing a shear thinning behavior. At the end of 300 seconds of analysis, shear rate was immediately reduced to 0.1 s^{-1} and viscosity increased up to 70% of the initial values, showing thixotropic behavior of formulation [68].

Shell 1 rheological evaluations are reported in Figure 27.

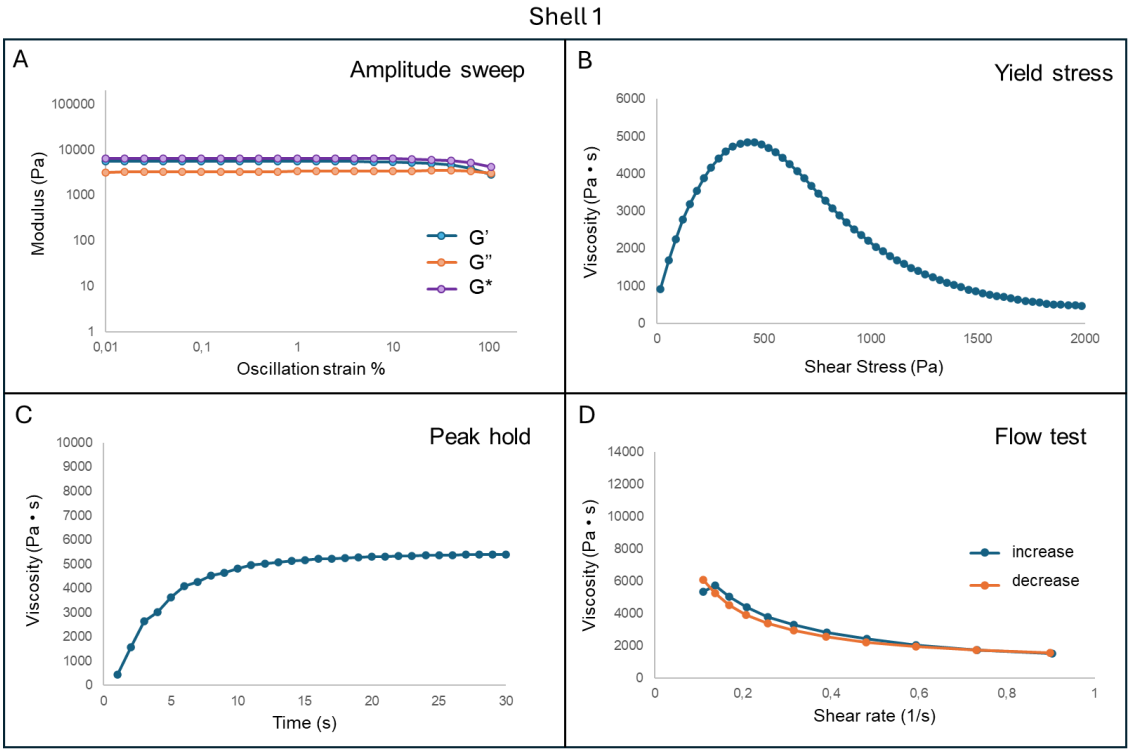

Figure 27. Rheological tests conducted on shell 1 hydrogel.

Amplitude sweep test curves are reported in Figure 27-A, showing a wide LVER where G' and G'' curves are running parallel, pointing at a very good stability to oscillation strain variation applied. From nearly the whole strain variation, G' assumes higher values respect to viscous modulus, highlighting a "solid-like" behavior of the hydrogel. The cross-over point was detected at 94 % oscillation strain. The intersection point between curves represents the flow point, over which the viscous component reaches higher values than the elastic one and the hydrogel assumes "liquid-like" characteristics. In Figure 27-B the yield stress test was reported on a linear scale. From obtained data a maximum peak of viscosity was observed at 4850.29 Pa·s, matching with a shear stress of 421.70 Pa and a shear rate of 0.09 s^{-1}. Given that, the following analysis of peak hold and flow test were conducted applying a shear rate higher than the yield point one.

Peak hold analysis was conducted at 25°C, at a fixed shear rate of 0,1 s^{-1} for 30 seconds, necessary to have stabilization of viscosity values. Results obtained are reported in Figure 27-C. The graph shows a viscosity plateau from which the limit value was obtained (media of the last six points of the curve) and identified as 5384.73 Pa·s. Flow test analysis (Figure 27-D) was conducted at 25°C, increasing shear rate from 0.1 to 1 s^{-1} (60 rpm at maximum) within 300 seconds and then immediately (without letting the sample to rest) reduced from 1 to 0.1 s^{-1} in other 300 seconds. Viscosity versus shear rate curve

was obtained on a linear scale. From data obtained the hydrogel showed a shear-thinning behavior, typical of non-Newtonian fluids, where viscosity decreased under increased shear rate. Then, the reducing shear rate translated into a sudden increase of viscosity which immediately returned to initial values. For this reason, the hydrogel was less thixotropic than core A and core B formulations. In the Figure 28 the rheological characterization of shell 2 hydrogel is reported.

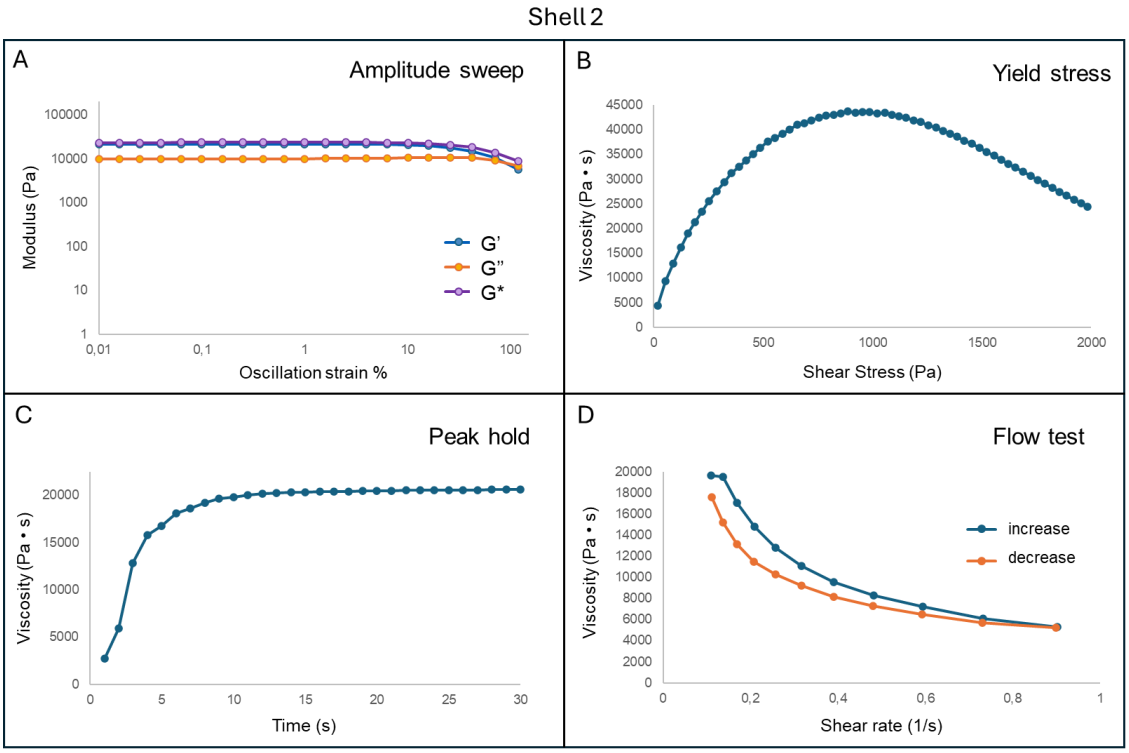

Figure 28. Rheological tests conducted on shell 2 hydrogel.

In the Figure 28-A the amplitude sweep test is reported. G' and G'' curves run parallel for nearly the whole duration of the test, describing a wide LVER region, highlighting an optimal stability of hydrogel to applied strain. Shell 2 hydrogel has a "solid-like" behavior, since elastic modulus was higher than viscous modulus, until the crossover point, observed at 88% oscillation strain, corresponding to 8097.21 Pa. In the region over the crossover point, viscous component overcomes the elastic one, giving to hydrogel flow characteristics "liquid-like". Then, in the Figure 28-B yield stress test is reported, the viscosity versus shear stress was shown on a linear scale. The yield stress indicated the limit of elastic behavior, corresponding to the minimum stress that is necessary to induce flow. [69] From obtained data is observed a maximum peak of viscosity at 43665.8 Pa·s, corresponding to 886.98 Pa of shear stress and 0.02 s^{-1} shear rate. Peak hold analysis

was conducted at 25°C, maintaining a fixed shear rate at 0.1 s^{-1} for 30 seconds, necessary to stabilize viscosity values. Figure 28-C showed viscosity values stabilization around 20575.5 Pa·s, calculated as media of last six points of the curve. At the end, flow test analysis was conducted at 25°C, increasing the shear rate from 0.1 to 1 s^{-1} (60 rpm maximum) within 300 seconds and then, without giving hydrogel time to rest, returning to 0.1 s^{-1} within 300 seconds. The curve viscosity versus shear rate (Figure 28-D) showed nearly a return to initial values of the viscosity, indicating a thixotropic behavior of the formulation.

Rheological analysis of shell 3 formulation is reported in Figure 29.

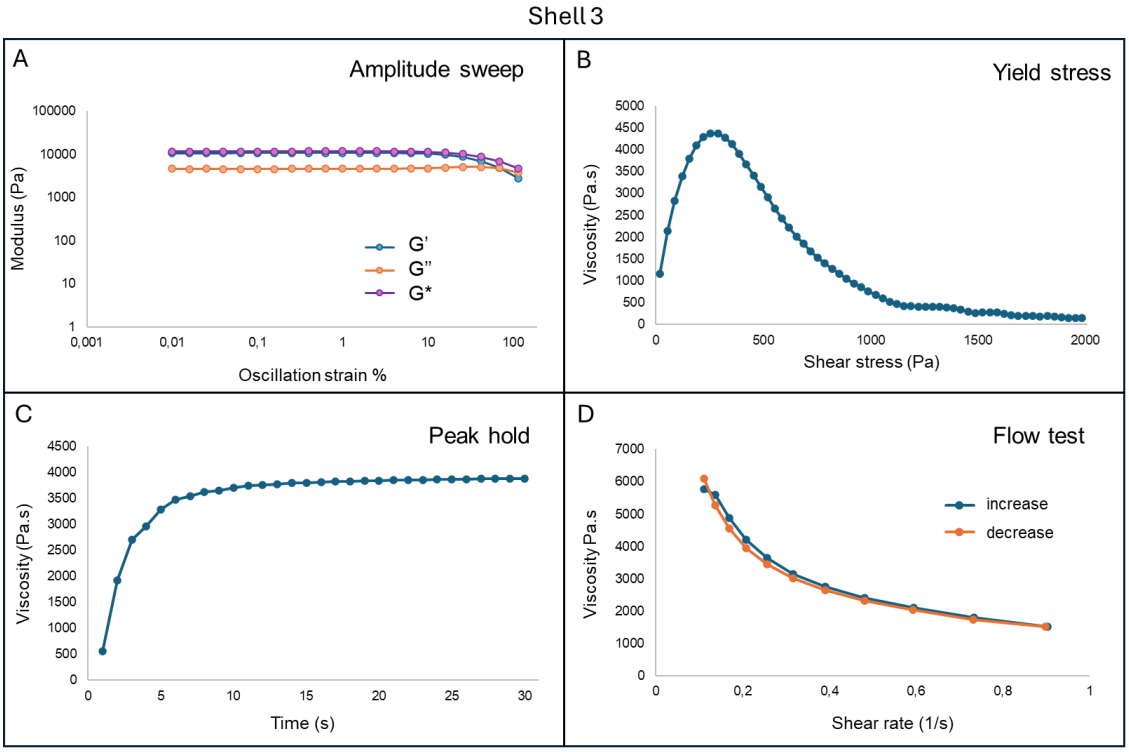

Figure 29. Rheological tests conducted on shell 3 hydrogel.

Amplitude sweep test is shown in Figure 29-A. Moreover, the elastic modulus (G') was higher than viscous modulus (G'') in this case, typical for "solid-like" behavior of hydrogels. The LVER was quite extended, showing good stability to applied strain. The cross-over point was reached at 71% oscillation strain, corresponding to 4721.08 Pa. At that point the formulation assumes flow characteristics "liquid-like", since the crossover point represents the sol-gel transition phase [69]. Yield stress test is reported in Figure 29-B where, applying increasing shear stress forces, a limit viscosity was obtained, over which flow of material is induced. The limit viscosity resulted to be 4370.6 Pa·s,

corresponding to 253.5 Pa shear stress and 0.06 s^{-1} shear rate. These values were used to set other rheological tests. Peak hold analysis was conducted at 25°C, maintaining a fixed shear rate at 0.1 s^{-1} for 30 seconds, necessary to stabilize viscosity values. The viscosity result is shown in Figure 29-C, calculated as a medium of the last six points of the curve. Viscosity stabilized around 3870.6 Pa·s. Flow test analysis (Figure 29-D) was performed following methods reported in section 3.1.2.3. The curve of the viscosity versus shear rate showed a shar-thinning behavior (viscosity dropping while increasing shear rate) with thixotropy behavior due to the return to initial viscosity values once shear rate was reduced. Shell 3 formulation showed fast thixotropy recovery, which contributed to ensure better shape fidelity [70]. The Figure 30 illustrates the results from rheological tests performed on shell 4 formulation.

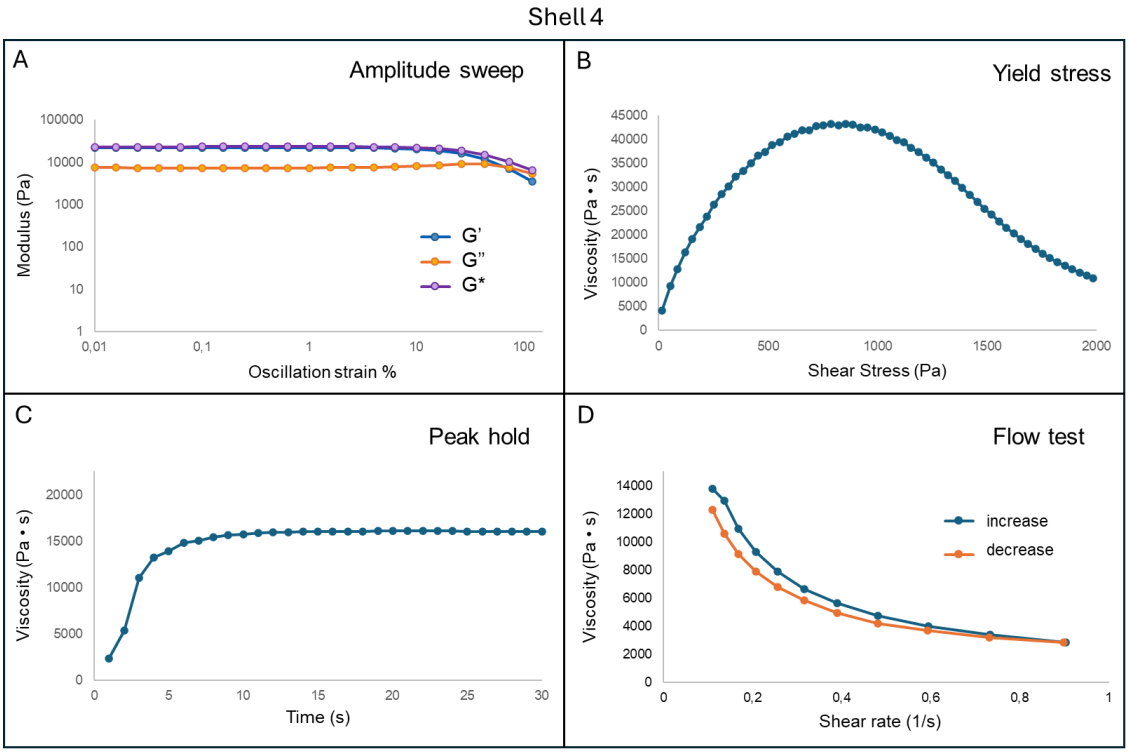

Figure 30. Rheological tests conducted on shell 4 hydrogel.

The amplitude sweep test (Figure 30-A) shows a large LVER, where G' exceeds G'' and both run parallel, indicating the formulation behaves in a "solid-like" behavior. Elastic components were overcoming the viscous ones. The crossover point was observed at 65% oscillation strain, which corresponds to a shear stress value of 7977.25 Pa. Over this point viscous components started to overtake the elastic ones, and the structure of the hydrogels start to lose its mechanical integrity, assuming "liquid-like" behavior. Yield stress is shown in Figure 30-B, reporting viscosity versus shear stress on a linear scale.

Maximum viscosity peak (also referred as yield point) was observed at 43235.4 Pa·s, corresponding to 854.21 Pa shear stress and 0.02 s^{-1} shear rate. These values represented the flowing limit of the formulation, over which hydrogel starts to flow under shear rate applied. Peak hold and flow test (Figure 30-C and D respectively) were performed applying a shear rate superior to the one associated with the yield point. Peak hold analysis allows to determine limit viscosity value at a fixed shear rate. Analysis was conducted at 25°C, with 0.1 s^{-1} shear rate for 30 seconds. Limit viscosity was calculated as medium of the last six point of the curve and resulted to be 16044.85 Pa·s. From flow test analysis, performed following method reported in section 3.1.23.1.2.3, the curve viscosity versus shear rate was obtained in linear scale. The formulation showed shear-thinning behavior, with returning to initial viscosity values once shear stress was reduced, typical of thixotropic characteristics.

Shell 5 formulation rheological analysis results are reported in Figure 31.

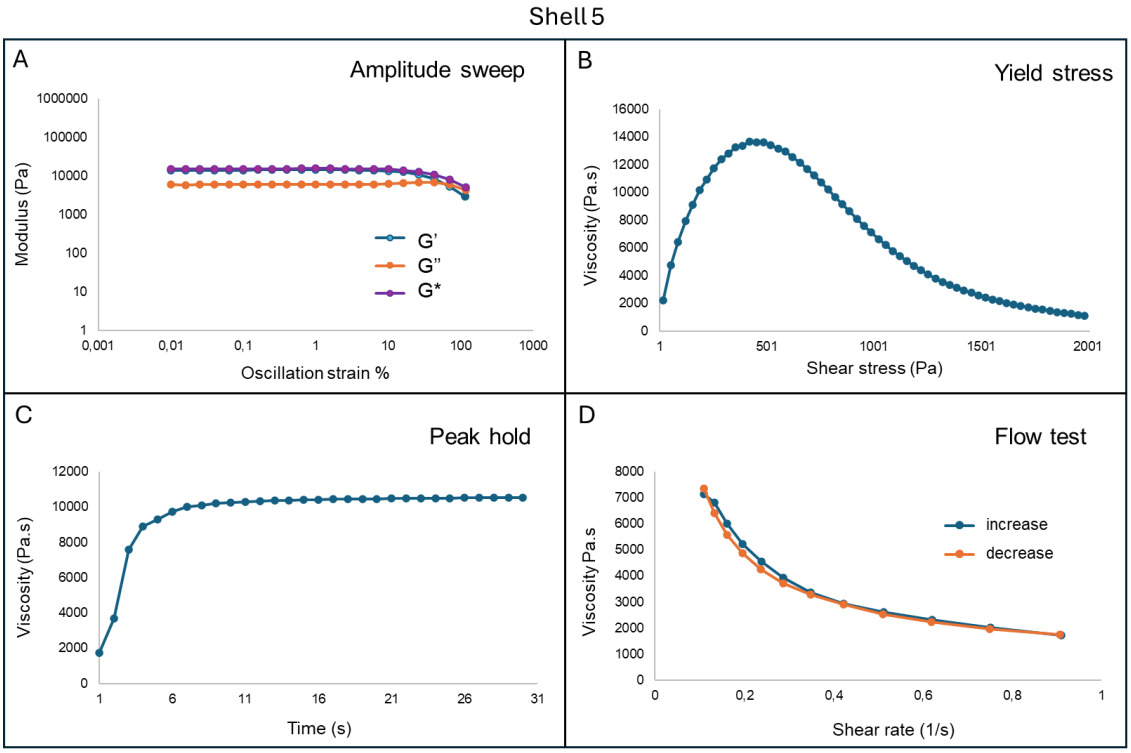

Figure 31. Rheological tests conducted on shell 5 hydrogel.

Even with amplitude sweep test performed with this hydrogel (Figure 31-A), a big LVER was observed, with G' and G'' running parallel. Within this region, elastic modulus resulted higher than viscous modulus, indicating "solid-like" behavior of the formulation. The crossover point was identified at 61% of strain and 6131.70 Pa shear stress. Then, with

yield stress test (Figure 31-B) yield point was identified, obtaining viscosity of 13642.2 Pa·s, shear stress of 421.7 Pa and shear rate of 0.031 s^{-1}, values necessary to set parameters for peak hold and flow test (Figure 31-C and D respectively). Peak hold analysis was conducted at 25°C stabilizing viscosity at 10531.3 Pa·s (obtained as medium of last six points of the curve) employing a shear rate of 0.1 s^{-1}. Finally, with flow test the behavior of formulation under increasing and decreasing ramp of shear rate was observed. Since viscosity of shell 5 reduced under increasing shear rate, the hydrogel possessed shear-thinning properties, essential property in extrusion processes. On the other hand, during the reduction of shear rate, viscosity returned to initial values, without hysteresis, showing thixotropic behavior ideal for 3D printing processes.

At last, shell 6 hydrogel rheological analysis results are shown in Figure 32

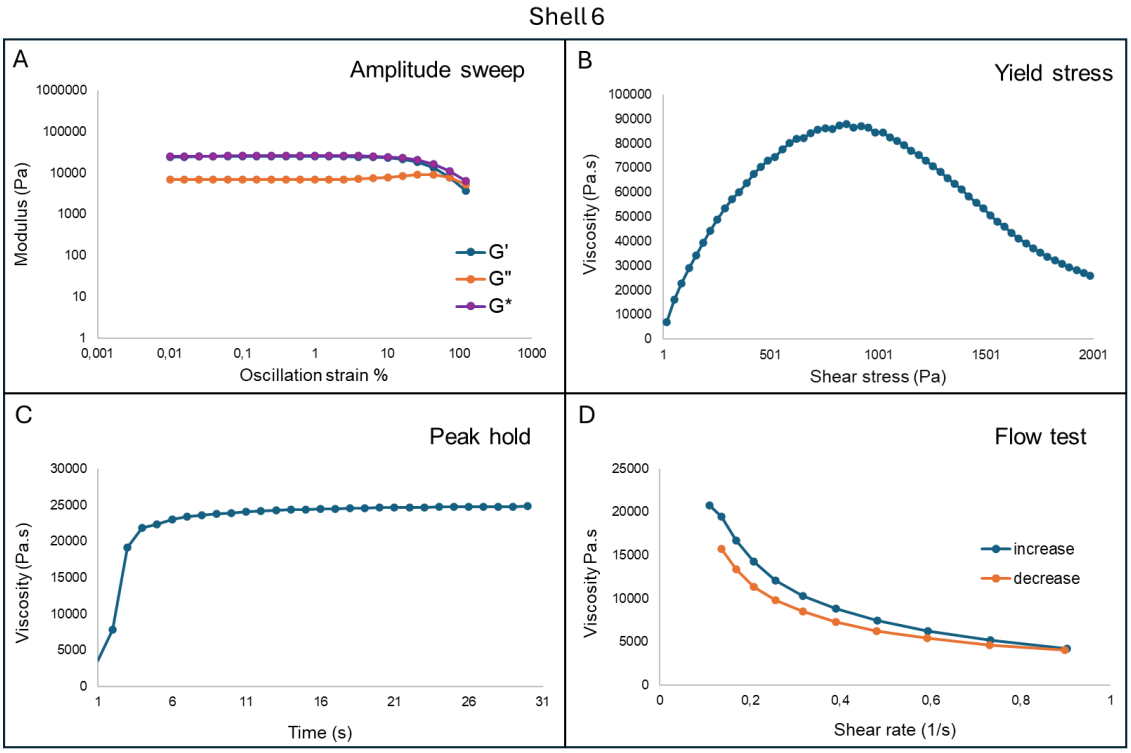

Figure 32. Rheological tests conducted on shell 6 hydrogel.

Amplitude sweep test performed is reported in Figure 32-A, showing a wide LVER where G' and G'' curves run parallel and elastic components overcome the viscous ones, typical of solid-like behaviours, The crossover point was observed at 72% oscillation strain, which corresponds to a shear stress value of 7952.22 Pa. From this point the structure of the hydrogel start to lose its mechanical integrity, assuming "liquid-like" behavior, due to viscous components overtaking the elastic ones. In Figure 32-B is reported the graph

from yield stress test, performed to identify the yield point, described by a viscosity of 87912.6 Pa·s, a shear stress of 854.2 Pa and a shear rate of 0.031 s^{-1}. Peak hold and flow test analysis were performed using values obtained from yield stress test (Figure 32-C and D, respectively). With peak hold test, carried out with a shear rate of 0.1 s^{-1} and at a constant temperature of 25°C, the viscosity obtained from a media of the last six points of the curve resulted to be stabilized around 24783.12 Pa·s. Finally, flow test analysis was conducted at 25°C, increasing the shear rate from 0.1 to 1 s^{-1} (60 rpm maximum) within 300 seconds and then, without giving hydrogel time to rest, returning to 0.1 s^{-1} within 300 seconds. The curve viscosity versus shear rate nearly returned to initial values, indicating a thixotropic behavior of the hydrogel.

3.1.3.9. Solid state investigation of reservoir formulations

3.1.3.9.1. X-Ray Diffraction

Solid state investigation was performed on dried core formulations (see Table 15 for composition) and printed reservoir formulations CC3, CC4, CH3, CH4, CH5 and CH6, following the methodologies reported in sections 3.1.2.4.1, 3.1.2.4.2 and 3.1.2.4.3.

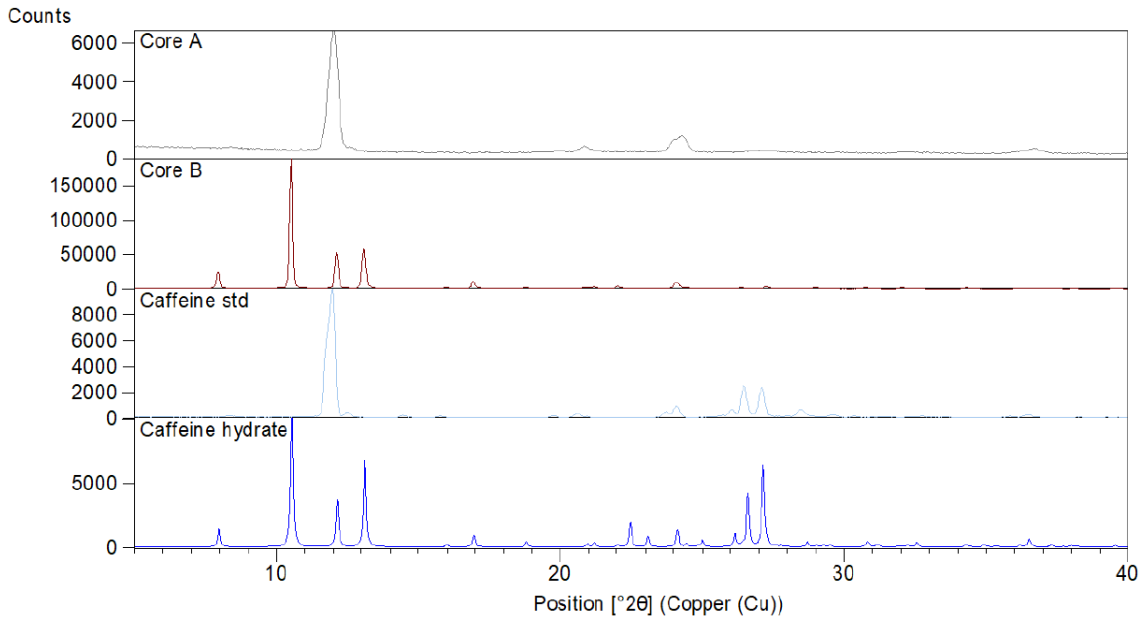

Figure 33. XRD of dried core formulations core A (grey) and core B (brown) compared to caffeine std (light blue) and caffeine hydrated form (blue).

Figure 33 reports the X-ray diffraction pattern of core A and B formulations employed within the 3D printing of reservoir solid forms (Table 17, Table 20 and Table 22). The diffractograms showed that within core A caffeine maintains the crystalline structure of the starting material and is not affected by the hydrogel formulation process nor the 3D printing process. On the other hand, there is a recrystallization of caffeine in the hydrated form in core B formulation, probably due to the temperature employed during 3D printing process (60°C). The temperature causes the dissolution of drug in the hydrogel formulation, which is extruded as a viscous solution. Once the layers of hydrogel are deposited, their temperature starts to decrease, causing recrystallization of caffeine as hydrate, obtaining solidification of the printed morphology [71]. Then, XRD analysis was performed on CC3 and CC4 solid forms, comparing the diffractograms obtained with pure caffeine and core A formulation already analyzed.

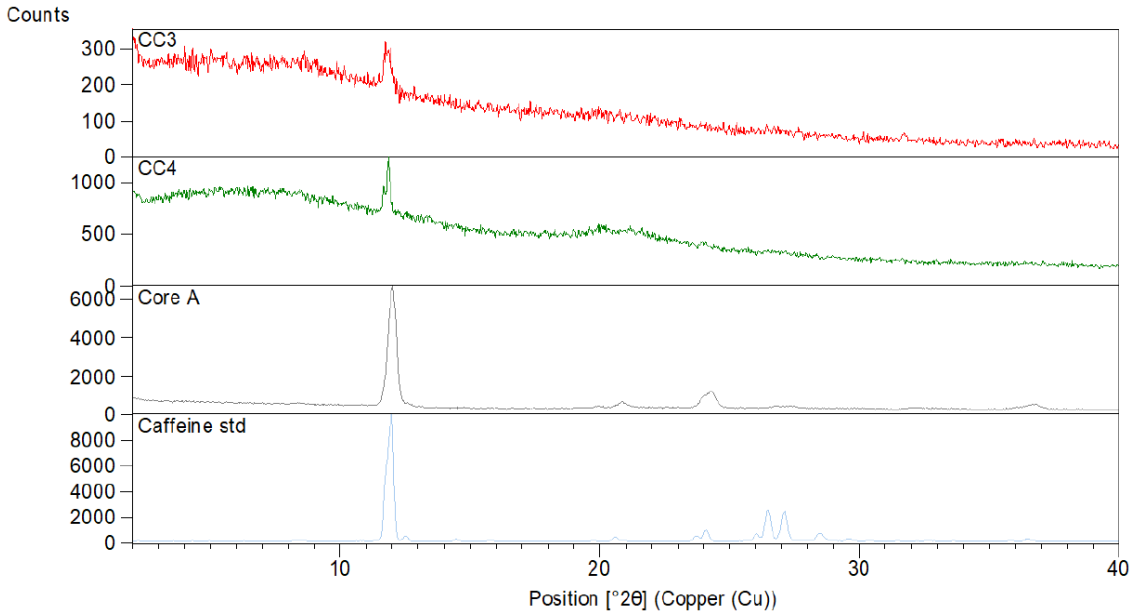

Figure 34. XRD of printed reservoir formulations CC3 (red) and CC4 (green) compared to caffeine std (light blue) and caffeine hydrated form (blue).

XRD analysis of printed and dried CC3 and CC4 formulations, reported in Figure 34, showed how the starting form of caffeine (form II, light blue curve) is maintained after extrusion and drying processes. Despite the high scattering and low intensity of signals, given by polymeric components of the formulations surrounding the matrixial drug enclosing core, the main distinctive peak at 12°2θ of standard caffeine is clearly visible. The extrusion process, carried out at room temperature, and the drying conditions

employed to achieve complete solidification, resulted to have not affected the polymorphic phase of the API.

After that, in Figure 35 the XRD analysis of CH3 - 6 formulations are reported.

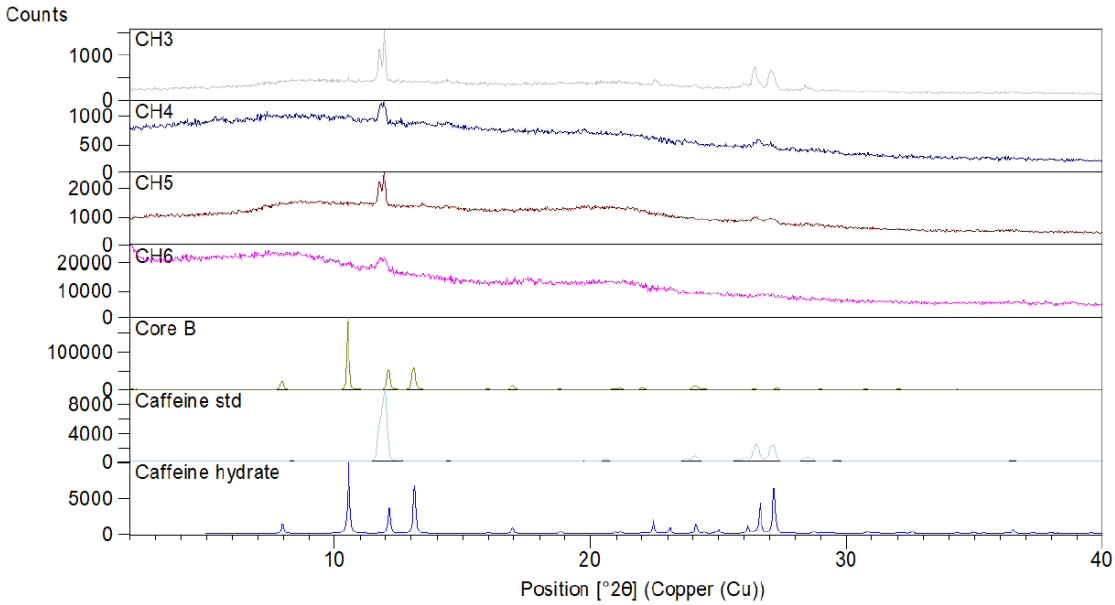

Figure 35. XRD of printed reservoir formulations CH3 (grey), CH4 (dark blue), CH5 (maroon) and CH6 (pink) compared to core B (dark yellow), caffeine std (light blue) and caffeine hydrated form (blue).

The XRD patterns of the CH3 - 6 3D printed reservoir formulations, reported in Figure 35, were compared with the spectra of core B formulation, caffeine standard (form II) and caffeine hydrated form. All the 3D printed formulations showed diffractograms with a scattered baseline, indicating the presence of amorphous phase, due to the high amount of cellulosic polymers. As already observed with CC3 and CC4 formulations (see Figure 3434), the main peaks of caffeine form II are detectable in the pattern of CH3 - 6. This is in contrast with the diffraction spectrum obtained with core B dried formulation, which showed the presence of recrystallized hydrated caffeine. Further analyses were performed on freshly printed and dried printlets (immediately after the end of the drying process) and reported in Figure 36.

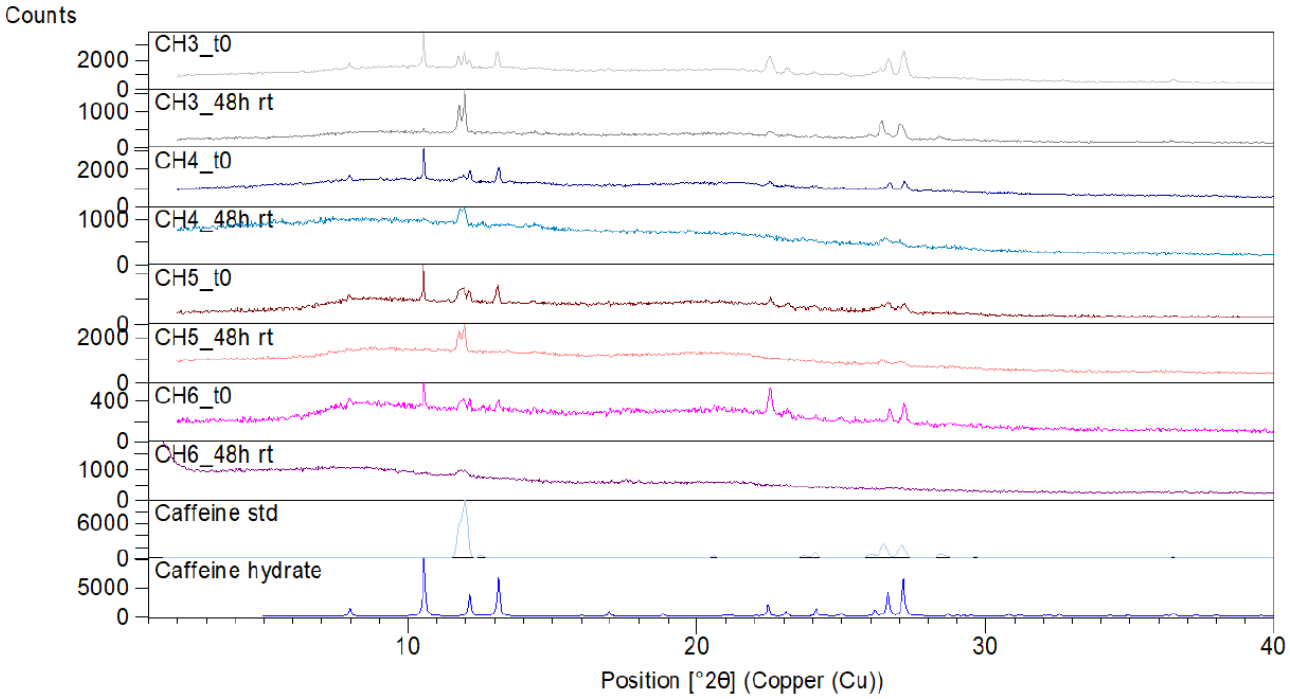

Figure 36. XRD of 3D printed formulations freshly dried and after 48h at ambient conditions compared with std caffeine (light blue) and caffeine hydrate (blue).

It is clearly notable how the freshly dried printed formulations show the presence of hydrated caffeine, like the dried core B formulation (Figure 3336). The situation changes with all the printlets after 48h at ambient conditions, where the “open air” conditions probably induce water mobility and hydrated caffeine transition towards the starting anhydrous form II.

This behaviour provides an explanation for the differences observed in the initial analysis reported in Figure 35. By the way, since both polymorphic forms’ solubility is high (21.8 mg/mL for the hydrate form and 49.7 mg/mL for the anhydrous one [72]) the release kinetics at the concentrations tested should not be affected by the API polymorphic form and the level of drying reached from the printlet.

3.1.3.9.2. Differential Scanning calorimetry

Anhydrous caffeine is known to exist in two polymorphic forms, form I (T_{mp} = 237.73 °C) and form II (T_{mp} = 158.88°C) [73,74], explaining the presence of the two endothermic peaks reported in the thermogram displayed in Figure 3737. The thermal behavior of caffeine starting material is reported in comparison to the curves obtained from the analysis of the 3D printed formulations.

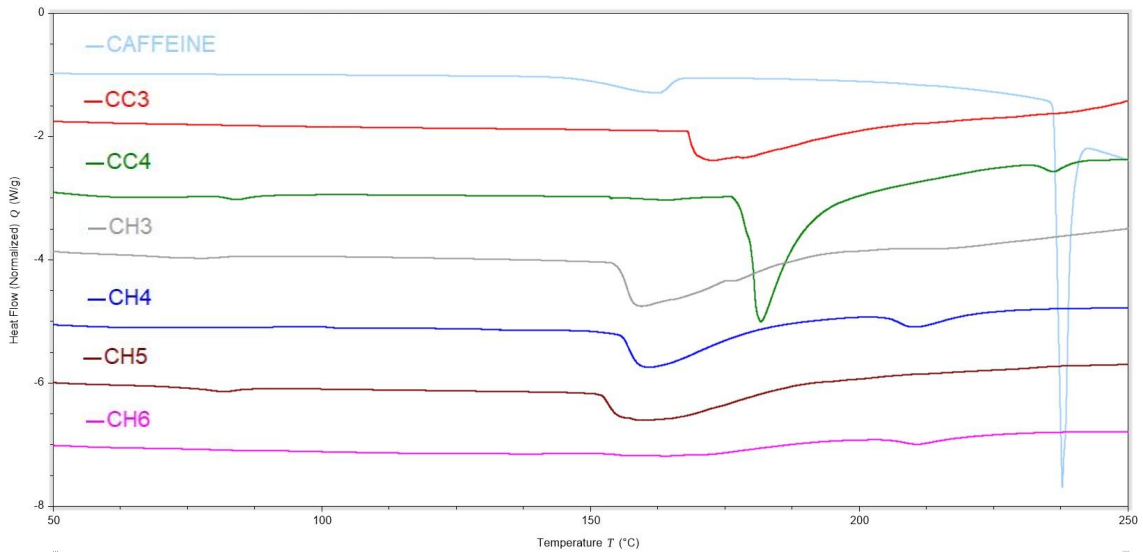

Figure 37. DSC of printed reservoir formulations compared to caffeine std.

Figure 37 shows similar behaviors between formulations printed with the same core type. 3D printed formulations from CH3 to CH6 display the melting of caffeine form II around 160°C, temperature similar to the one observed during the API analysis. The melting of caffeine form II is present also in CH6, with a very low intensity. The latter melting of caffeine form I is clearly visible only with CH4 and CH6, observed at lower temperature with respect to standard caffeine (210°C instead of 237°C). With formulations CH3 and CH5 the melting of caffeine form I is masked and not visible, suggesting that some different interactions could happen at high temperatures between caffeine form I and HPMC K4 or K15. On the other hand, formulations CC3 and CC4 showed the melting of caffeine form II at higher temperatures if compared to standard caffeine. Solid formulation CC3 exhibits the melting of caffeine form II at 173°C, with the subsequent melting of form I masked and not displayed. Formulation CC4 behaved differently, clearly showing the presence of caffeine form I, melting at 235°C, coupled with the endothermic peak, attributed to melting of caffeine form II, which shifted to 181°C and with the highest intensity observed so far. The composition of CC4 formulation probably could help to stabilize the API which requires more heat to melt and convert to the most stable polymorph. Polymeric excipients at these concentrations could have a “solvent effect” on API, potentially justifying the different thermograms observed [75].

3.1.3.9.3. Scanning Electron Microscopy (SEM)

SEM images of the surface of reservoir formulations are illustrated in Figure 38.

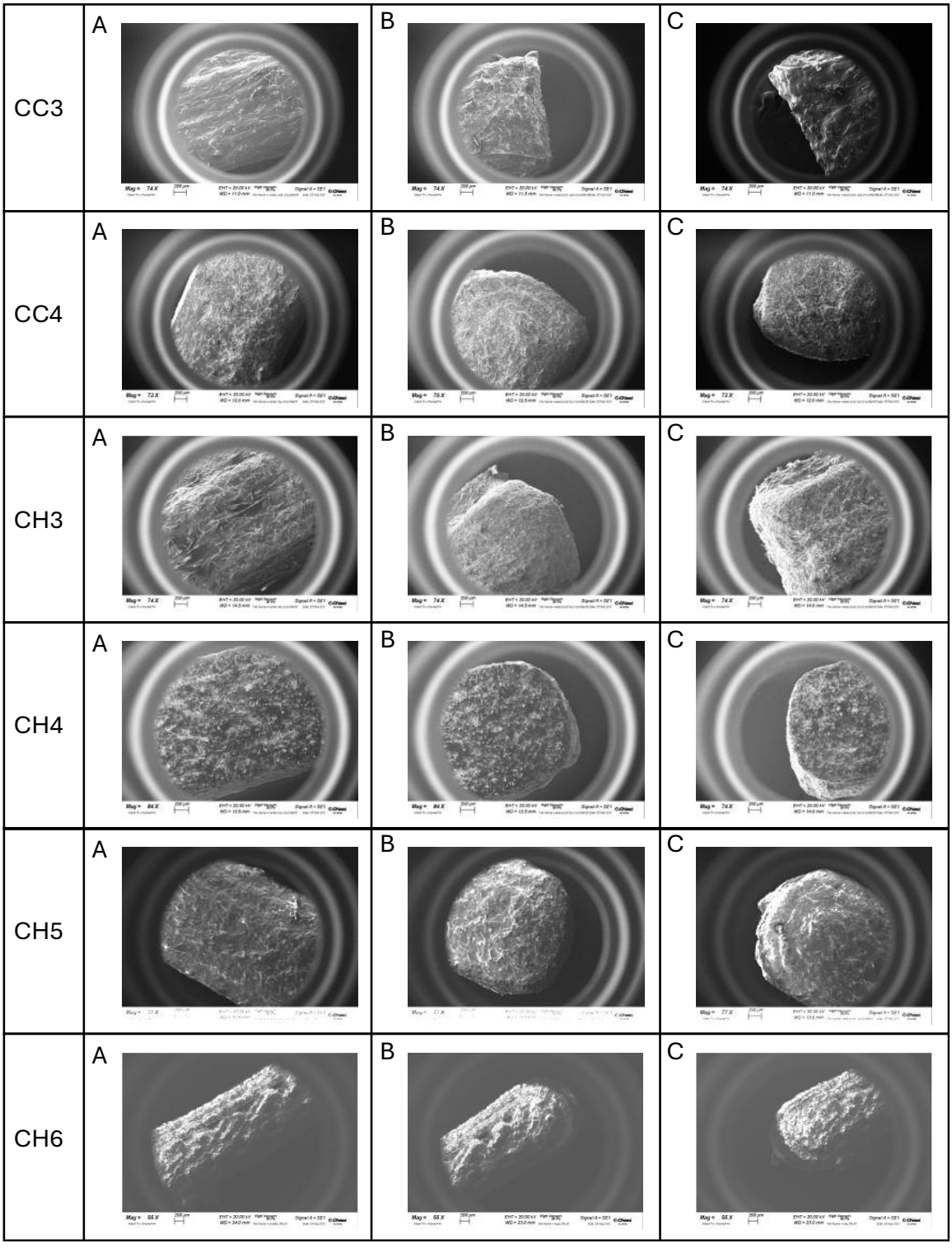

Figure 38. Scanning electron microscopy images obtained with 3D printed reservoir formulations (top views).

SEM images showed the top surface of printed formulations. From that it is possible to notice how the extruded strands of material are all melted together and barely distinguishable. The path followed during printing process was cancelled by the material incorporation into a unique layer. Anyway, from the side view of CH4 formulation shown in Figure 39 below, is possible to see how the various layers printed on top of each other are well defined and their morphology perfectly maintained, confirming the accuracy of the printing process. Both from top view or lateral view, neither overlapping nor empty spaces are observed within all the formulations printed.

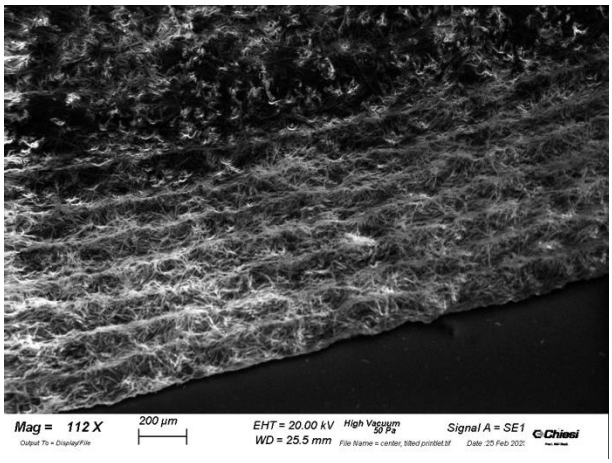

Figure 39. CH4 reservoir formulation side view.

3.1.3.10. In vivo administration in rats

For the *in vivo* oral administration evaluation, CC3 and CH5 were selected as SSE 3D printed formulations with caffeine. Each of the selected printlets was administered successfully to the rats without complications, following methodologies reported in section 3.1.2.8.1. Commercial Torpac® size 9 gelatin capsules filled with pure caffeine were considered as reference. The corresponding mean pharmacokinetic profiles of 3D printed solid forms and reference, are illustrated in parallel within Figure 40 below, enabling a comparative evaluation of their absorption characteristics and systemic distribution. Relevant mean plasma PK parameters are reported in Table 25. PK parameters of the commercial reference gelatin capsule are also reported for comparison.

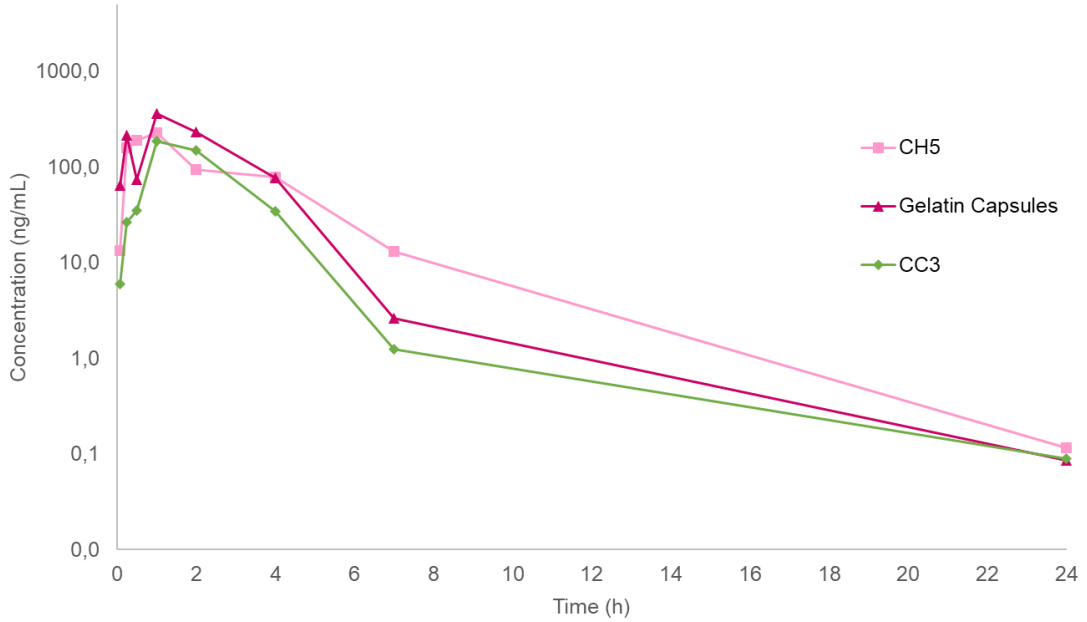

Figure 40. Caffeine plasma profile after oral administration of printed formulation CC3 (green) and CH5 (pink) compared to reference gelatin capsule (dark pink). Plasma levels were normalized per dose.

Table 25. Mean plasma pharmacokinetic parameters for caffeine after oral administration of selected 3D printed formulations and reference commercial gelatin capsule size 9.

Formulation ID	Cmax (ng/mL) Mean ± SD	AUC0-24 (h*ng/mL) Mean ± SD	MRT0-24 (h) Mean ± SD	$t_{1/2}$ (h)	AUC/D (ng·kg / mL·mg) Mean ± SD	Cmax/D (ng·kg / mL·mg) Mean ± SD
CC3	509 ± 432	1157±971	2.5±0.523	5.8	448±377	198±172
CH5	1503± 1071	4215± 879	2.98±1.276	1.9	935± 239	337± 253
Gelatin Capsules	1417±454	3594±1386	2.11±0.147	2.1	916±303	362±96.6

CH5 printed formulation showed favorable characteristics respect to commercial and CC3 ones, with increased AUClast and Cmax relative to the reference, indicating a moderate enhancement in bioavailability.

In contrast, the CC3 formulation resulted in a lower Cmax and AUClast, despite a slightly earlier Tmax, suggesting a faster but less efficient release of caffeine. Moreover, CC3 was associated with a prolonged terminal half-life (T1/2), which may reflect a delayed elimination phase or a formulation-specific release mechanism, although this did not translate into improved systemic exposure.

Mean residence time (MRTlast) values were relatively consistent across the 3D-printed formulations, ranging from 2.5 to 2.98 hours, and slightly exceeded that of the gelatin capsule (2.11 h), suggesting a modest extension of drug presence in the systemic circulation. When normalized per dose, both AUC/D and Cmax/D values showed improved dose-normalized exposure of CH5 compared to the gelatin capsule, while CC3 remained less effective across all parameters.

The plasma PK curves obtained underscore the essential role of *in vivo* testing in assessing the physiological release kinetics of solid dosage forms, considering that the relationship observed between CC3 and CH5 in Figure 23 is reversed under these conditions.

These data support the hypothesis that semi solid extruded 3D printed formulations can be strategically employed to fine-tune the pharmacokinetic behavior of oral formulations, even though deeper optimization of hydrogel formulations should be performed. Among the tested printlets, CH5 demonstrate potential for further development, offering an enhanced PK profile that could serve as a foundation for optimizing oral delivery of 3D printed caffeine formulations.

3.2. Direct Powder Extrusion

This section investigates direct powder extrusion 3D printing technology. Some parts of the formulation development and composition studies for 3D printed samples were performed in collaboration with the Department of Biomolecular Sciences, University of Urbino Carlo Bo. The content of this section was published [76].

3.2.1. Materials

Caffeine powder from Carlo Erba (Milan, Italy) was selected as model drug. Polyvinyl alcohol (PVA) in the forms of powder (05 fine, VIVAPHARM®, 4.6-6 mPas, JRS Pharma, Rosenberg, Germany), pellets (MOWIFLEX™ 3D 2000, Kuraray Poval, Frankfurt, Germany), and micronized powder (GOHSENOL™ EG-05P, 4.8-5.8 mPas/ EG-03P, 27-33 mPas, Farmalabor, Milan, Italy) was tested. Hydroxypropyl celluloses (HPC-L MW 140 kDa, and HPC-SSL MW 40 kDa) were obtained from Nippon Soda (Tokyo, Japan), while hydroxypropyl methylcellulose (AFFINISOL™, HPMC HME 15LV and AFFINISOL™, HPMC HME 100LV) from DuPont (Wilmington, USA). Kollidon® VA 64 (copovidone) was obtained from Basf (Ludwigshafen, Germany), and Eudragit® L 100-55 (poly-methacrylic acid-co-ethyl acrylate 1:1) from Evonik GmbH (Essen, Germany). Polyox WSR N10 (PEO, MW 100 kDa) was purchased from Colorcon (Gallarate, Italy); while mannitol from Farmalabor (Milan, Italy) and PEG 6 kDa from Merck (Darmstadt, Germany). The salts (NaCl, KCl, $Na_2HPO_4*2H_2O$, KH_2PO_4) employed for preparing PBS, methanol and formic acid were purchased from Merck (Darmstadt, Germany). All solvents used were analytical grade.

3.2.2. Methods

3.2.2.1. 3D printing process

M3DIMAKER™ (FabRx, London, UK) was the 3D printer involved in the project execution, equipped only with a direct powder extrusion nozzle. The printhead employed was a single-screw powder extruder with a nozzle diameter of 0.2mm. Printbed temperature was set to 80°C and the extrusion temperature adjusted depending on the various properties of the formulations (170-180°C). Infill density was kept at 100% and layer height at 0.4mm. The default speed employed was 5 mm/s during extrusion while travel speed was set at 50 mm/s. Three layers of skirt were added to provide continuity to the flow of material.

3.2.2.2. Selection of printable cellulose-based polymeric excipients

Prior printing, each batch (5 g) was prepared by weighing the components, drying overnight at 40 °C, and finally the blend was homogeneously shaker mixed for 15 minutes at 100 rpm (Galena Top powder mixer, Ataena, Ancona, Italy). The prepared blend was directly fed into the printing unit (Tumaker NX Pro, Gipuzkoa, Spain) prior preheating the equipment approximately for 15 minutes. After each trial, the printhead was disassembled and cleaned preventing cross-mixing between the formulations.

Firstly, the extrudability was evaluated, considering formulations “extrudable” when a good flowability and a uniformity of filaments coming out from the nozzle were observed. Subsequently, the extrudable formulations were considered “printable” when the layer-by-layer deposition of the molten material led to the production of the desired design.

The matrix excipient was first blended with 10% w/w of the selected model drug corresponding to an administrable rodent dose of 1.65 mg/unit during preclinical studies. If the formulation was not extrudable or the printability was not adequate, different percentages of additional excipients were considered according to the necessities. Mannitol, PEO 100 kDa or PEG 6000 were added as plasticizers to control the flowability of the material and/or as binders to enhance the layer-layer adhesion. Table 26 report the composition of each formulation tested with 10% w/w of caffeine (not included in the table).

Table 26. Composition of the powder blends containing 10% w/w of caffeine.

Formulation	Matrix Excipient	Polyox WSR N10	Mannitol	Kollidon® VA 64	PEG6000
F1	PVA 05 fine	-	-	-	-
F2		10%	-	-	-
F3	PVA MOWIFLEX™ 3D 2000	-	-	-	-
F4	PVA GOHSENOL™	-	-	-	-
F5		-	-	-	-
F6	PVA Farmalabor	-	-	-	-
F7	HPC-L	-	-	-	-
F8		10%	-	-	-
F9		-	10%	-	-
F10	HPC-SSL	-	-	-	-
F11		-	10%	-	-
F12		5%	10%	-	-
F13	Eudragit® L 100-55	20%	-	-	-
F14	Kollidon® VA 64	15%	-	-	-
F15		20%	-	-	-
F16	Affinisol™ HPMC HME 15LV	-	-	-	-
F17		-	10%	-	-
F18		10%	-	-	-
F19		-	-	-	10%
F20		-	10%	-	5%
F21	Affinisol™ HPMC HME 100LV	-	-	-	-
F22		-	10%	-	-
F23		10%	-	-	-
F24	Affinisol™ HPMC HME 15LV	-	-	10%	-
F25	Affinisol™ HPMC HME 100LV	10%	-	10%	-
F26		-	-	20%	-
F27		-	-	40%	-

3.2.2.3. Optimization of the printing process parameters

Since the printlets are intended for eventual *in vivo* studies in rats, it is necessary to choose the appropriate size and shape. Thus, based on the cannula's inner dimension that is employed for the administration of a size 9 capsule by gavage, a rectangular shape (8.6 mm length x 1.8 mm height x 1.8 mm width), was designed using a freeware CAD tool (see section 3.1.2.2). The .stl file was converted to G-code using Simplify3D software (Figure 41). The optimization of the printing parameters was performed using a nozzle of 0.2 mm diameter, to achieve a better resolution of the printed form. The printing temperature was set at 170-180 °C and to improve the adhesion, the bed was heated at 80 °C. When the adhesion of the material to the printing bed was still poor, a polypropylene (PP) adhesion sheet was added. The infill density was kept at 100% and different infill patterns were investigated (*e.g.*, rectilinear, aligned, grid). The aligned was considered the most suitable, providing good structural accuracy in terms of final outcome of the printlet. The default speed was set at 5 mm-s, while the travel speed was 50 mm-s. Three layers of skirt were added to provide continuity to the material's flow.

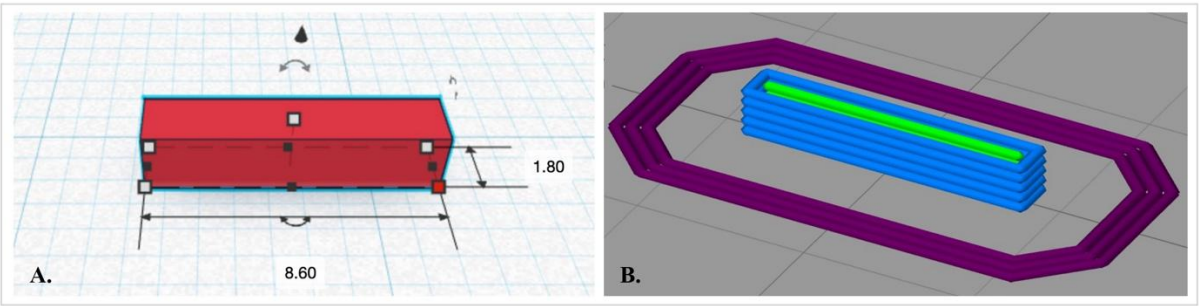

Figure 41. (A) CAD model of the printlets and (B) printing preview after slicing process.

3.2.2.4. Powder blend uniformity

To confirm the homogeneity of the formulation, random samples were collected after mechanical mixing and analyzed using UV-Vis spectrometry (UV-1900 i, Shimadzu, Tokyo, Japan). Specifically, the powder blends were dissolved in PBS (1 mg-mL) and stirred until complete dissolution. The spectrum mode, in the range 200-400 nm was applied for the analyses. The intensity of the resulting absorbance was visually compared among three replicates from the same formulation.

3.2.2.5. Solid state characterization

3.2.2.5.1. X-Ray diffraction (XRD)

The solid state of 3D printed forms was investigated by X-ray powder diffraction with Empyrean V2.0 (Malvern Panalytical, Almelo, Nederlands) equipped with Cu radiation source (Cu Kα 1.5406 Å), generator voltage set to 40 kV and the current to 40 mA. Samples were acquired under transmission mode spinning with revolution time 0.5s. The measurements were scanned over 2Theta range from 2° to 45°, step size 0.02°, soller slit 0.02 rad, divergence slit 1-2°, antiscatter slit 1-2°.

3.2.2.5.2. Differential scanning calorimetry (DSC) and Thermogravimetric analysis (TGA)

The thermal behaviour of the pure model drugs, excipients, the physical blends and the final 3D printed formulations was investigated through DSC (DSC 6000, Perkin Elmer, Shelton, US), and TGA (TGA 4000, Perkin Elmer, Shelton, US) analyses. Specifically, for the DSC measurements, approximately an average mass of 5-10 mg of sample was placed in an aluminium pan and heated up from 25°C to 275°C at 10°C-min. Nitrogen flow rate was kept at 30 mL-min. While for TGA analysis, scans were run from 25°C to 550°C, at a speed rate of 10°C-min, using nitrogen as purge gas. Data collection and analyses were performed using Pyris Manager software (Perkin Elmer, Shelton, US).

3.2.2.5.3. Morphological characterization by scanning electron microscopy

The morphology of the 3D printed formulations was observed with a SEM microscope (FEI, Hillsboro, US). The instrument was employed in low-vacuum mode, applying a specimen pressure chamber of 0.8 mbar and an acceleration magnitude of 25.0 kV. The magnitude ranged between 100-255x, while the working distance ranged between 8.7-9.6 mm. The images were performed using the large field detector (LFD).

3.2.2.5.4. Fourier-Transform infrared spectroscopy

FTIR (Spectrum Two, Perkin Elmer, Shelton, US) was employed to investigate the chemical composition of the physical blends and the pointlets; and compare it with the raw materials. Measurements were carried out at 400–4000 cm^{-1} with a resolution of 4 cm^{-1} and a total of 64 scans.

3.2.2.6. Uniformity of dosage units

Mass uniformity was assessed according to the method described in the European Pharmacopoeia (Eur. Ph. XI Ed.) for uncoated tablets of mass < 80 mg, the deviation is set at ±10% from the average. A total of 20 dosage units, taken randomly, were analysed.

3.2.2.7. Drug content

HPLC (Agilent 1260 Infinity II, Agilent, Santa Clara, US) was employed for quantitative detection of caffeine. The analysis was conducted using an Agilent Zorbax Eclipse Plus C18, 150×4.6 mm, 5 µm column (Agilent, Santa Clara, US), at room temperature. 0.5% formic acid (FA) in water and methanol (60:40) were selected as mobile phases, setting the flow rate at 1 mL-min and the injection volume at 20 µL. The detection signal was recorded at 274 nm. Calibration curves were also performed, and linearity was guaranteed in the interval of 1-40 µg-mL and 0.5-10 µg-mL, with the R^2 values equal to 0.9999.

3.2.2.8. In vitro drug release

The cumulative drug release profile of the drug from the 3D printed formulations was evaluated adapting the method described in the European Pharmacopoeia (Dissolution Test, Eur. Ph. XI Ed.). The analysis was carried out using a PTWS 120D Dissolution apparatus (Pharma Test, Hainburg, Germany) equipped with a basket stirring tool. Stirring was fixed at 60 rpm and the temperature kept at 37°C. To mimic the physiological condition, different pH media were used. Specifically, the printlets were immersed in 75 mL of HCl 0.1N pH 1.2 for the first 2h, mimicking the stomach acidity, then 25 mL of Na_2HPO_4 0.2M were added and pH adjusted to 6.8 with minimum amount of NaOH 2M simulating the transit to the intestine until complete dissolution of the printlet. Time points

were recorded each 15 minutes for the first hour and then each 30 minutes. Samples of 1mL were withdrawn at each time point and then replaced with fresh medium. Quantification studies were carried out using UV-HPLC. The analytical method is described in section 3.2.2.7. The analysis was carried out in triplicate. Also, for each formulation, size 9 capsules were manually filled with powder blends, and the drug release profile was assessed at the same conditions described above.

3.2.2.9. Mechanical properties

A compression test was performed to assess the mechanical properties of the 3D printed formulations with a TA.XTplus Texture Analyzer, (Stable Micro Systems, Surrey, UK) equipped with a 50 Kg load cell. Tests were conducted using a compression probe of 2 mm diameter, a constant compression speed of 0.03 mm-sec, and a trigger force of 100 g, to achieve a strain of 100%. The analysis was carried out at room temperature and for a total of five samples for each formulation. Data was collected as stress vs strain. The peak force (N) registered at 100% strain and the Unconfined Compressive Strength (UCS, MPa) were defined, while the Young's Modulus (YM, MPa) and the Yield Point (YP, MPa) were determined from engineering the stress-strain curves.

3.2.2.10. In vivo administration in rats

The methodologies employed to perform *in vivo* oral administration in animal models (rats) are detailed within section 3.1.2.8 and administration of DPE 3D printed caffeine formulation has been performed following the same as with SSE 3D printed formulations.

3.2.3. Results

3.2.3.1. Selection of printable cellulose-based polymeric excipients

In the identification of the optimal formulation, appreciable flowability is a fundamental prerequisite for a good resolution of the printing performance. Hence, the extrudability and printability were evaluated for each blend.

Since for F3, the drug was not homogeneously distributed around the pellets, the formulation was discarded.

Most of all formulations were extrudable, however, the filaments obtained from F1, F4, F5 and F6 were rough and brittle, in addition, when increasing the temperature an over-extrusion was observed and the filament browned. Despite the addition of Polyox WSR N10 (F2), PVA has not proved adequately processability in combination with the model drugs, probably due to the narrow range between the melting and degradation temperature. In addition, when the nozzle was clogged avoiding the printing process, a formulation was discharged, like in the case of formulation F13.

Considering HPC-based formulations loaded with caffeine, F7 and F10, extrusion was difficult and not constant, being characterized by under-extrusion followed by over-extrusion. Suggesting the need for an additional excipient such as a plasticizer, Polyox WSR N10 or mannitol, to facilitate and control the flow. However, Polyox WSR N10 (F8), was not appropriate, providing a plasticizing effect without controlling the amount of extruded material. Conversely, the addition of mannitol (F9) showed promising results. The extrusion of Kollidon® VA 64 with caffeine proved difficult. Even in the presence of plasticizers which could help the extrusion, the formulations tend to adhere to the screw (F14 and F15).

Two different grades of HPMC at lower and higher molecular weight (15LV and 100LV, respectively) were tested. Formulations containing only the caffeine (F16 and F21) or with the addition of mannitol (F17 and F22) were easily extrudable, with a good control over the flow, while the addition of Polyox WSR N10 (F18 and F23) lead to a loss of control over the flow that turned out to be too slow. PEG6000 was also selected as a binder for the HPMC-based formulations (F19) but it led to a very sticky blend that clogged the nozzle during the extrusion. HPMC100LV was also combined with Kollidon® VA 64 at different concentrations, at 10% (F24) high temperatures were required to obtain a sufficient flow from the nozzle, leading to the darkening of the filament. The addition of mannitol (F25), helped lowering the extrusion temperature, thus avoiding the darkening of the filament but a complete lack of flow control was experienced. Higher concentrations of Kollidon® VA 64 were added to the mixture (F26 and F27) but led to the extrusion of a filament that was too stiff and brittle. Overall, the formulations containing HPMC at lower molecular weight resulted in a more controlled and smooth extrusion through the nozzle.

Taking into consideration the extrudability test, a preliminary printing trial was performed with the selected formulations (F9, F11, F12, F16, F17 and F20). By comparing the formulations, HPC-L based composition (F9) provided a superior accuracy of the design over HPC-SSL based ones (F11 and F12). Concerning the HPMC15LV-based

formulations (F16 and F17), the good extrudability did not lead to a good outcome of the printing process. This was due to a quick cooling of the filament and complete lack of adhesion to the printing bed and layer to layer. Hence, the addition of 5% of PEG6000 (F20) was selected to enhance the “stickiness” of the blends resulting in a good layer adhesion and printing accuracy. Thus, formulations F9 and F20 were selected as candidates for the manufacturing of the printlets loaded with caffeine. The printed products are represented in Figure 42. After printing, the devices were measured using a digital caliper (Mitutoyo, Milan, Italy) and a good accuracy to the selected CAD dimension was observed.

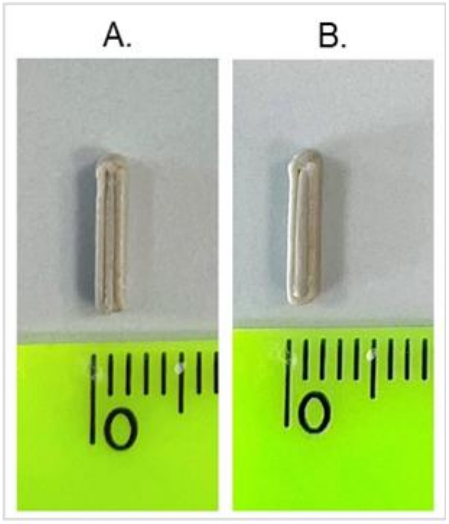

Figure 42. Top view of the caffeine loaded printlets: (A) HPC-L-based formulation (F3); (B) HPMC 15LV-based formulation (F20). The scale is expressed in cm.

3.2.3.2. Powder blend uniformity

To evaluate the homogeneity of the powders’ blend, random samples (triplicate) of the same formulation were collected after mechanical mixing. For all the formulations, HPC-L and HPMC-based, the resulting intensity of the UV bands overlapped, confirming the homogeneity of the blends after mechanical mixing.

3.2.3.3. Solid state characterization

3.2.3.3.1. Differential scanning calorimetry (DSC) and Thermogravimetric analysis (TGA)

DSC analysis was carried out to assess the thermal stability of the excipients and APIs in formulations at the operating temperatures and after printing. Thermograms are reported in Figure 43. As already discussed in section 3.1.3.9, anhydrous caffeine is known to exist in two polymorphic forms, form I, T_p = 237.73 °C and form II, T_p = 158.88°C [73,74], explaining the presence of the two endothermic peaks in the thermograms. Mannitol and PEG 6000 show their melting peaks at T_p = 168.16°C and T_p = 66.57°C, respectively. Cellulose-based polymers are instead amorphous and glass transition temperatures are hardly detectable as previously reported [77,78,79]. Thermograms display a broad endothermic event at low temperatures T < 100°C which can be attributed to the evaporation of the moisture absorbed [80]. The peak is anyway weak as the amount of water incorporated is very low due to the overnight drying of the physical blends.

When considering the physical mixtures and 3D printed formulations, significant changes in the thermal behavior were detectable. Caffeine-based formulations display a reduction, in terms of temperature and intensity of the peaks, suggesting a good miscibility of the drug and excipients. Moreover, although caffeine melts at higher temperatures than the printing conditions, the “molten environment” allows the API to easily dissolve. Still, after cooling to room temperature, caffeine recrystallizes quickly [81], also explaining the lack of total amorphization of the drug. Specifically, in formulation F9, caffeine recrystallizes in form I, while in F20 it is present in form II, as assessed through the XRD analysis (section 4.2.3.3.3).

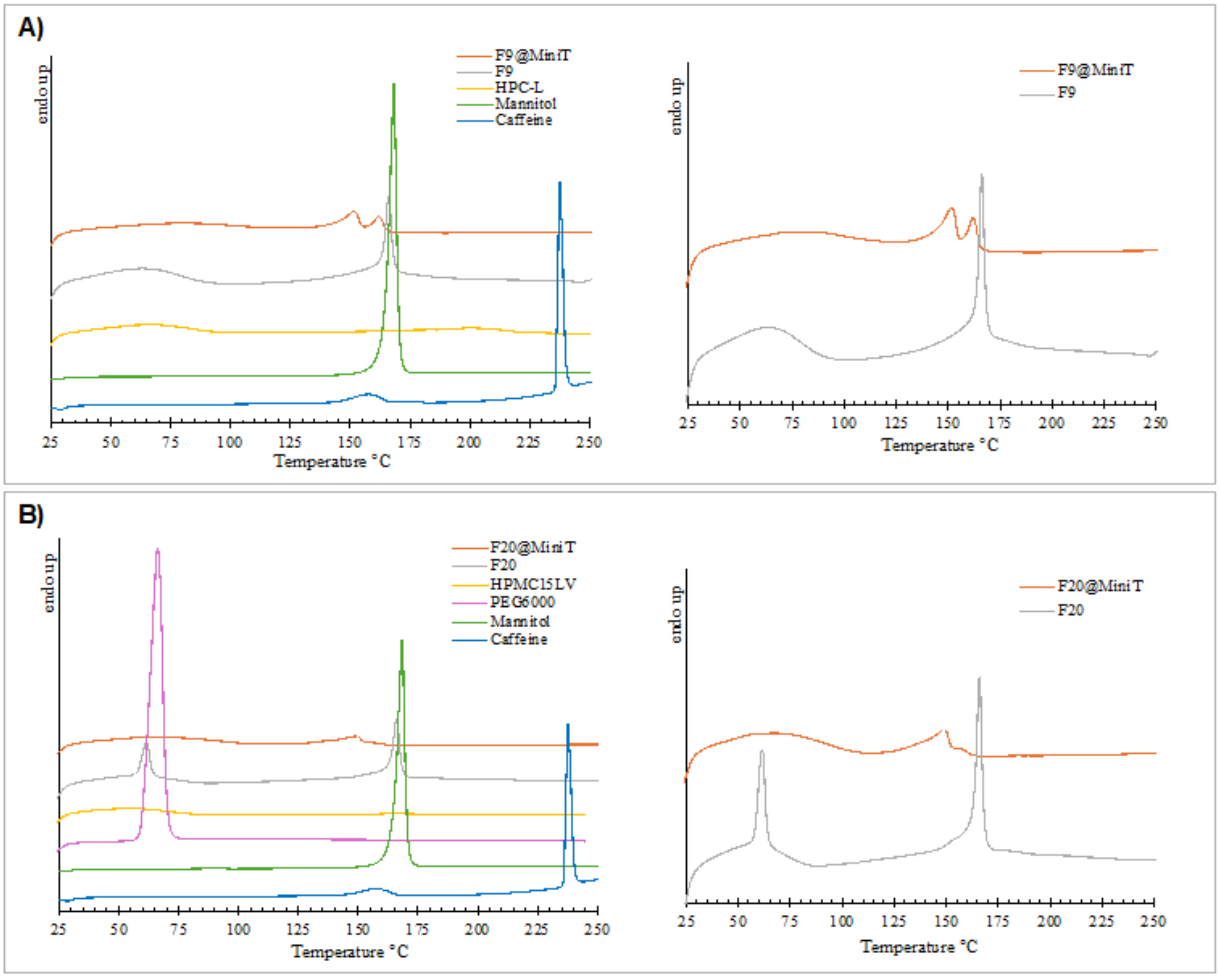

Figure 43. DSC thermograms of caffeine loaded formulations (A) HPC-L and (B) HPMC 15LV. The graphs on the right represent a clear view of the thermograms for the powder blends (grey) and the printlets (orange).

Since the materials are exposed to high temperatures during the 3D printing manufacturing process, it is essential that all formulations are processed at conditions that are clearly below the decomposition critical points; ideally, at the lowest feasible processing temperatures [82]. The primary benefit of DPE over FDM is that the powder blends only need to go through the hot stage once because creating the filament is not a required step.

Based on the weight variations, the TGA thermograms of the caffeine, excipients, physical mixtures and 3DP formulations were examined (Figure 44). It was evident that the printing temperatures, which range between 170°C and 180°C, are far below these critical points. Until 200°C, indeed, a negligible weight loss was observed for all samples (1.2 – 2.3 %,

due to the release of the moisture absorbed), demonstrating the chemical stability of the materials during the printing process.

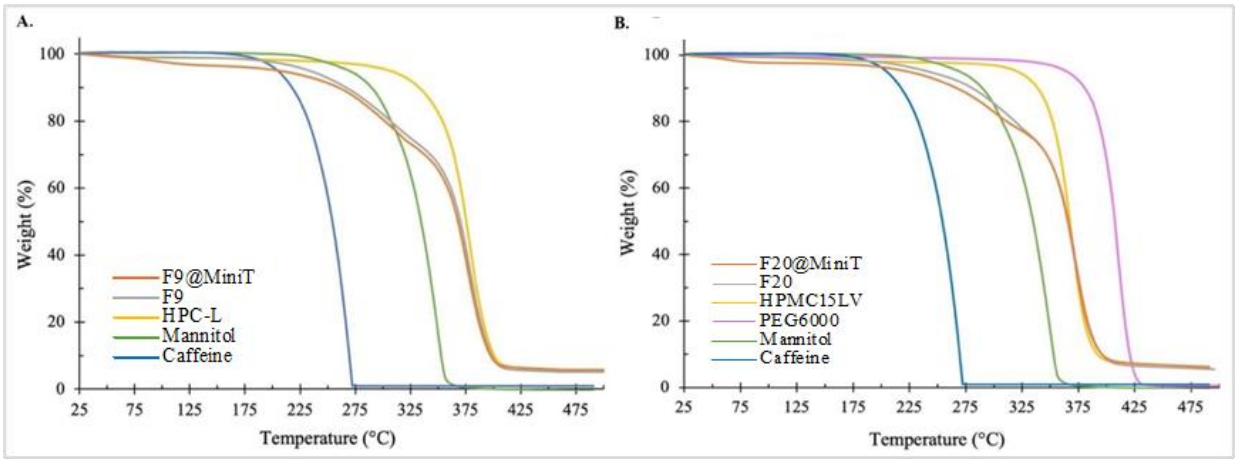

Figure 44. TGA thermograms of caffeine loaded formulations in the two different polymer matrices (A) HPC-L and (B) HPMC 15LV.

3.2.3.3.2. Fourier-transform infrared spectroscopy (FTIR)

FTIR spectra were collected from analyzing the raw materials (excipients and caffeine), the powder blends and final 3D printlets, as shown in Figure 45. All the significant peaks observable in the spectra were confirmed with the ones found in literature. HPC-L and HPMC 15LV showed their significant peaks around 3200-3400 cm^{-1}, broadband, due to the O-H stretching vibrations in the pyranose ring of the sugar, at 2926 and 2856 cm^{-1} attributed to the C-H asymmetric and symmetric vibrations, and a broad band at 1050 cm^{-1} due to the C-O-C asymmetric stretches [83]. In the PEG 6 kDa spectrum, the peak at 1100 cm^{-1} is due to the stretching vibration of C–O–C bonds, while the strong peaks around 2800-2900 cm^{-1} to the stretching vibrations of C-H and OH functional groups, respectively [84,85]. Mannitol spectrum displays the main peaks at 3310 cm^{-1} (broadband, O-H stretching vibrations), at 1348 cm^{-1} and 1080 cm^{-1} (C-H and C-O stretching vibration respectively) [86]. Caffeine has its characteristic peaks at 1670 cm^{-1} (C=O stretching), and at 1638 cm^{-1} (C=N stretching) of the xanthine. [87] Both the spectra of the powder blends and the final 3D printed formulations feature the main peaks of the raw materials (excipients and API), and no unknown peaks appear, nor significant ones disappear, suggesting a good compatibility among the excipients and caffeine but also within the manufacturing method.

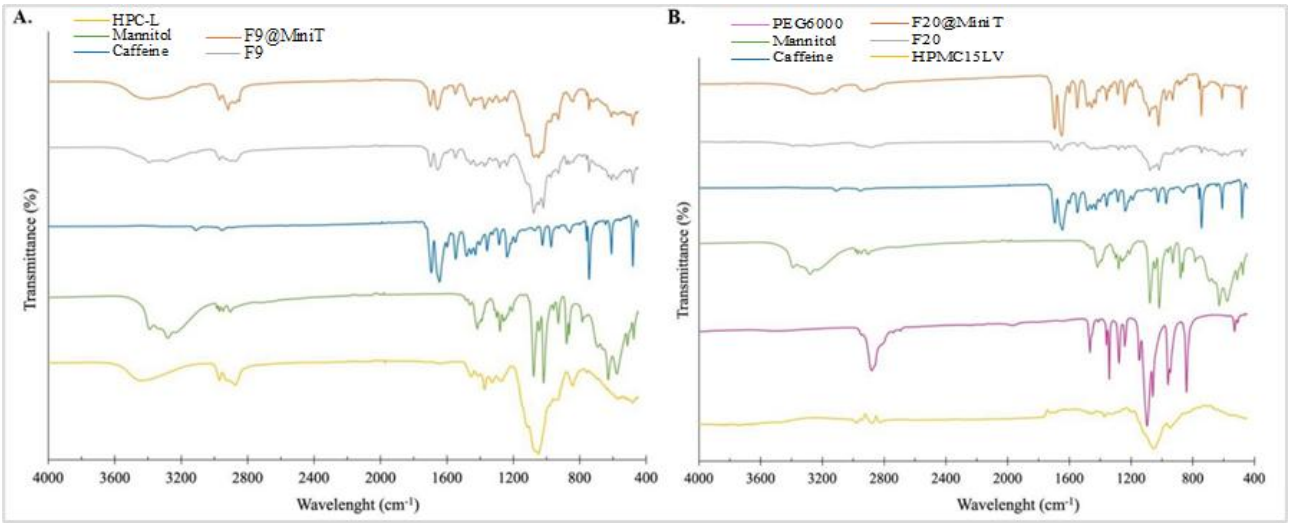

Figure 45. FTIR spectra of the raw materials, physical blends and printlets. Caffeine-loaded formulations F9 and F20 in the two different polymer matrices (A) HPC-L and (B) HPMC 15LV.

3.2.3.3.3. X-ray diffraction (XRD)

X-Ray diffraction spectra were acquired on the final 3D printed forms formulations F9 and F20, under transmission mode. Looking at Figure 46, in formulation F9, it was clear the presence of both caffeine recrystallized in form I and Delta form of mannitol. This was mainly caused by the temperatures reached by the printing process (170-180°C) which were higher than the melting temperatures of caffeine form II (present in the physical powder blends) and Alpha form of mannitol, leaving only the two polymorphs described above as present in the final 3D printed form. This behaviour provided also the indication that molten HPC-L had a "solvent effect" on caffeine [75]. Figure 47 shows in F20 the presence of recrystallized Delta form of mannitol, but less intense than in F9, and form II of caffeine instead of form I, suggesting that the presence of PEG 6 kDa and HPMC 15LV lower the "solvent effect" of the polymer matrix on caffeine.

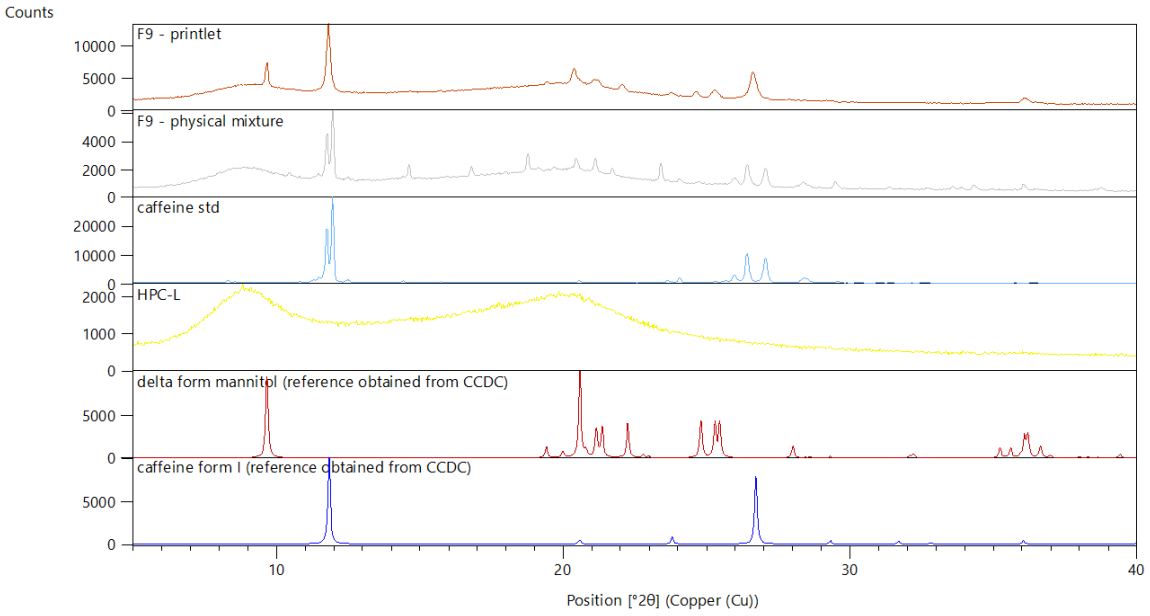

Figure 46. XRPD diffractograms of the raw materials, physical blend and 3D printed formulation F9.

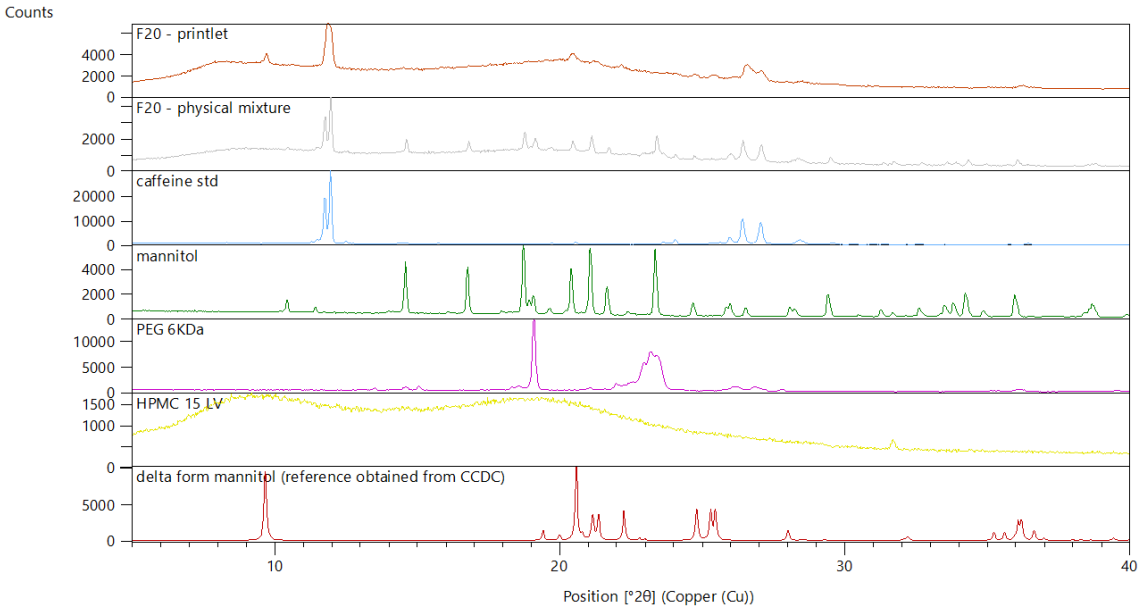

Figure 47. XRPD diffractograms of the raw materials, physical blend and 3D printed formulation F20.

3.2.3.3.4. Morphological characterization by scanning electron microscopy (SEM)

SEM images shown in Figure 48-A and B reveal a smooth surface for the 3D printed formulations. The layered structure appeared accurate both from top (left) and lateral view (right), confirming the accuracy of the printing process; indeed, neither overlapping nor empty spaces are observed. Moreover, in accordance with the results obtained at the XRD analysis, in Figure 48-C, the presence of crystalline structures in the matrix of the caffeine-loaded 3D printed formulations is highlighted.

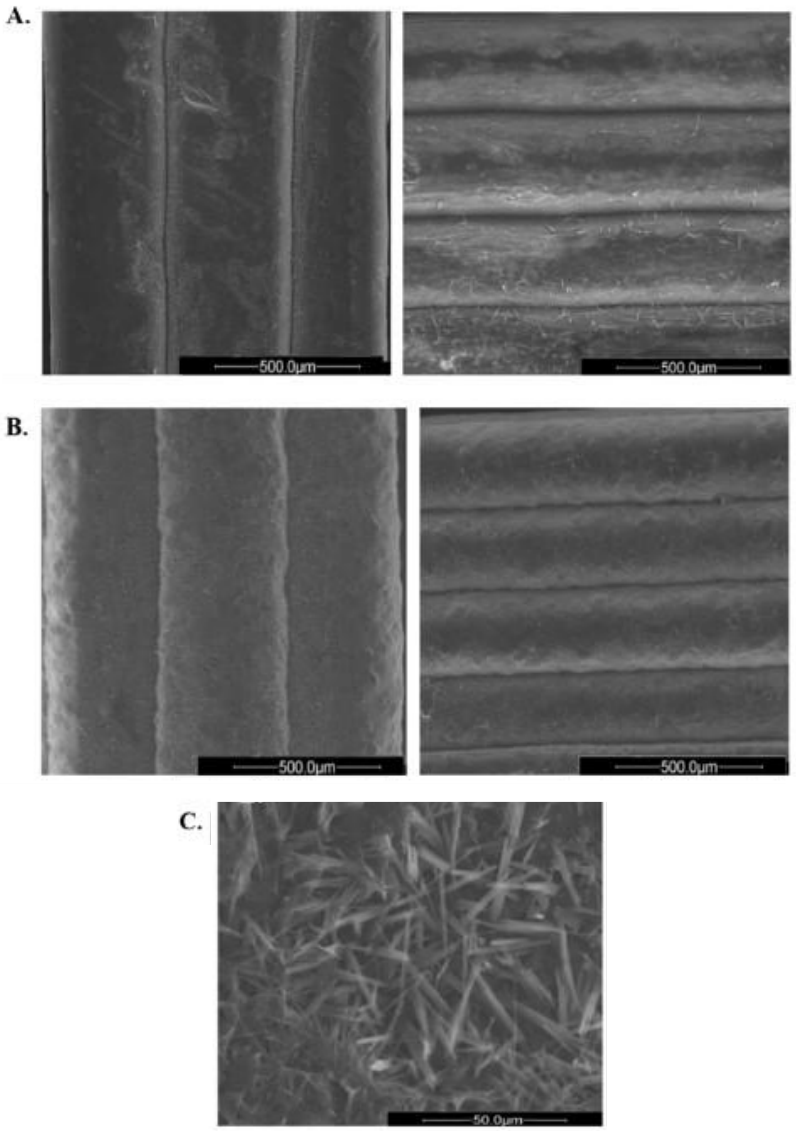

Figure 48. (A) SEM images of top and lateral view of printlet F9. (B) SEM images of top and lateral view of printlet F20. (C) SEM image focused on caffeine recrystallized.

3.2.3.4. Uniformity of dosage units

Uniformity of mass was assessed for the 3D printlets. The one obtained from HPC-L-based formulations (F9) showed an average mass of 23.1±1.8. While, for the one obtained from HPMC 15LV (F20) the average mass was of 27.1±1.6 mg. European Pharmacopoeia states that individual masses of no more than two tablets can differ from the average mass by more than 10% when it comes to uncoated single-dosage units with an average mass lower than 80 mg. Since in this case no printlet exceeded the 10% limit, for both the HPC-L and HPMC 15LV-based formulations, the Eur. Ph. requirement was satisfied. Indeed, each batch's relative deviation from the mean mass was low, confirming a good reproducibility of the manufacturing method and satisfying control over the dosage-units' uniformity.

3.2.3.5. Drug content

The effective drug content in the 3D printed formulations was evaluated through quantitative characterization (UV-HPLC, see section 3.2.2.7) and referred to the theoretical caffeine amount loaded in the powder pre-processing at the 3D printer. Drug loading efficiency was 92.4% for HPC-L based formulation (F9) and 95.3% for HPMC 15LV-based formulation (F20). Overall, the amount of caffeine loaded in the final printlets is satisfying and considered acceptable even though a loss of drug is present due to the manufacturing method with very limited amount of material to work with.

3.2.3.6. In vitro drug release

The release profile of caffeine from the different cellulose-based matrices were evaluated through dissolution studies, in accordance with the Eur. Ph. XI. As shown in Figure 49 (yellow plot), unfortunately, the release ratio of caffeine from the HPC-L matrix is fast and immediate, with a 77.83 ± 2.67 % released in 60 minutes and is only slightly slowed when the formulation matrix is switched from HPC-L to HPMC 15LV, 54.41 ± 2.70% after 60 minutes (Figure 49, blue plot). Moreover, the different outcome is not to be look at the presence of mannitol in the formulation as it works only as a plasticizing agent for the manufacturing process without affecting the release profile of the drug from the matrix. This behavior could be ascribed to burst effect as previously experienced with semisolid formulations, as already described in the section 3.1.3.3.

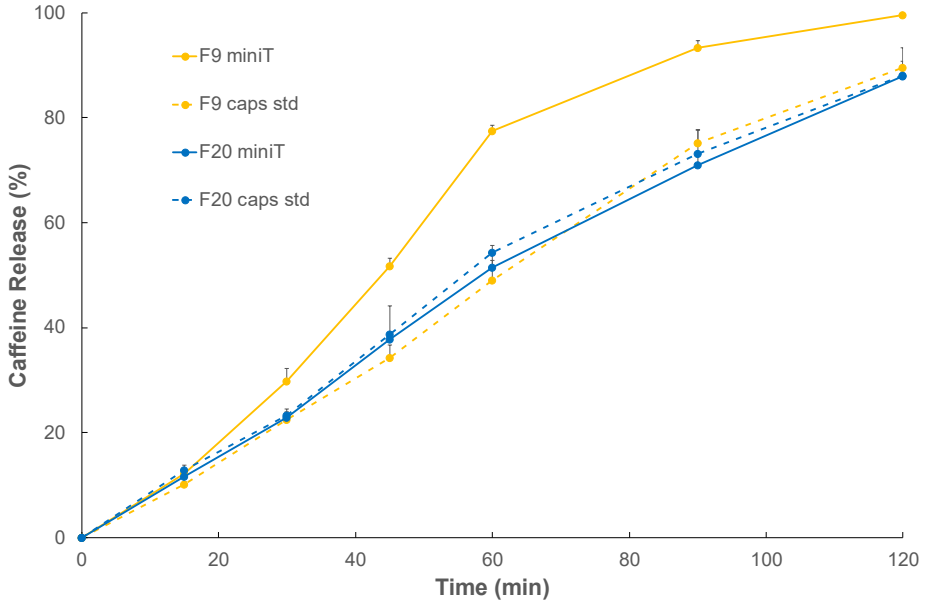

Figure 49. Drug release profiles of size 9 capsules filled with physical blends vs 3D printed formulations.

The dissolution tests were also caried out on capsules size 9 filled with physical blends and the resulting data compared with the ones obtained for the printlets as shown in Figure 49, dotted plots. Comparing the two formulations (3D printed forms and conventional blends filled in size 9 capsules), no significant variation was observed within the release kinetics of the oral dosage forms, highlighting the requirement to move towards different formulation concepts (es. reservoir) to obtain the desired sustained release.

3.2.3.7. Mechanical properties

A compression test was performed on the 3D printed formulations to evaluate their mechanical behavior. In Table 27, for each formulation, the peak force (N), UCS (MPa), YM (KPa), and YP (MPa) are listed. The 100% strain was obtained without any breakage occurring in the printlets, demonstrating their high toughness and resistance. YM measures the resistance of a material to elastic deformation under load, thus a stiff material has a high YM and changes its shape only slightly under deforming stresses [88]. Overall, the strength needed to reach a strain of 100% was similar for all the tested formulations.

Table 27. Mechanical characteristics of the 3D printed formulations.

Formulation	Peak Force (N)	UCS (MPa)	YP (MPa)	YM (MPa)
F9	238.49 ± 8.10	18.99 ± 4.33	4.42 ± 1.01	0.24 ± 0.12
F20	253.84 ± 13.91	21.03 ± 3.16	3.30 ± 2.03	0.21 ± 0.13

3.2.3.8. In vivo administration in rats

F9 was selected as DPE 3D printed caffeine formulation for *in vivo* oral administration. The dosing to the rats was performed, together with commercial capsules size 9 filled with pure caffeine as reference, without complications. The corresponding mean pharmacokinetic profiles of 3D printed formulation are illustrated in Figure 50, in parallel with the reference capsule data, enabling a comparative evaluation of their absorption characteristics and systemic distribution. Relevant mean plasma PK parameters are reported in Table 28, together with PK parameters of the reference capsule size 9.

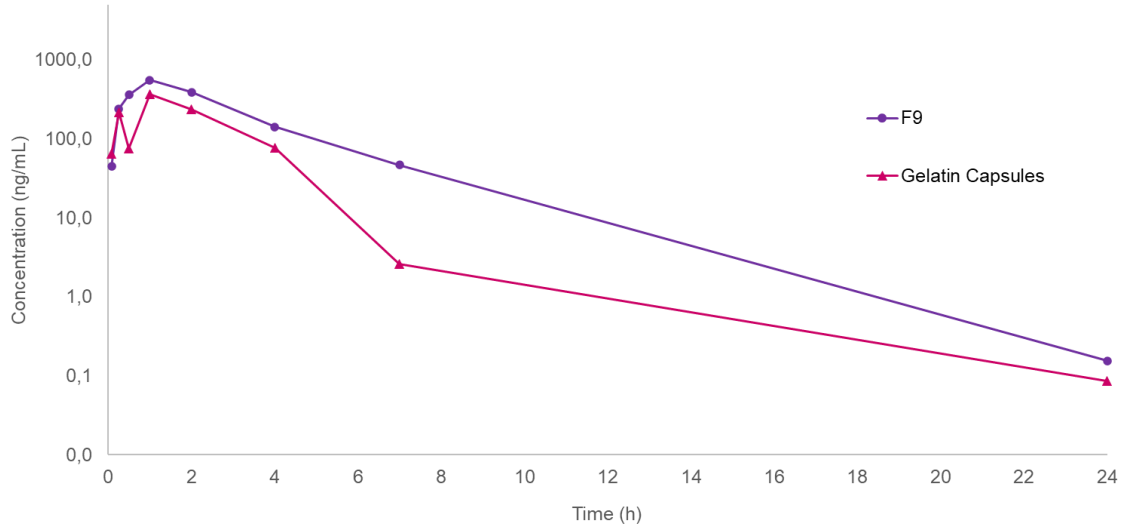

Figure 50. Caffeine plasma profile after oral administration of printed formulation F9 (purple) compared to reference gelatin capsule (dark pink). Plasma levels were normalized per dose.

Table 28. Mean plasma pharmacokinetic parameters for caffeine after oral administration of selected 3D printed formulations and reference commercial gelatin capsule size 9.

Formulation ID	Cmax (ng/mL) Mean ± SD	AUC0-24 (h*ng/mL) Mean ± SD	MRT0-24 (h) Mean ± SD	t1/2 (h)	AUC/D (ng·kg / mL·mg) Mean ± SD	Cmax/D (ng·kg / mL·mg) Mean ± SD
F9	3615± 417	10904± 404	2.90±0.096	1.95	1665± 37.2	554± 96.5
Gelatin Capsules	1417±454	3594±1386	2.11±0.147	2.095	916±303	362±96.6

The selected printed formulation (F9) exhibited a markedly improved pharmacokinetic profile, characterized by a substantial increase in both peak plasma concentration (Cmax) and systemic exposure (AUClast) compared to the commercial gelatin capsule filled only with caffeine.

Mean residence time (MRT last) value slightly exceeded the one of the gelatin capsules (2.90 vs 2.11 h, respectively), suggesting a modestly sustained drug presence in the systemic circulation. When normalized per dose, both AUC/D and Cmax/D values further confirmed the superior performance of F9 (AUC/D = 1665 h·ng·kg/mL·mg; Cmax/D = 554 ng·kg/mL·mg), reinforcing its potential as a highly efficient oral delivery system.

These data support the hypothesis that 3D printing can be strategically employed to fine-tune the pharmacokinetic behavior of oral formulations. F9, the tested 3D printed formulation, stands out as a promising candidate for further development, offering a significantly enhanced PK profile that could serve as a foundation for optimizing oral delivery of caffeine and potentially other active pharmaceutical ingredients. In contrast to the findings from *in vitro* dissolution studies (refer to section 3.2.3.6), where sustained release conditions were not achieved, *in vivo* administration demonstrated a prolonged release compared to the commercial capsule containing pure drug. This outcome underscores the significance of physiological differences between release tests in evaluating the release kinetics of solid formulations.

3.3. Comparison of *in vivo* administered 3D printed formulations

A comparison of all the plasma profiles obtained with *in vivo* administration of selected 3D printed caffeine formulations and commercial size 9 gelatin capsules filled with pure API is reported in Figure 51 below.

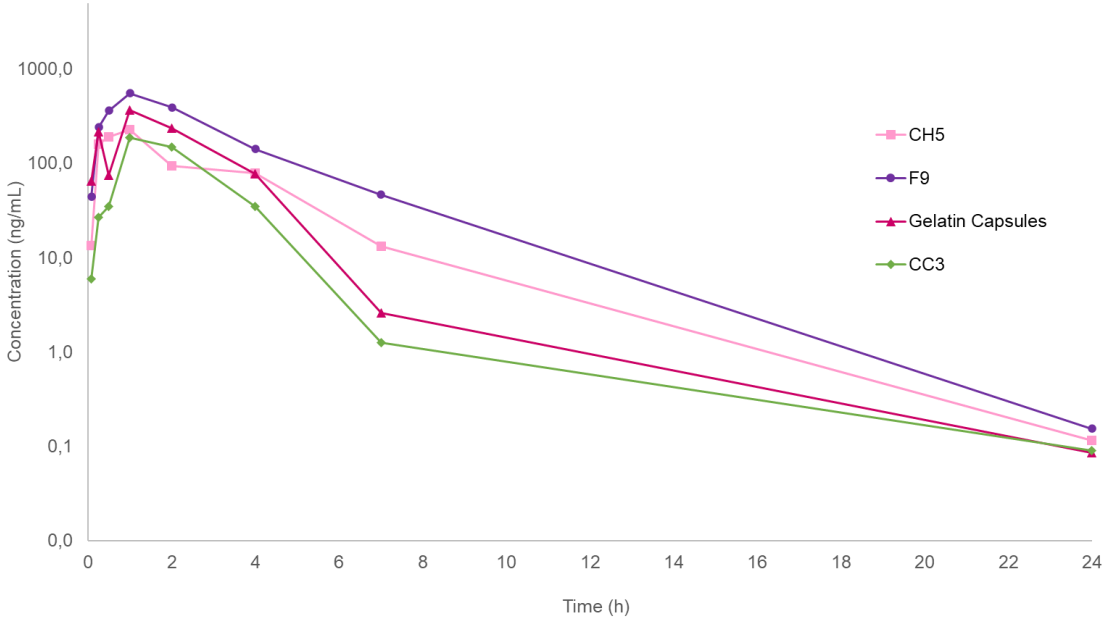

Figure 51. Comparison of caffeine plasma profile after oral administration of selected 3D printed formulations and commercial size 9 capsules filled with pure API.

From the reported comparison it is clearly visible how the DPE 3D printed formulation exhibits the most sustained release kinetics among all the formulations tested. Also the formulation CH5, which was prepared with SSE 3D printing technology and based on HPMC K4 (see section 3.1.3.4), resulted to be more sustained than commercial gelatin capsule filled with pure caffeine, although the difference between the two release profiles is thin. At last, CC3 formulation showed not to be advantageous respect to commercial gelatin capsule. Overall, within this testing environment, the formulation prepared with DPE 3D printing technology proved to be the best one in achieving a more sustained release of caffeine as model drug.

3.4. Conclusions

In the initial part of this project, the use of 3D printing emerged as a highly effective approach for the design and fabrication of pharmaceutical formulation prototypes with modified release properties, specifically employing caffeine as a model API. Two different formulations were developed and fully characterized: the first was prepared using Semi Solid Extrusion (SSE) technology, while the second was obtained through Direct Powder Extrusion (DPE). With the first studied technology, both matrixial and reservoir formulations were evaluated. An alternate dual head printing was developed to prepare reservoir formulations, which required a deeper refinement of CAD model and instrumental set up. Regarding DPE printing technology, only matrixial formulations were printed, due to intrinsic limitation of the 3D printer employed for the study.

Both prototypes were successfully produced in sizes suitable for oral administration in preclinical murine models. *In vitro* release experiments in simulated gastric environment were performed, demonstrating different behaviors between the formulations tested. SSE prepared formulations showed a significant modulation of the drug release kinetics compared to commercial capsules filled with pure caffeine. On the contrary, DPE prepared formulations resulted to reproduce the dissolution behavior of the reference commercial capsule employed in the test, without improving the duration of drug release.

Notably, *in vivo* studies were performed with both SSE and DPE prepared formulations. DPE formulation tested, exhibited an improved pharmacokinetic profile which suggested a modestly sustained drug presence in the systemic circulation. In contrast to the findings from *in vitro* dissolution studies, where sustained release conditions were not achieved, *in vivo* administration demonstrated a prolonged release compared to the commercial capsule containing pure drug, highlighting once more the capacity of 3D printing technologies to tailor release profiles. On the other hand, with SSE 3D printed reservoir formulations, which resulted in achieving a sustained release with *in vitro* dissolution experiments, within the *in vivo* evaluation turned out to have a modest extension of drug presence in the systemic circulation, indicating a moderate enhancement in bioavailability respect to commercial capsule filled with pure API. These results underscore the importance of *in vivo* studies to better understand the behavior of api within physiological conditions, which could influence the results obtained with *in vitro* preliminary tests.

The solid state of the final printed formulations was deeply characterized, showing how both the printing technologies did not influence the chemical and physical characteristics of caffeine.

4. 3D printlets for naproxen immediate release

4.1. Semisolid Extrusion

4.1.1. Materials

Naproxen was the second active ingredient selected as model drug, purchased from BLD Pharm (Reinbek, Germany). Cyclodextrins (Sulfobutyl-Ether-β-Cyclodextrin, α-cyclodextrin, β-cyclodextrin and γ-cyclodextrin) were purchased by Cyclolab (Budapest, Hungary). Calcium chloride, carboxymethylcellulose sodium salt (NaCMC, viscosity 50-200 cP, c=4% H_2O at 25°C), chitosan, cholesterol, citric acid, gelatine, glycerol, Kolliphor® EL, mannitol, polyethylene glycol 400-3350-6000, polyvinyl pyrrolidone, sodium alginate, sodium dodecyl sulfate (SDS) and sorbitol were purchased from Merck Life Sciences (Darmstadt, Germany), while hydroxy propyl celluloses (HPC-SSL MW 40.000, -SL MW 100.000 and -H MW 1.000.000 kDa) were kindly donated by Nippon Soda (Tokyo, Japan). Croscarmellose Sodium (Ac-Di-Sol®) was supplied by Roquette (Alessandria, Italy), while soy phosphatidylcholine was purchased from Avanti Polar Lipids (Birmingham, USA). Hydroxy propyl methyl celluloses (HPMCs): Methocel K4M, K15M, K100M and E5 premium LV were obtained from Colorcon (Gallarate, Italy). Kollicoat® IR (Macrogol Poly [Vinyl alcohol] grafted copolymer), Kollidon® CL (crospovidone) and Soluplus® (Polyvinyl caprolactam-polyvinyl acetate-polyethylene glycol graft copolymer) were provided by BASF (Ludwigshafen, Germany). Capryol 90, Capryol PGMC, Labrafac lipophile WL 1349, Labrasol ALF, Maisine CC, Plurol oleique CC 497 and Transcutol HP were obtained from Gattefosse (Milan, Italy) while Phosal® 50 PG was obtained from Lipoid (Ludwigshafen, Germany). Simulated gastric fluid (FaSSGF) prepared for dissolution studies in acidic medium was obtained from Biorelevant (London, UK). All deionized and purified water was obtained with MilliQ® systems (Merck Life Sciences, Darmstadt, Germany). All the other solvents used were analytical grade.

4.1.2. Methods

4.1.2.1. Preliminary formulative assessment

Prior to printable hydrogels preparation, different formulative approaches were explored, which are described in the following paragraphs.

4.1.2.2. Cyclodextrins (CD)

Inclusion trials of naproxen in CD with water were performed before the preparation of hydrogels. Starting from 100mg of naproxen 1 and 2 equivalents of α-cyclodextrin, β-cyclodextrin, γ-cyclodextrin and sulfobutyl-ether-β-cyclodextrin were weighed and stirred at room temperature with progressive amounts of water, in order to reach complete dissolution. In the end, naproxen was added to the CD solutions and left under magnetic stirring at room temperature for two days, to achieve equilibration. Samplings of naproxen-CD suspension were aliquoted and filtered with 0.2 µm Verex PTFE filters vials (California Phenomenex, USA) before moving to drug quantification (see section 4.1.2.13).

4.1.2.3. Lipid excipients solubility and emulsification

Prior to hydrogel preparation with lipidic excipients, a preliminary solubility screening was performed with naproxen. Concentrations of 15 and 30 mg/ml were explored, adding naproxen to lipid excipients under magnetic stirring at room temperature or raising temperature up to 40°C when a solution was not obtained. Then, if complete solubilization was achieved, the lipidic solution was emulsified with water for subsequent gelification or already preformed hydrogel, with the help of high-speed homogenizer T10 basic Ultra-turrax® (IKA, Staufen, Germany).

4.1.2.4. Liposomes preparation

Naproxen- liposome formulation was prepared using Thin Layer Evaporation (TLE, also referred as thin film hydration) method, followed by membrane extrusion. The preparation method was illustrated in Figure 52. Briefly, soy PC, cholesterol and naproxen (70-30-5, molar ratio) were dissolved in pure ethanol. The API was weighed to achieve a final theoretical concentration of 15 mg/mL. The solvent was then removed using a rotary vacuum evaporator adapting rotation speed and vacuum to the behavior of the solution. The obtained thin film was hydrated at above the transition temperature (Tm) of the employed lipid, with 10 ml of phosphate buffered saline (8.10 mM Na_2HPO_4, 1.47 mM KH_2PO_4, 137 mM NaCl

and 2.68 mM KCl, PBS, pH 7.4). The suspension was kept under magnetic stirring at 100 rpm for at least 2 hours to ensure complete hydration of the lipid film and promote the formation of stable liposomal vesicles. Naproxen-liposomes obtained from thin film complete hydration were then extruded through polycarbonate membrane (Isopore™, Merck Millipore, UK) with pore sizes of 0.8 µm.

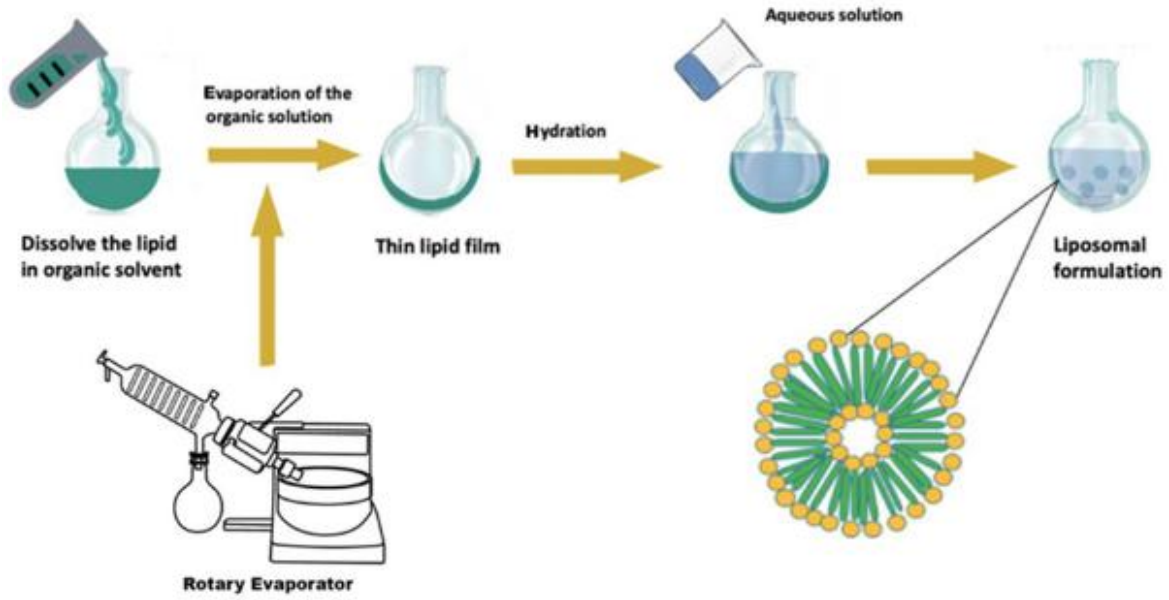

Figure 52. TLE liposomes formulation process flow. Naproxen was dissolved in the organic solvent together with lipidic components (reproduced from [89]).

4.1.2.5. Liquisolid formulation

Liquisolid formulations were prepared following the methodology reported in the work performed by Tiong et al. [90], with some adaptations. To begin with, naproxen was added to Kolliphor® EL using mortar and pestle. Then, after obtaining an homogeneous suspension, carriers and excipients were gradually incorporated. In the end, the obtained blend was slowly added to hot water (85°C) under continuous magnetic stirring, until complete homogenization and gelification of the formulation, that was left resting overnight at room temperature.

4.1.2.6. Hydrogel preparation

The detailed description of the hydrogel preparation was already present in the section 3.1.2.1. In fact, hydrogels were prepared following the procedures already used with caffeine as model drug.

4.1.2.7. 3D printing process

The printing process was carried out with a Cellink BIOX (Cellink Life Sciences, Gothenburg, Sweden), equipped with interchangeable printheads. See section 3.1.2.2 for further details on printer specifications.

4.1.2.8. Solid state characterization

The solid state characterization of naproxen 3D printed formulations was performed using the same equipment and method employed for caffeine. For XRD see section 3.1.2.4.1, for DSC see section 3.1.2.4.2 while for SEM refer to section 3.1.2.4.3.

4.1.2.9. Liposomes characterization

Liposomes physicochemical characterization includes the determination of average particle size, polydispersity index (PDI), and zeta potential by Dynamic Light Scattering (DLS), the evaluation of shape and morphology through optical microscopy, and the investigation of encapsulation efficiency and drug loading through LC/UV/MS methods. The *in vitro* drug release profile was also measured. For this kind of investigation, an additional step of dialysis is required, followed by drug content quantification using chromatographic and spectrophotometric techniques.

4.1.2.10. Particle size and zeta potential evaluation

The particle size and ς-potential of liposomes were both determined using a dynamic and electrophoretic light scattering instrument (Zetasizer Nano ZS, Malvern Panalytical, UK). Particle size measurements were performed at 25°C using a sample volume of 40 µL in disposable micro cuvettes (Malvern, UK), after 30 s equilibration time, and acquired at a backscattered detection angle of 173°. Each measurement was run in triplicate. For zeta potential determination, a High Concentration Zeta Potential Cell (Malvern, UK) was employed under the same experimental conditions, and measurements were carried out as a single acquisition.

4.1.2.11. Encapsulation efficiency

In order to calculate encapsulation efficacy (%EE), the first step was to separate non-entrapped (free) drug from drug-loaded liposomes. Centrifuge and exclusion columns were used for separation. In this study, the lipid formulation of naproxen was loaded into Vivaspin® 50K centrifugal concentrators (Sartorius, Germany). The devices were used to separate the free drug present in the supernatant from the formulation-associated fraction retained in the pellet, through size-exclusion provided by the 50 kDa molecular weight cut-off membrane. Centrifugation was performed at 7830 G and 4°C for 1 h and 30 min. Both the supernatant and pellet fractions were subsequently analyzed by ultra-high-performance liquid chromatography (UHPLC) to determine the naproxen content. Additionally, particle size and zeta potential were measured in the pellet fraction to confirm that the physicochemical properties remained consistent with those of the initial formulation.

To calculate liposomes encapsulation efficiency, naproxen content was determined by UHPLC analysis applying the following method. The chromatographic system was composed of UHPLC Waters Acquity (Milford, Massachusetts, USA), equipped with UV detector (Tunable UV, TUV, Waters, USA). Samples (standard solution for calibration curve: API in ethanol, range concentration 0.0001-0.1 mg/ml; liposomes dissolved in Ethanol, dilution 1:3000) were automatically injected into a C18 column (Kinetex 1.7µm EVO C18 100A, 150x2.1mm, Phenomenex, Torrance, California, USA) and eluted with a gradient: water + 0.2% formic acid (phase A) and methanol: propanol (80:20 v-v) + 0.2% formic acid (phase B) with a flow rate of 0.35 mL-min. Gradient timetable is shown below.

Table 29. Gradient timetable for naproxen quantification method with liposomal formulations.

Time (min)	A (%)	B (%)
0.00	100	0
0.10	100	0
10.00	50	50
20.00	20	80
25.00	0	100
28.00	0	100
30.00	100	0
32.00	100	0

The column temperature was set at 25°C. The detection wavelength was set at 270 nm. Calibration curve and samples were prepared using pure ethanol. The quantification of the active compound in the samples of the manual experiment was performed using a calibration curve obtained from standard solutions of the pure analyte, prepared at known concentrations by appropriate dilutions of a stock solution. In addition to the calibration standards, a system suitability test (SST) was performed in order to verify the accuracy and reliability of the calibration curve. For each standard concentration, the area under the UV peak was measured and plotted on a graph, with the x-axis representing the concentration of the active compound (µg/mL) and the y-axis the corresponding peak area. The best-fitting line through the experimental data points was determined using the least-squares method. Based on the equation of this line and the measured UV peak area, the concentration of each sample was calculated in mg/mL. Fullscan acquisition was performed to evaluate eventual presence and nature of impurities or degradation products. The data are presented as average ± standard deviation of three experiments.

MS instrument:	Waters QDa
Acquisition Mode:	Fullscan MS scan
Polarity:	ES+
Mass range:	30-1250
Injection colume (µL):	5
Sample solvent:	Ethanol
Cone voltage QdA	3V

4.1.2.12. Release test from liposomes

The API release from liposomal formulations was examined by the membrane-diffusion technique. This method utilizes an appropriate dialysis membrane with a specific molecular-weight cut-off (MWCO) to physically separate the released drug molecules from microparticles by allowing the free drug to pass easily through the membrane into the release medium. Drug release is usually assessed with samples taken from the external solution outside the dialysis membrane over time. Liposomal formulation as prepared and 3D printed were placed in a 0.5 mL dialysis cassette Slide-A-Lyzer® 2K (Thermo scientific, USA) with 2000 Da MWCO, and immersed in 40 mL of freshly prepared FaSSGF (Biorelevant, UK) kept under constant magnetic stirring at 37°C. The released amount of

Naproxen from both formulations was determined by UHPLC method (see section 4.1.2.11) with the reported check point: 1h, 2h, 4h, 6h, 24h and 28h.

4.1.2.13. Naproxen quantification in hydrogels and 3D printlets using UHPLC

The quantification of naproxen in hydrogels and 3D printlets was determined using the same equipment and method used for caffeine (see section 3.1.2.5). The data are presented as average ± standard deviation of three experiments.

4.1.2.14. Dissolution test

Dissolution profile of 3D printed formulations compared to commercial capsules size 9 (Torpac®, Fairfield USA) filled with pure naproxen was investigated. The dissolution test was conducted on 3D printed formulations using a USP 27 dissolution apparatus II: Sotax AT 7 Smart (Sotax, Milan, Italy) equipped with basket stirring tool to avoid printlet floating and guarantee the sink condition during the test. The drug release was assessed with Fasted State Simulated Gastric Fluid (FaSSGF, Biorelevant, London, UK) by itself and additioned of a 0.5% w/v of SDS. In each vessel, two printlets were placed into 300 ml of acidic medium with surfactant. Temperature was set to 37 ± 0.5°C and paddle rotation was kept at 75 rpm. During dissolution test, samples of 1 ml were withdrawn at prefixed timepoints, the filtered with 0.2 µm Verex PTFE filters vials (California Phenomenex, Torrance, USA). After every sampling the dissolution medium volume was restored with 1 ml of fresh one, kept at 37°C.

4.1.2.15. X-Ray micro-computed tomography

The micro-CT evaluation of naproxen 3D printed formulations was performed using the same equipment and method employed for caffeine and reported in section 3.1.2.7.

4.1.3. Results

To further investigate and optimize the 3D printing technology of SSE-printed hydrogels, the research was moved to naproxen, selected as model drug for its poor aqueous solubility [91] and classified by Biopharmaceutics Classification System (BCS) as a Class II compound. This intrinsic limitation is particularly challenging in achieving efficient drug loading, uniform distribution, and predictable release profiles within semi-solid extrusion (SSE) formulations. Overcoming low solubility in such systems necessitates innovative strategies in excipient selection and formulation design to enhance dissolution and bioavailability, making naproxen an ideal test case for exploring advanced solubilization and strategies approaches in SSE 3D printed formulations.

4.1.3.1. Cyclodextrins

The initial approach considered was to utilize well-established solubilizing excipients, such as cyclodextrins [7, 92, 93]. The primary objective was to enhance the aqueous solubility of naproxen using cyclodextrins, followed by gelification of the resulting solution with a water-soluble (and preferably erodible) polymer [49], in combination with disintegrants or water-soluble excipients. This strategy aimed to optimize the release kinetics of naproxen during dissolution testing in simulated gastric fluid. Therefore, inclusion tests of the active ingredient in various cyclodextrins (CDs) were conducted (see section 4.1.2.2), investigating Sulfobutyl-Ether-β-Cyclodextrin (SBE-CD), α-cyclodextrin, β-cyclodextrin and γ-cyclodextrin, with the results reported below in Table 30. Both 1 and 2 equivalents of cyclodextrins were explored in ratio with drug, without noticing any improvement in the inclusion levels reached between them.

Table 30. Solubility of naproxen in water reached with the help of cyclodextrins.

Cyclodextrin (CD)	1 eq of CD (mg/ml)	2 eq of CD (mg/ml)
α-cyclodextrin	0.15	0.12
β-cyclodextrin	0.68	n-a
γ-cyclodextrin	0.24	0.20
Sulfobutyl-ether-β-cyclodextrin	12.43	14.58

The data obtained showed the maximum concentration achievable in solution with each of the CD employed. β-cyclodextrin was not moved to 2 equivalents trial. The amount of water

used to solubilize 1 equivalent of β-CD was already excessive to prepare a printable hydrogel. The best CD to be used in this case turned out to be SBE-CD. The solubility of drug in water reached with SBE-CD improved, settled around 13 mg/ml (12.4 mg/ml with 1 equivalent and 14.6 mg/ml with 2 equivalents of CD), with an increase of around 1000 folds respect to starting solubility of pure drug in water [91]. Unfortunately, even the maximum solubility achieved with Sulfobutyl-B-cyclodextrin was quite high, it was not sufficient to reach the target dosage in potential printed forms, since naproxen drug loading within these hydrogels should range around a concentration of 30 mg/ml.
For this reason, the use of CDs to improve naproxen solubility was no further investigated.

4.1.3.2. Lipidic excipients

The next formulative strategy adopted involved the use of lipidic excipients [94, 95]. It was decided to test lipidic excipients due to the lipophilic nature of API studied. The idea was to obtain solubilization of API in the lipid excipient, prepare an emulsion O-W with the lipidic solution, mimicking the work published by Al-Ashawy et al [96] and Johannesson et al [94], and achieve gelification of the entire system. It was performed a quick solubility screening (see section 4.1.2.3 for details) with the goal to obtain solutions at 30mg/ml concentration, target loading of hydrogels as stated before (see section 4.1.3.1). As lipidic excipients capryol 90, capryol PGMC, labrafac lipophile WL 1349, labrasol ALF, maisine CC, plurol oleique CC 497, transcutol HP and Phosal® 50 PG were tested. It was discovered that naproxen is soluble at concentrations of 30mg/ml in capryol 90 and Phosal® 50 PG (at 50°C), while at 15mg/ml with transcutol HP. Since capryol 90 was the best in solubilizing the drug at room temperature, it was decided to start from that one to study how lipidic excipients could work for the scope.
Before starting with the formulation trials to obtain emulsions, since a water insoluble lipidic excipient was selected, a preliminary naproxen release in acidic media in sink conditions was tested, mimicking a potential *in vitro* release test. A solution of naproxen in capryol 90 at 30mg/ml was prepared and 50µl (1.5mg of naproxen, the target dose) were sampled and additioned to 100ml of simulated gastric fluid kept at 37°C and under magnetic stirring. Right after the addition of the lipidic solution, no dispersion of the lipidic part and no precipitation of naproxen were observed. The hydrophobic drug was retained in capryol 90, without being released to the aqueous part. This behaviour brought to discard capryol 90 as a lipidic excipient. It was then decided to move towards Phosal® 50 PG and once again explored its incorporation ability in water, discovering that is still not soluble but homogeneously

scattered, giving a fine suspension. For that reason, a naproxen solution in Phosal® 50 PG was prepared, in order to progressively obtain O-W emulsion. Acidic water was prepared by dissolving 1% w-v citric acid in 2 mL of hot water (80°C), in anticipation of the chemical cross-linking of HPMC for hydrogel formation from the emulsion. Then, 1ml of Phosal® 50 PG solution (30mg/ml) with the naproxen was continuously added to the hot water under high-speed homogenization with IKA T10 basic Ultra-turrax®. Once the lipidic solution was fully mixed into water, Ultra-turrax® was removed, adding HPMC K4 at 10% w/v (relative to water), and completely dispersing it before turning off the heat to allow formulation gelification. The obtained formulation resulted in having an apparent viscosity suitable for the printing process and was left at 5°C overnight before moving it to extrusion trials. Its complete composition is reported in Table 31.

Table 31. Naproxen semi solid formulation composition obtained with Phosal® 50 PG.

Formulation	Phosal® 50 PG (ml)	Naproxen (mg)	Citric acid (mg)	HPMC K4 (mg)	H2O (ml)
LN-1	1	30	20	200	2

Extrusion trial with LN-1 emulsion was carried out loading the hydrogel into 1ml syringe equipped with 3D printer's nozzle (22G) and manually extruding it on a microscope's glass slide. The extruded material obtained was left to dry overnight at ambient conditions before evaluating it. The dried deposited formulation resulted maintaining its shape and crossed areas and was subsequently moved to printing trial to evaluate its behavior during a complete printing process. After loading the hydrogel into the printing cartridge, a centrifugation step of 15 minutes at 3000 rpm was carried out to remove eventual air bubbles trapped in the polymeric network. After centrifugation step, the formulation was moved to printability assessment. A complete printing process was carried out with the parameters reported in Table 32.

Table 32. Printing parameters employed for formulation LN-1.

Formulation	Extrusion pressure (kPa)	Printing speed (mm-s)	Printing temperature (°C)	Layer height (mm)	Preflow (ms)	Postflow (ms)
LN-1	183	1	-	0.4	-200	200

Since after extrusion trials the filament obtained from LN-1 resulted not completely dried after overnight resting at ambient conditions, freeze drying of the final 3D printed form was carried out, after pe-freezing the printlet at -80°C. After 3 days at 0.5 mpas the printlet was taken out from the freeze-dryer and resulted still not completely dried. The obtained formulation was analyzed by XRD, showing the presence of recrystallized naproxen, as showed in Figure 53.

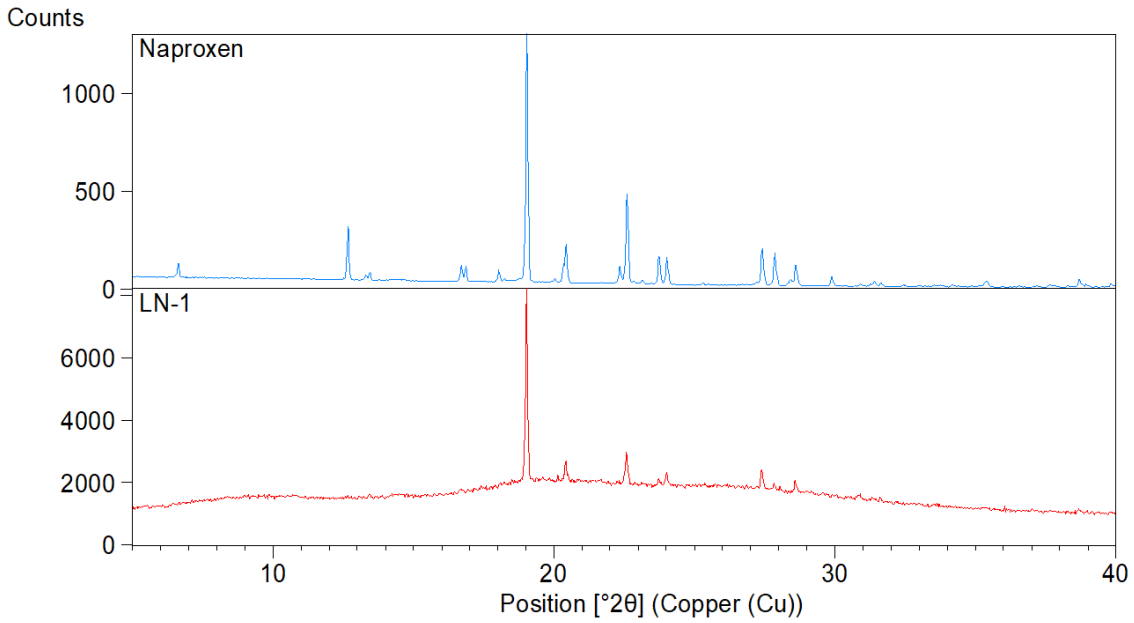

Figure 53. XRPD analysis of LN-1 after freeze drying compared with naproxen standard. Samples acquired in transmission mode.

After this result also Phosal® 50 PG formulation was discarded and moved on with other lipidic excipients.

Other lipidic excipients tested were considered not suitable due to their low solubilizing activity with naproxen. Only Transcutol HP could have been taken into consideration but, in addition to its low solubilizing activity towards the naproxen, reaching only 15mg/ml like with SBE-CD, it is water soluble and therefore not able to form emulsions O-W. The solubilizing properties of Transcutol HP may be useful in developing alternative formulations. However, studies by Tiong et al [90] and Alskar et al [97] indicate that the selected API can achieve higher concentrations when dissolved with other solubility enhancers. Consequently, Transcutol HP was not selected for further use.

Due to these last results, lipidic excipients as vehicles to obtain O-W emulsions were discarded, focusing on other types of formulations.

4.1.3.3. Liposomes preparation

The primary focus of this part of work was to enhance the release kinetics of BCS Class II drugs through formulations produced via 3D printing technologies. Due to the high hydrophobicity of the selected active compound, liposomal formulations were investigated as an enabling strategy to improve its solubility and maintain the drug in solution. Although liposomes were expected to inherently provide a sustained release profile [7], they were incorporated into a three-dimensional printed matrix to explore whether additive manufacturing could modulate the release behavior. Specifically, this approach aimed to determine whether the structural and compositional features introduced by 3D printing could counterbalance the naturally sustained release of liposomes and ultimately promote a faster release of the active compound.

Naproxen-liposome formulation was prepared using TLE method followed by extrusion. The preparation method details are reported in section 4.1.2.4. The characteristics of the liposomal suspension are strongly influenced by the conditions applied during and after their preparation. Prior to extrusion, liposomes typically display a polydisperse size distribution; nevertheless, the quality of the thin lipid film is highly dependent on the duration of the rotary evaporation step. An extended and well-controlled evaporation generally promotes the formation of a more homogeneous film, which in turn favors the generation of vesicles with narrower size distribution. In addition, parameters applied during the hydration step, such as mixing speed and temperature, critically affect vesicle formation, bilayer organization, and ultimately encapsulation efficiency. Careful monitoring and optimization of these variables are therefore essential to obtain liposomes with reproducible physicochemical properties and improved stability [89].

The liposomes obtained were extruded to obtain acceptable liposome particle size populations. Images acquired with polarized light optical microscopy were taken to observe the correct formation of liposomes and the encapsulation of API, therefore indicated by the absence of recrystallized naproxen in the surrounding water environment. The pictures obtained are reported in Figure 54 below. The prepared liposomal formulation, renamed LN-2, was stored at 5°C before analytical characterization.

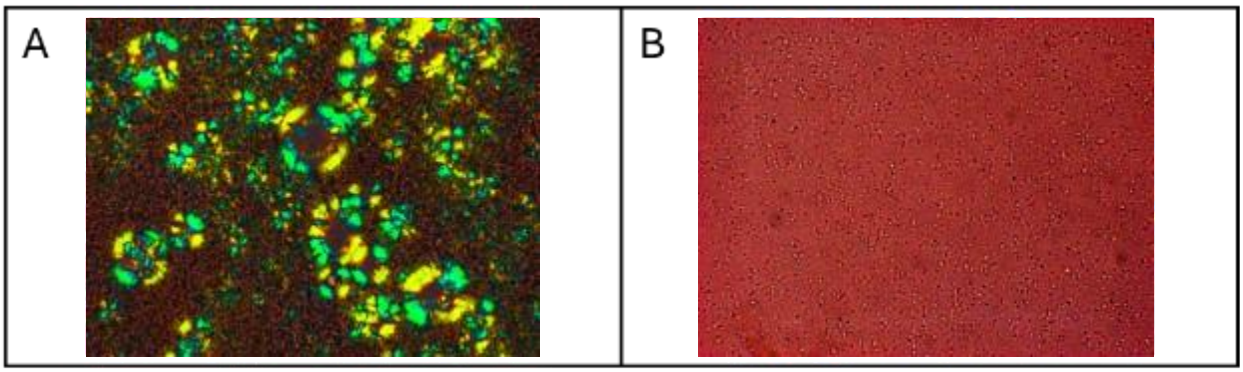

Figure 54. LN-2 formulation observed with polarized light microscopy. (A) Before extrusion, 50x magnification. (B) After extrusion, 50x magnification.

4.1.3.4. Liposomes characterization

Liposomal formulation with naproxen was characterized following methodologies reported in section 4.1.2.9. To evaluate the physicochemical properties of the naproxen-loaded liposomal formulation, DLS and ζ-potential analyses were performed. These measurements provide essential information on vesicle size, size distribution and surface charge, which are key parameters influencing the stability, reproducibility and performance of liposomal systems. In particular, the mean hydrodynamic diameter, PDI and ζ-potential were determined through a Zetasizer Nano ZS and the results are summarized in Table 33.

Table 33. LN-2 analytical characterization results after extrusion at 800 nm.

Formulation	Particle size (nm)	PDI	ζ-potential (mV)
LN-2	~ 1000	0.5	~ 0

The characterization of naproxen-loaded liposomes showed a mean particle size of approximately 1 μm, a PDI of 0.5, and a ζ-potential close to zero. The neutral ζ-potential is consistent with the lipid composition, as the absence of charged components prevents the development of a significant surface charge. The relatively broad size distribution indicated by the PDI suggests some degree of heterogeneity in the vesicle population. Overall, although there remains room for optimization in terms of size uniformity and potential improvements in stability, the observed physicochemical properties are in line with the expected behavior for this type of liposomal system and can be considered suitable for preliminary formulation studies.

4.1.3.5. Drug content and encapsulation efficiency

The analytical characterization of the naproxen-loaded liposomes was performed to determine both the drug content and the encapsulation efficiency (%EE). Encapsulation efficiency is the percentage of a total amount of drug successfully trapped within the liposomal structure. It is a critical parameter for evaluating the quality of the formulation and directly reflects the concentration of active ingredients available for delivery. In addition, these parameters are crucial to assess the actual amount of naproxen incorporated into the vesicles and to evaluate the performance of the formulation in terms of drug loading capacity. The analysis was performed following the method reported in section 4.1.2.11 and the obtained results are discussed below.

Table 34. LN-2 drug content and encapsulation efficiency analytical results.

LN-2 drug content (mg/ml)	Centrifugated pellet drug content (mg/ml)	Encapsulation Efficiency (%)
15	14	93

The %EE was determined following a centrifugation step, which separated the free drug from the liposome-encapsulated fraction. The total naproxen content in the formulation was found to be 15 mg/mL, and the fraction of drug successfully encapsulated within the vesicles reached 93% confirming the high loading capacity of the liposomal system and demonstrating the effectiveness of the formulation procedure.

4.1.3.6. Liposomal hydrogels formulation

Following the preparation of naproxen-loaded liposomes, various formulations were investigated by carefully adding swelling polymers to formulation LN-2 at room temperature. This approach aimed to attain an apparent viscosity appropriate for the 3D printing extrusion process. The performed liposomal hydrogel formulation trials are reported in Table 35 below.

Table 35. Composition of liposomal hydrogel formulations performed starting from LN-2.

Trial	LN-2 (ml)	PBS (ml)	H2O (ml)	Gelatine (mg)	SA (mg)	HPMC E5 (mg)
LN-2-1	0.2	0.8	-	-	100	-
LN-2-2	0.4	0.6	-	100	-	-
LN-2-3	0.4	0.6	-	100	50	-
LN-2-4	0.4	0.6	-	150	50	-
LN-2-5	0.4	-	0.6	100	-	200
LN-2-6	0.4	-	0.6	100	50	50
LN-2-7	0.4	0.6	-	200	-	-
LN-2-8	0.4	0.6	-	200	50	-

To obtain the liposomal hydrogels described in Table 35, an amount of LN-2 was diluted with PBS or water, because of the high concentration and the too small amount of liquid environment available to enable the gelification process. Then, the proper amount of excipients was added to the liposome diluted formulation and left to hydrate under gently magnetic stirring at room temperature overnight. The first trial was LN-2-1, where sodium alginate was employed alone as gel former. The obtained hydrogel resulted to be too liquid and could not maintain the extruded filament morphology. The same behavior was observed with LN-2-2 and LN-2-3. LN-2-4 exhibited viscosity and retained its morphology after being left to dry overnight, maintaining the deposited structure after complete drying. This allowed it to be suitable for the full printing process. The application of HPMC E5 as main polymer in LN-2-5 or as adjuvant in LN-2-6 was investigated. The first hydrogel was too viscous for extrusion, while the second had appropriate viscosity and maintained its shape after drying overnight. The formulation was then moved to the 3D printing process, together with LN-2-4. The other hydrogels prepared (LN-2-7 and LN-2-8) proved to be suitable as well for printing process but the filaments obtained from extrusion trials were less uniform than the one from LN-2-4, probably due to the higher amount of gelatine loaded. For that reason, they were not further moved to 3D printing process and discarded.

From manual extrusion trials only two liposomal hydrogels were selected for a complete 3D printing process, LN-2-4 and LN-2-6. The printing process was carried out employing the printing parameters reported in Table 36 below and according to the CAD model prepared in advance and showed in Figure 55-C.

Table 36. Printing parameters employed for liposomal formulations LN-2-4 and LN-2-6.

Formulation	Extrusion pressure (kPa)	Printing speed (mm-s)	Printing temperature (°C)	Layer height (mm)	Preflow (ms)	Postflow (ms)
LN-2-4	65	1	-	0.4	-100	200
LN-2-6	40	1	-	0.4	-100	200

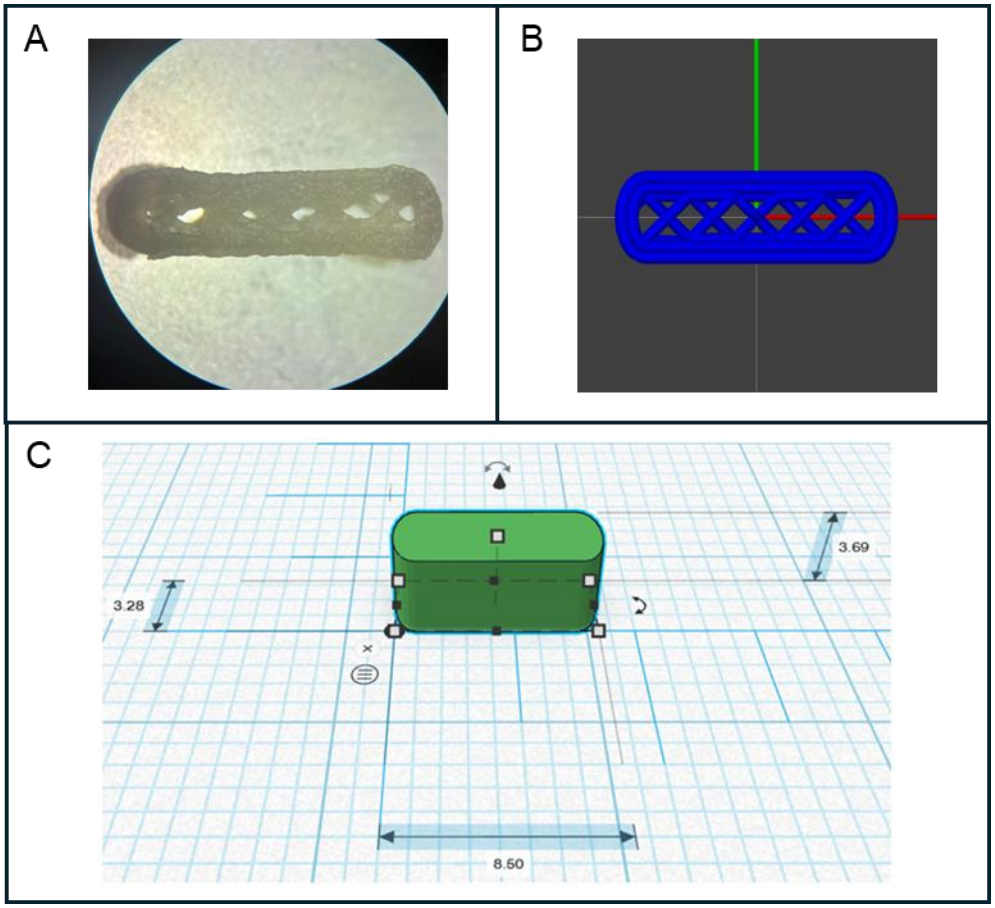

Figure 55. (A) Optical microscopy image of printed LN-2-4 formulation, (B) virtual model employed to print LN-2-4 formulation with 30% infill, (C) CAD model prepared to print naproxen liposomal formulations.

The CAD model was prepared on the base of matrixial formulations; however, to speed up the drug release, the design did not consist of full infill. Before starting the 3D printing process, a new slicing process was designed, intentionally generating empty areas within the dried printlet. The virtual model employed is reported in Figure 55-B and is characterized by a 30% infill density with alternate rectilinear infill pattern. This approach aimed to increase

the exposed surface area, thereby potentially enhancing the dissolution rate in the chosen medium [98, 99]. Formulation LN-2-6 was successfully printed following the same virtual model with 30% infill density. Both the printed formulations were left to dry overnight at standard laboratory conditions before collection. After a visual observation of the obtained printed forms, formulation LN-2-4 was selected to be further analysed with *in vitro* release test. An image of printed LN-2-4, taken with optical microscopy (2x magnification) is reported in Figure 55-A.

4.1.3.7. Release test from liposomes

After performing analytical characterization shown above (see sections 4.1.3.4 and 4.1.3.5), the liposomal formulation underwent gelification and 3D printing process, obtaining LN-2-4 (see section 4.1.3.6). The selected printlets were investigated in terms of drug release, together with LN-2 starting formulation. Methodology employed is reported in section 4.1.2.12 and the obtained release curves are shown in Figure 56 below.

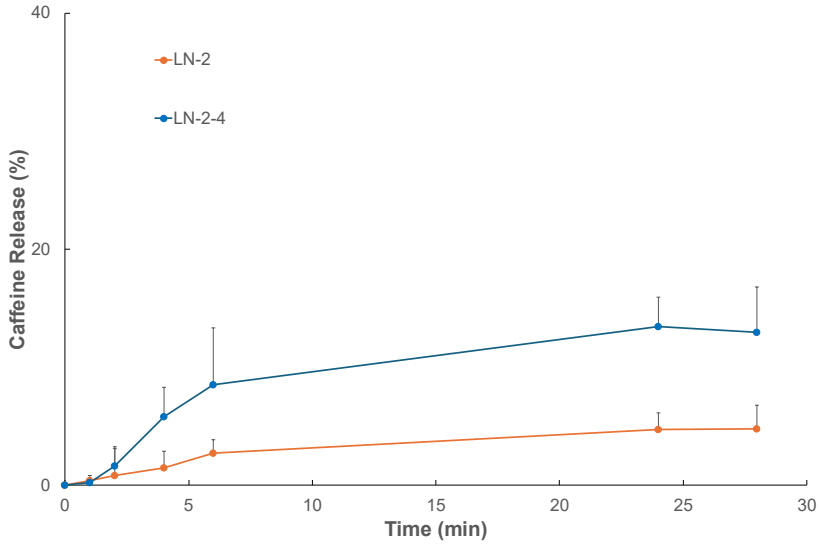

Figure 56. Release curves obtained from release test with LN-2 and LN-2-4 formulations.

The curves report the release profiles of both the liposomal formulation and the corresponding 3D printed system, including standard deviations derived from three independent replicates for each formulation. The release profiles indicated a slow and limited drug release for both systems, over the 28-hour testing period. Although the 3D printed solid form exhibited a slight increase in the release rate of naproxen, the difference

between the two profiles was not considered significant, with both dosage forms ultimately reaching a comparable cumulative drug release of approximately 10%. These results suggest that, in the current formulations, the release kinetics are predominantly governed by the liposomal component rather than by the structural features introduced through additive manufacturing. Nonetheless, this does not exclude the possibility that further optimization of the gel composition or printing and slicing parameters could lead to improved release profiles in future studies. However, this outcome indicates that the 3D printing process did not compromise the physicochemical integrity of the liposomes, which retained their ability to control drug release in a comparable manner to the original suspension. This result is particularly relevant, as several factors associated with the printing process (such as mechanical stress during extrusion or incorporation into a dense polymeric matrix) could potentially compromise liposome structural integrity and functionality. Nevertheless, the release profile demonstrates that these parameters did not negatively affect the system, confirming that the liposomal carriers maintained their characteristics even after processing. Moreover, the data clearly indicates that the 3D-printed formulation does not further slow-down the release of naproxen. This suggests that the dense polymeric matrix surrounding the liposomes does not act as an additional diffusion barrier for the drug. Instead, the release kinetics remain dictated by the intrinsic properties of the liposomal carriers, which regulate drug retention and diffusion through their bilayer structure. In other words, in this case the solid form functions primarily as a structural support for the formulation, without significantly interfering with or modifying the release behavior. This finding reinforces the idea that the liposomal system itself is the main determinant of drug release, even after being embedded within a solid dosage form.

These findings highlight the capacity of liposomes to effectively retain naproxen within their structure, preventing its interaction with the surrounding hydrogel both before and after 3D printing. However, the current hydrogel composition did not support an immediate release, indicating that further optimization is required to improve the release rate. It is worth noting that the preservation of liposomal functionality after integration into a solid dosage form highlights the potential of 3D printing as an innovative pharmaceutical technology, enabling the development of tailored drug delivery systems while maintaining the structural integrity of sensitive carriers such as liposomes.

It should be emphasized, however, that these findings are limited to the *in vitro* conditions of the present study; *in vivo* investigations will be necessary to determine whether the additional excipients used in the 3D-printed solid dosage form provide a real advantage in

terms of drug release, or whether enzymatic activity in the biological environment will simply promote the degradation of the matrix [100]. The reduced *in vitro* release rate from these liposomal formulations makes them unsuitable for the purpose of this project, highlighting the need to move towards other types of formulations. Nevertheless, further confirmation through *in vivo* release tests could prove that this system could be satisfactory, since the enzymatic and physiological components of the gastric environment can play a crucial role in the release kinetics of drugs from lipid-based formulations. The presence of enzymes like lipases is particularly important, as they significantly contribute to the metabolism and digestion of the phospholipids that make up the outer layer of liposomal micelles [101].

4.1.3.8. Liquisolid formulations

In the investigation of new formulations appropriate for the project, the requirement to achieve solubilization of the naproxen before gelification was omitted. Based on the approach by Tiong et al. [90], an increased release rate under simulated gastric conditions could be achieved by utilizing non-volatile liquid vehicles, which enhance wetting properties of API and expand the surface area available for drug particle dissolution. To adapt liquisolid formulations to 3D printing, the same formulation composition was replicated up to but not including the compression stage. In this method, polymers and water would be added to the powdered formulation producing an hydrogel suitable for 3D printing, as described in section 4.1.2.5. Since in the work already performed by Tiong et al. the naproxen solubility was assessed in different non-volatile liquid vehicles [90], it was decided to base the following formulation trials on the employment of Kolliphor® EL as wetting agent.

The formulation trials started preparing liquisolid formulations with some changes in the composition. Firstly, naproxen was incorporated in Kolliphor® EL with mortar and pestle, then cellulose microcrystalline (Vivapur®102) was slowly added with the same mixing technique. Then, HPMC E5 was added as gelling agent and Kollidon® CL as disgregant, still aiming for a fast release formulation. In the end the powdered mass was slowly added to 1ml of hot water (85°C) under high-speed magnetic stirring, until an homogeneous paste was obtained. The amount and composition of this formulation (called TN1) was reported in Table 37.

Table 37. TN1 liquisolid formulation composition, prepared loading 30mg of naproxen.

Formulation	Kolliphor® EL (mg)	Vivapur 102 (mg)	Kollidon® CL (mg)	HPMC E5 (mg)	H2O 85°C (ml)
TN-1	100	400	30	50	1

TN-1 prepared formulation was left at rest overnight at ambient conditions, to let HPMC hydrate and stabilize polymeric network. Then, the paste was centrifugated at 4000rpm for 30 minutes and loaded into an empty cartridge with 22G plastic nozzle, to perform an extrusion trial with the 3D printer. The paste turned out to be too viscous and no extrusion was obtained, even employing the highest pressure available (195 kPa). The formulation turned out to be very dense and hydrogel from HPMC E5 could not be obtained. For that reason, formulation TN-1 was discarded. Then, some modifications were applied to TN-1 to obtain a new set of formulations. The new formulations composition is reported in Table 38 below.

Table 38. New naproxen liquisolid formulations composition. All formulations were prepared with 1ml of water at 85°C and 30mg of naproxen.

Formulation	Kolliphor® EL (mg)	Vivapur 102 (mg)	Kollidon® CL (mg)	HPMC E5 (mg)	NaCMC (mg)	Citric acid (mg)
TN-2	100	400	30	100	-	-
TN-3	100	400	30	-	100	10
TN-4	100	400	30	-	50	5

With TN-2 the amount of HPMC E5 was doubled respect to TN-1, trying to improve the kneading effect of hydrogel. Within formulations TN-3 and TN-4, NaCMC was employed as swelling polymer, in a ratio 10:1 with citric acid, as previously experienced with caffeine (see section 3.1.3.1). Taking into consideration the dissolution results obtained with caffeine matrixial formulations (see section 3.1.3.3), NaCMC was chosen as possible useful cellulosic swellable polymer to reach the desired fast release in combination with naproxen, surfactant and disintegrants. The same concentrations as HPMC E5 (TN-1 and TN-2) were examined, to obtain a comparison between the two cellulosic excipients in terms of gelling and release ability. The formulations were prepared employing pestle and mortar as previously explained for formulation TN-1. After preparation and incorporation into water, they are left at standard laboratory conditions overnight. Then, formulations were

centrifugated at 4000 rpm for 30 minutes and loaded into printhead cartridges to attempt material extrusion and eventually subsequent printing. Formulation TN-2 resulted in not being homogeneous and solid and liquid phases were separated. Similar behavior was observed with TN-4 formulation, where the paste resulted to have low viscosity and the extruded morphology was not maintained during drying process. TN-3 proved to be the only one extrudable and was moved to 3D printing trial with the parameters reported below in Table 39.

Table 39. Printing parameters employed with formulation TN-3.

Formulation	Extrusion Pressure (kPa)	Printing Speed (mm-s)	Printing Temperature (°C)	Layer height (mm)	Preflow (ms)	Postflow (ms)
TN-3	40	1	-	0.4	-200	200

3D printing process was not carried out successfully since frequent nozzle occlusion was experienced, interrupting the printing process quite often. Looking at the occluded nozzle with optical microscopy, some aggregates were observed, probably cellulose microcrystalline or disintegrant not well dispersed. For that reason, formulation TN-3 was no further investigated too, and new formulations were prepared, replacing Vivapur 102 with Avicel ph-101, due to its smaller particle size and shape. The composition of the new set of formulations is reported in Table 40.

Table 40. New naproxen liquisolid formulations composition. All formulations were prepared with 1ml of water at 85°C and 30mg of naproxen.

Formulation	Kolliphor® EL (mg)	Avicel ph-101 (mg)	K-CL (mg)	Mannitol (mg)	SiO_2 (mg)	NaCMC (mg)	CA (mg)
TN-5	100	400	30	-	20	100	10
TN-6	100	400	-	50	20	100	10
TN-7 (GN1)	100	400	30	-	20	150	15

Within the new set of formulations, as mentioned before, Avicel ph-101 was employed as a cellulosic carrier, instead of Vivapur 102, evaluating a smaller type of MCC. Moreover, silicon dioxide was added in this new set of formulations, as filling agent and disintegrant. The formulations were prepared with mortar and pestle, starting from a suspension of naproxen

and Kolliphor® EL. With TN-5 only the effects of smaller MCC and addition of silica were investigated, maintaining NaCMC at 10% w-v respect to water, in a ratio 10:1 with citric acid. TN-6 was prepared replacing Kollidon® CL with mannitol as pore former, evaluating its ability to speed up the eventual printed formulation dissolution. At last, with TN-7 mannitol was abandoned, returning to utilize Kollidon® CL as disintegrant but increasing NaCMC concentration up to 15% w/v respect to water, still maintaining ratio 10:1 with citric acid. The formulations prepared were left overnight at ambient conditions at rest and the subsequent day were loaded into printhead cartridges and centrifugated at 4000rpm for 30 minutes. Then, extrusion trials were carried out, discovering that all of them were extrudable and suitable for printing trials. They were moved to 3D printing trial, following parameters reported in Table 41.

Table 41. Printing parameters employed with formulations TN-5-7

Formulation	Extrusion Pressure (kPa)	Printing Speed (mm-s)	Printing Temperature (°C)	Layer height (mm)	Preflow (ms)	Postflow (ms)
TN-5	50	1	-	0.4	-100	100
TN-6	45	1	-	0.4	-100	100
TN-7 (GN1)	70	1	-	0.4	-100	100

TN-7 turned out to be the only formulation printable with satisfying results. The extruded material morphology was well retained, layer to bed and layer to layer adhesion was efficient. Pressure required to extrude the material was low and the flow of material was constant, without observing occlusions. On the other hand, TN-5 and TN-6 resulted to be printable without occlusions like TN-7, but an excessive swell of deposited formulation was observed during the printing, yielding to defects in the final printed forms. Probably, at least 15% w/v concentration of NaCMC is required to obtain a satisfactory complete printing process. Formulation TN-7 was then renamed GN1 and moved to release studies into acidic media. Together with formulation GN1, a new liquisolid formulation was prepared (TN-8) adding mannitol, to further study it pore forming ability within fast releasing formulations. The new prepared and printed formulation was renamed GN2 and its composition and printing parameters are reported in Table 42 and Table 43, respectively.

Table 42. TN-8 liquisolid formulation composition. The formulation was prepared with 1ml of water at 85°C and 30mg of naproxen.

Formulation	Kolliphor® EL (mg)	Avicel ph-101 (mg)	K-CL (mg)	Mannitol (mg)	SiO_2 (mg)	NaCMC (mg)	CA (mg)
TN-8 (GN2)	100	400	30	50	20	150	15

Table 43. Printing parameters employed with formulation TN-8.

Formulation	Extrusion Pressure (kPa)	Printing Speed (mm-s)	Printing Temperature (°C)	Layer height (mm)	Preflow (ms)	Postflow (ms)
TN-8 (GN2)	90	1	-	0,4	-200	100

The two liquisolid formulations were printed following the same CAD model reported in Figure 55-C, but infill density and pattern were not generated by the printer proprietary software. An appropriate g-code was prepared in advance with free software PrusaSlicer (version 2.9.2), embedding a 30% rectilinear infill. The obtained virtual model of prepared g-code together with the printed formulations GN1 and GN2, are shown in Figure 57.

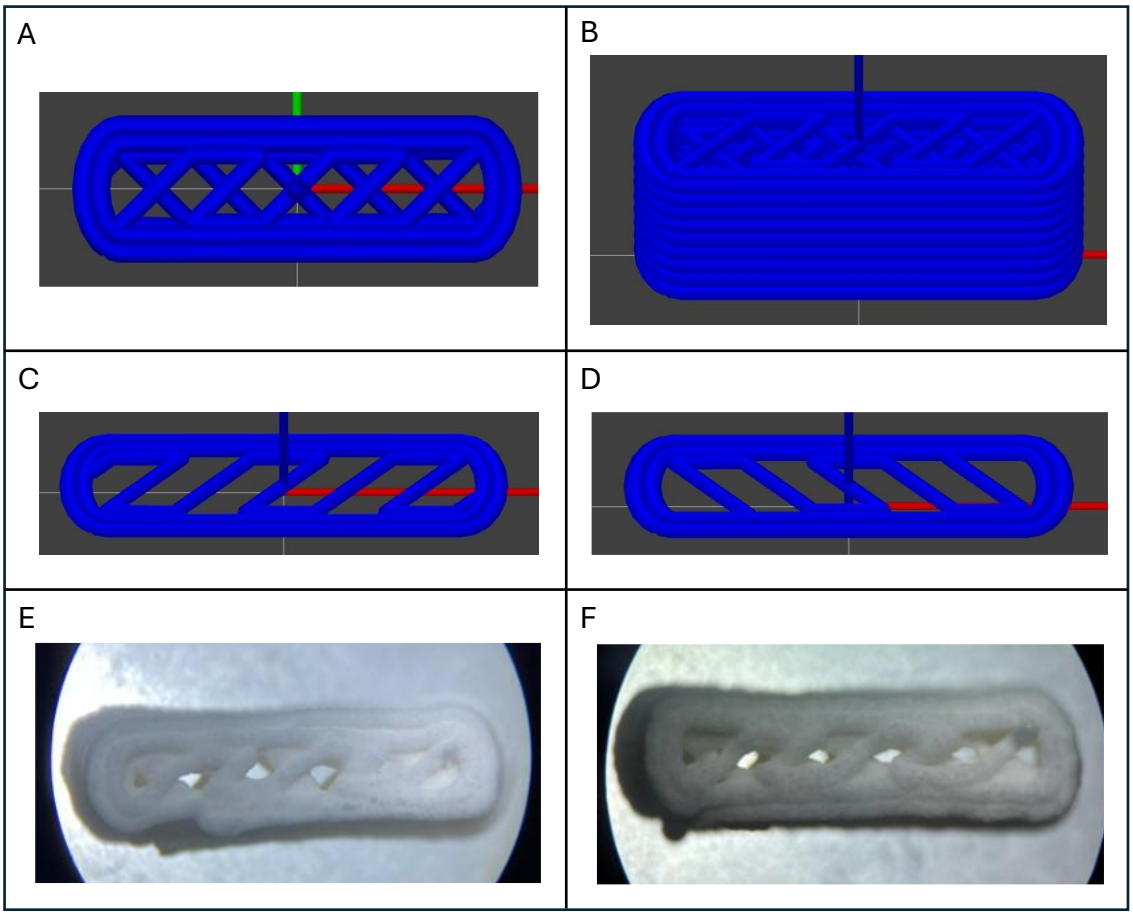

Figure 57. Virtual model employed for GN1 and GN2 printing with 30% infill density and rectilinear pattern: (A) top view, (B) side view, (C) side view of first layer, (D) side view of second layer. GN1 (E) and GN2 (F) printed formulations, images taken with optical microscopy at 4x magnification.

Printed formulations GN1 and GN2 were then analyzed in terms of drug content (and content uniformity) and preliminary dissolution profile following methodologies reported in sections 4.1.2.13 and 4.1.2.14, respectively. Obtained results are reported in Table 44 and Figure 58.

Table 44. Naproxen quantification and content uniformity analysis performed on printed liquisolid formulations (mean value ± deviation standard, n = 3).

Formulation	Drug content (mg-cpr)
GN1	1.73 ± 0.13
GN2	1.84 ± 0.02

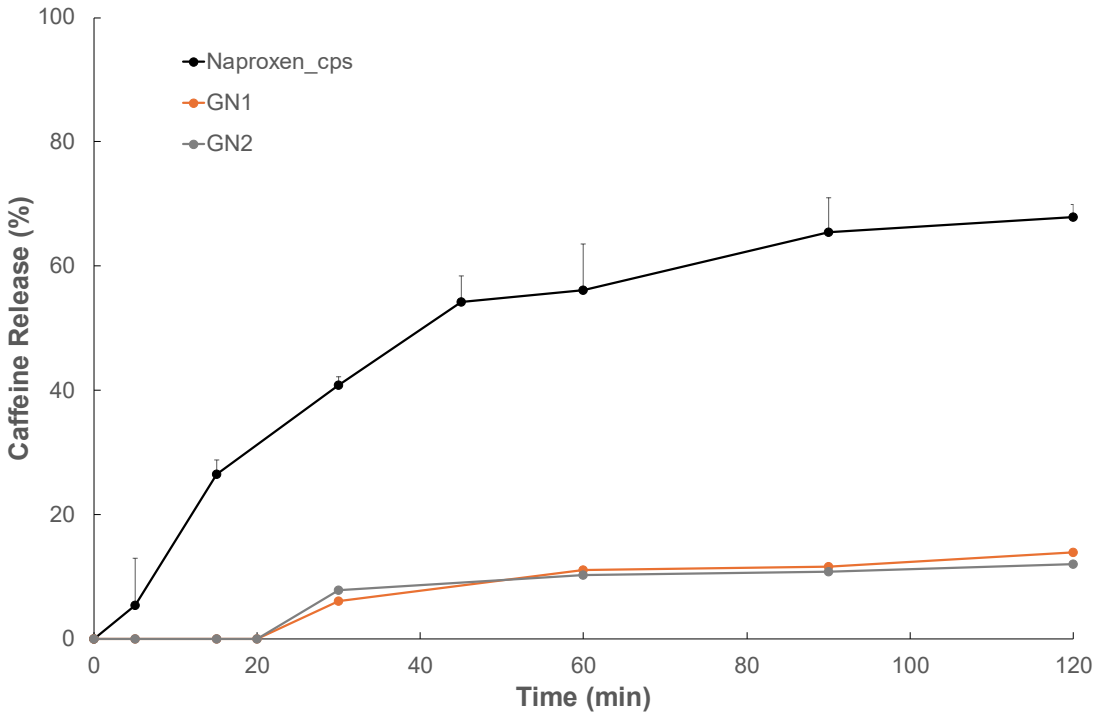

Figure 58. Dissolution curves in FaSSGF media obtained in house with liquisolid formulations GN1 (orange) and GN2 (grey), compared with naproxen std in Torpac® capsules (light blue).

In terms of drug loading and content uniformity, the 3D printed liquisolid formulations resulted in having a slightly high amount of loaded naproxen (target dose of 1.65 mg-printlet for eventual administration in rodents) and an acceptable SD for preclinical purposes (below 10%). On the other hand, looking at dissolution test, the printed forms showed a much slower release rate, compared to standard capsules size 9 filled with pure naproxen. Standard capsules managed to achieve 27% of drug release within the first 15 minutes, reaching a 41% at 30 minutes timepoint. The printed formulations instead, at 15 minutes were still intact, without releasing anything and reached only a 6% (GN1) and 8% (GN2) release after 30 minutes from the beginning of the test. These data are far away from the definition of "immediate release" (*i.e.* 75% of the active substance dissolved *in vitro* within 45 minutes, Ph. Eur. 5.17.1 [2]) and by that, the formulations needed to be deeply modified. Since the analyzed printlets remained intact at the end of the dissolution test, the initial approach was to modify the formulations composition in order to achieve a disintegrating system.

First, an evaluation of the gel-forming polymer was performed, to understand if NaCMC could be the best option to achieve the fast release. Hydrogels of NaCMC 20% w/v, HPMC E5 40% w/v and HPC-SL 50% w/v in water were prepared and a predefined amount was

manually extruded and dried on a microscope glass plate. The polymer selection was based on their fast-dissolving characteristics [52, 102,103]. The concentrations tested were derived from retaining morphology visual observation after manual extrusion of hydrogels with increasing concentrations. Each of the dried extruded materials was then dropped in 100ml of freshly prepared FaSSGF, kept at 37°C under magnetic stirring and their dissolution time was visually observed. The initial test revealed that HPMC E5 and HPC-SL dissolved more rapidly than NaCMC when exposed to simulated acidic media. From that, the inclusion of disintegrating agents was investigated. Kollidon® CL, Ac-Di-Sol® and PEG 6000 were selected as dissolution enhancer excipients [104-108].

The Inclusion test began with each of the disintegrants loaded into each hydrogel at a concentration of 10% w/v of water, during hydrogel preparation, following the procedure reported in section 3.1.2.1. HPMC E5 turned out to be suitable for inclusion of all the disintegrants tested (one at a time), maintaining a good filament morphology after extrusion and during drying process at ambient conditions. On the other hand, HPC-SL showed poor morphology retaining properties, with all the excipient composition tested and by that, was discarded as fast dissolving polymer. By that, a set of formulations was prepared, with HPMC E5 as gelling agent and different ratio and composition of disintegrants. The formulations composition is reported in Table 45.

Table 45. HPMC E5 based formulations composition. The formulations were all prepared with 1ml of water at 85°C, $CaCl_2$ in ratio 1:10 with HPMC and 30mg of naproxen.

Formulation	Kolliphor® EL (mg)	SDS (mg)	Ac-Di-Sol® (mg)	PEG 6K (mg)	K-CL (mg)	PVP (mg)	HPMC E5 (mg)
E1	-	-	200	-	-	-	400
E2	-	-	100	100	-	-	400
E3	-	-	100	-	100	-	400
E4	-	-	100	100	100	-	400
E5	-	-	300	-	-	100	400
E6	100	-	100	-	100	-	400
E7 (CN1)	100	-	100	100	100	-	400
E8	100	-	200	100	-	-	400
E9 (CN2)	100	-	150	-	150	50	300
E10 (CN3)	100	-	100	100	-	-	400
E11 (CN4)	-	10	100	100	-	-	400
E12	-	10	200	100	-	-	400
E13	-	10	150	-	150	50	300

For each formulation prepared, a manual extrusion test was conducted on a defined quantity of hydrogel (100µl) to assess both the smoothness and the ability of the extruded filaments to maintain their shape. With formulations E1-E5 only disintegrants were added to hydrogels, adapting type and amount but maintaining Ac-Di-Sol® always present. From formulation E6 up to E10 Kolliphor® EL was added to hydrogels, adapting liquisolid formulations from the work performed by Tiong et al. [90]. Within formulations E11-E13 the impact of SDS as surfactant was examined, adapting the work performed by García-Herrero et al. [109]. The first formulation attempted envisaged the employment of Ac-Di-Sol® alone in a ratio of 1:2 with HPMC. The resulting hydrogel was extrudable and maintained the extruded morphology also during ambient conditions overnight drying. The same behavior was observed with E2, where the impact of PEG as pore former and API solubility enhancer was examined [107]. On the other hand, E3 showed to be less dense than E1 and E2 and looking at extruded filaments with optical microscopy were clearly visible few agglomerates within the gelified network, probably Kollidon® CL not well dispersed. Same results were obtained with formulation E4, where all the disintegrants tested were added to the same HPMC hydrogel, but not homogeneously mixed. For these reasons, formulations E3 and E4

were discarded. Then, adapting the work performed by Suárez-González et al [105]. interaction between Ac-Di-Sol® and PVP in a ratio of 3:1 was investigated. The resulting hydrogel showed to be very dense and maintained the extruded morphology after overnight drying at ambient conditions. These first 5 formulations were taken as references and replicated (in few cases with minor modifications) with the inclusion of 100mg of Kolliphor® EL as surfactant and dissolution enhancer [90]. The discarded formulations E3 and E4 were replicated with the addition of surfactant, to investigate if the disintegrants could be better disperse obtaining an homogeneous hydrogel (E6 and E7 respectively). The resulting formulations turned out to be easily extrudable, retaining the deposited morphology after overnight ambient conditions drying. Formulation E2 was reproduced with the same composition, giving formulation E10 which showed the same extrudability and morphology retaining characteristics of its predecessor. On the other hand, formulation E1 was not maintained, adding 100mg of PEG 6K other than Kolliphor® EL, to give hydrogel E8, which maintained the good characteristics shown by previous formulation. Formulation E9 is the most changed formulation. The intention was to adapt formulation E5 but, since the material obtained resulted to be very dense and viscous, the new formulation composition was modified, reducing the amount of Ac-Di-Sol®. The ratio with PVP was maintained at 3:1 but Kollidon® CL was added in equal amount of croscarmellose sodium. To avoid excessive viscosity also the amount of HPMC E5 was reduced to 300mg, maintaining the ratio of 10:1 with $CaCl_2$. Moving on, the effect of another surfactant, SDS, employed together with HPMC E5 was investigated [109]. Formulations E8, E9 and E10 were reproduced substituting Kolliphor® EL with 10mg of SDS, giving formulations E11, E12 and E13. Formulation E11 resulted to be easily extrudable, and the material deposited maintained the shape also after overnight drying at ambient conditions. On the other hand, E12 and E13 turned out to be not extrudable, observing nozzle occlusions during the trials. For that reason, the last two formulations obtained were discarded.

From all the new liquisolid formulations prepared, only four were selected to move towards dissolution studies. Formulations E7, E9, E10 and E11 were selected as the most interesting-promising and moved to a complete 3D printing process. The formulations were renamed respectively from CN1 to CN4 and printed with the parameters reported in Table 46.

Table 46. Printing parameters employed with formulations CN-1-4.

Formulation	Extrusion Pressure (kPa)	Printing Speed (mm-s)	Printing Temperature (°C)	Layer height (mm)	Preflow (ms)	Postflow (ms)
CN1	60	1	-	0,4	-200	200
CN2	120	1	-	0,4	-100	200
CN3	50	1	-	0,4	-100	100
CN4	80	1	-	0,4	-100	100

The 3D printing process was carried out following the g-code prepared in advance and showed in Figure 57, leaving 30% infill to obtain holes in the printed forms. The resulting printlets were left to dry overnight at ambient conditions and then moved to content evaluation and dissolution studies.

4.1.3.9. Drug content on new liquisolid formulations

3D printed formulations were analyzed in terms of drug quantification and content uniformity following the methodology reported in section 4.1.2.13. The results obtained are reported in Table 47 below.

Table 47. Naproxen quantification and content uniformity analysis performed on printed liquisolid formulations (mean value ± deviation standard, n = 3).

Formulation	Drug content (mg/cpr)
CN1	1.33 ± 0.05
CN2	1.31 ± 0.07
CN3	1.58 ± 0.09
CN4	1.56 ± 0.17

Formulations CN1 and CN2 are completely in line both in terms of drug quantification and content uniformity. The printed forms resulted to be homogeneous with a low SD. The content is slightly lower than the target one, achieving 1.33 and 1.31 mg-printlet instead of 1.65 mg-printlet. The amount of naproxen loaded into hydrogel must be adjusted for the future. On the other hand, CN3 showed a drug content in line with the target, coupled with a low SD, sign of homogeneity between the printed forms. Finally, CN4 showed a drug

content in line with the target too, but with a SD of 0.17, which is the limit of acceptability in terms of homogeneity.

4.1.3.10. Dissolution test on new liquisolid formulations

Dissolution test in simulated gastric fluid was performed on new liquisolid printed formulations following the methodology reported in section 4.1.2.14. Figure 59 shows the released amount (%) of naproxen from printed formulations, compared to a commercial Torpac® capsule size 9 filled with pure naproxen. The release test was performed with pure FaSSGF as dissolving media.

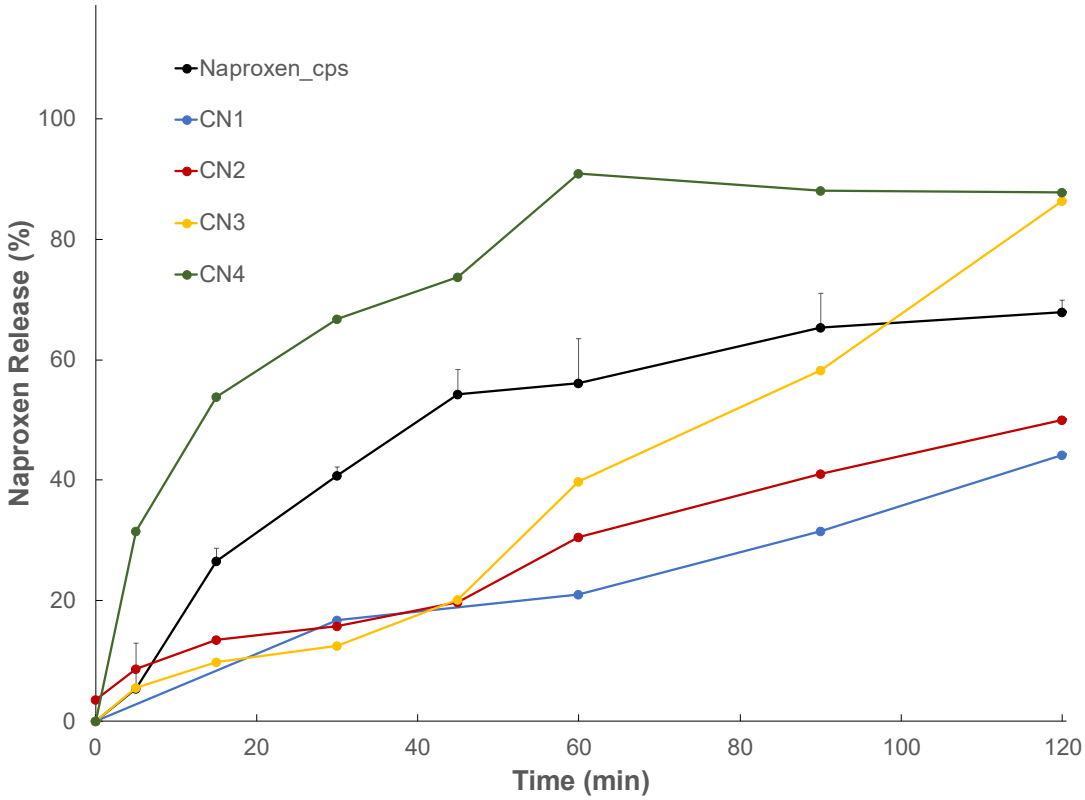

Figure 59. Dissolution curves in FaSSGF media obtained in house with liquisolid formulations CN1 (blue), CN2 (red), CN3 (yellow) and CN4 (green), compared with naproxen std in Torpac® capsules (black).

The curves reported in Figure 59 showed how the release of drug was enhanced only with formulations CN4 (see Table 45 for its composition) compared with std Torpac® capsules filled with pure naproxen. With all the other formulations (CN1, CN2 and CN3) the API release was always slower than the commercially available capsule. However, since at 45 minutes checkpoint, a release of 73.8% was reached with formulation CN4, the faster one,

the conditions to define an immediate release were not met yet (Ph. Eur. 5.17.1 [2]). These dissolution results showed how even a smaller amount of SDS coupled with HPMC E5 works better than Kolliphor® EL in speeding up the release of the poorly soluble BSC class II drug naproxen. Starting from these encouraging results obtained, a new dissolution test was performed, employing the same reference and 3D printed formulations, but adding SDS to the dissolving media (see 4.1.2.14). Dissolution curves obtained are reported in Figure 60.

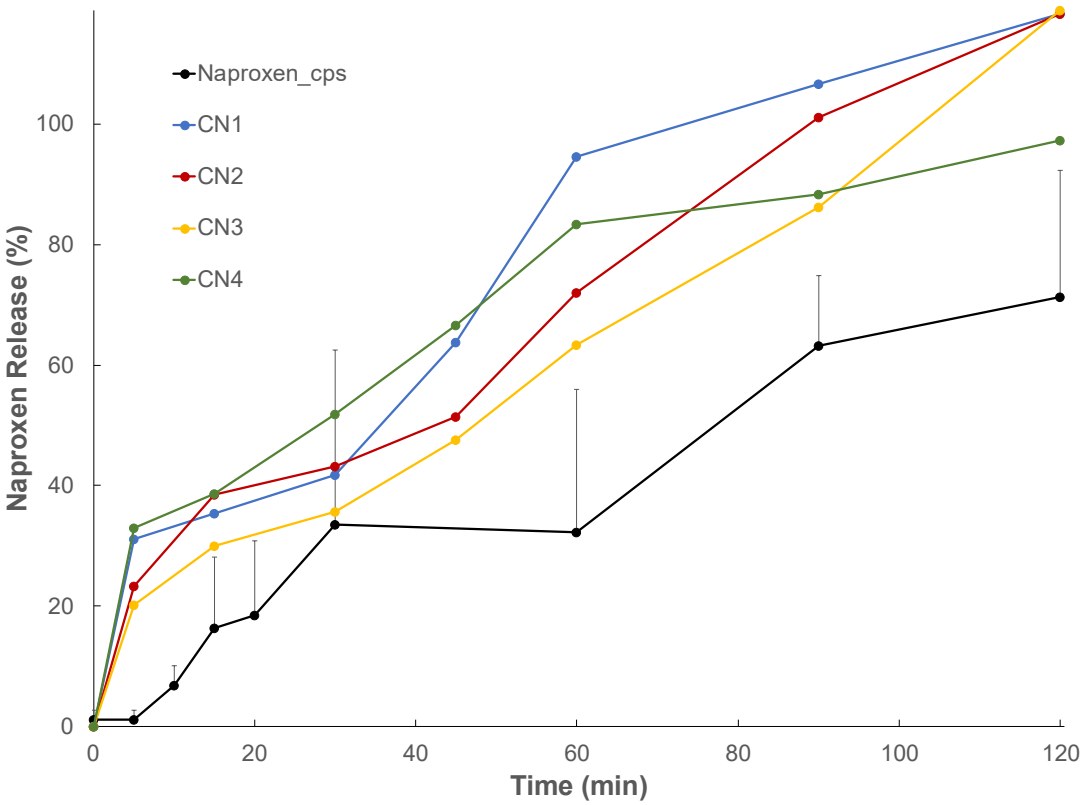

Figure 60. Dissolution curves in FaSSGF with SDS media, obtained in house with liquisolid formulations CN1 (blue), CN2 (red), CN3 (yellow) and CN4 (green), compared with naproxen std in Torpac® capsules (black).

The curves reported in Figure 60 showed how the addition of SDS to the dissolving media resulted in a positive influence over the release rate from CN1, CN2 and CN3 3D printed formulations, compared with commercial capsules filled with pure naproxen. Nonetheless, immediate release was not achieved with all the four formulations tested. Moreover, the release rate of CN4, compared with the same test performed without SDS addition to the dissolving media, resulted to be slightly lower at 45 minutes checkpoint: 66.6% vs 73.8%, probably due to the amount of SDS already present into the CN4 formulation composition. Then, a new dissolution test was conducted, selecting CN4 and CN1 respectively as

formulation that showed the faster release rate and formulation including Kolliphor® EL as surfactant agent, and employing FaSSGF additioned of SDS as dissolving media. Within this new test, instead of changing again the formulations composition, the formulations were printed reducing the infill percentage and pattern of the prepared CAD model, already shown in Figure 55-C. A new g-code was prepared, consisting of a 35% infill and a different filling pattern from before, which created bigger holes. The new prepared g-code is shown in Figure 61, where a comparison with the previous one is reported (Figure 61-C vs D).

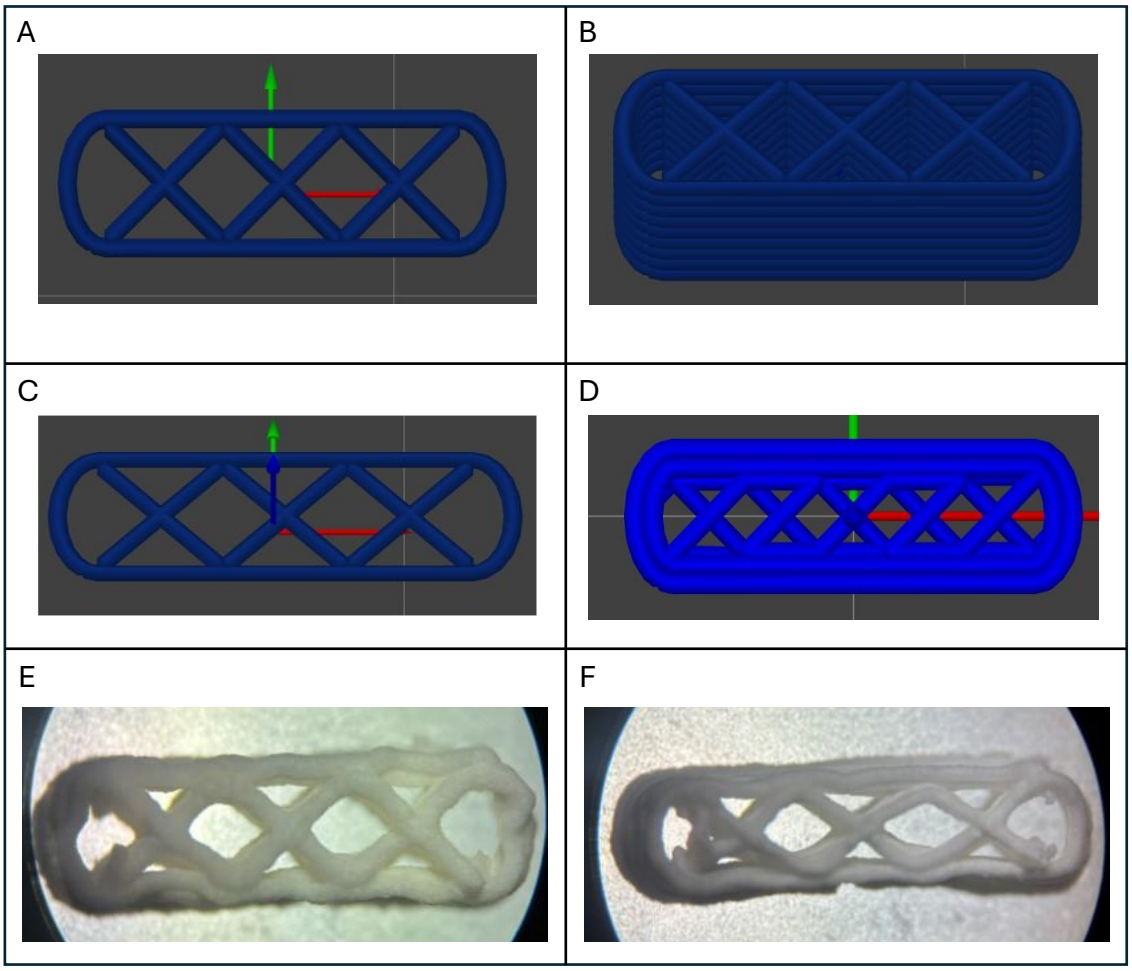

Figure 61. New virtual model employed for printing with 35% infill density and grid pattern. (A) top view, (B) side view, (C) side view of first layer, (D) top view of previous g-code employed, to compare holes generated. CN1-v2 (E) and CN4-v2 (F) printed formulations, images taken with optical microscopy at 4x magnification.

This new model was applied to formulation CN4, generating a printed form renamed CN4-v2, which was printed with the same parameters reported in Table 46. At the same time, a comparison with a new version of CN1 obtained with new g-code (CN1-v2) was performed, taken as reference for the slow releasing formulations tested previously (see Figure 59), to better investigate the effects of reduced density on the release speed of the drug. The new

dissolution trial results are reported in Figure 62 below. CN1-v2 was printed with increased pressure, to obtain better reproducibility between virtual model and printed form.

The reported curves showed how the reduced density of newly 3D printed forms greatly affected the release rate of naproxen [99]. The comparison between old and new printed formulations revealed how CN1 and CN4 improved their release kinetics together with the reduction of infill density. Both the new printed formulations reached 100% of released naproxen within the 120 minutes of the dissolution test. CN1-v2 released 100% of naproxen within 60 minutes, while CN4-v2 had already reached 100% of release after 30 minutes checkpoint, perfectly falling into the definition of immediate release for the European Pharmacopoeia (Ph. Eur. 5.17.1 [2]). In the same way, a big improvement was obtained with CN1-v2, which reached 91.5% of naproxen released after 45 minutes of the test, indicating the realization of an immediate release solid formulation too, to be confirmed with a new dissolution test (n=1 as preliminary test).

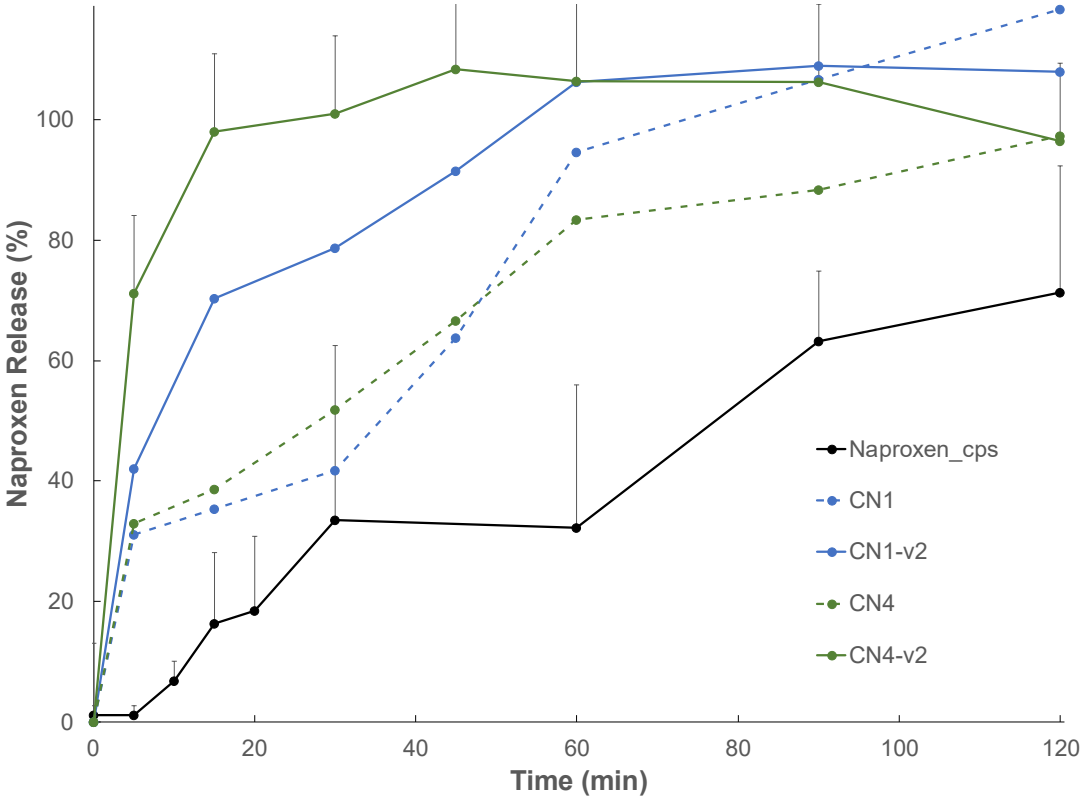

Figure 62. Dissolution curves in FaSSGF with SDS media, obtained in house with liqui-solid formulations CN1-v2 (blue) and CN4-v2 (green), compared with CN1 (blue dotted line), CN4 (green dotted line) and naproxen std in Torpac® capsules (black).

Both the new 3D printed formulations CN1-v2 and CN4-v2, prepared following the new g-code with reduced infill density, were analyzed in terms of drug loading and content uniformity, with the results reported in Table 48.

Table 48. Naproxen quantification and content uniformity analysis performed on CN1-v2 and CN4-v2 printed liquisolid formulations (mean value ± deviation standard, n = 3).

Formulation	Drug content (mg/cpr)
CN1-v2	1.32 ± 0.08
CN4-v2	1.06 ± 0.02

Despite the reduction of infill density, CN1-v2 maintained the same drug content observed before (see Table 47), together with acceptable SD. This is probably due to the increased pressure employed to print these latest printlets. CN4-v2 instead, showed a much lower drug content coupled with stabilized SD, indicating good homogeneity of printing process. The reduced content highlights the necessity to increase naproxen loading in formulation preparation, to reach the target dose set at 1.65 mg-printlet for eventual *in vivo* dosing in rodents.

4.1.3.11. X-Ray micro-computed tomography

Naproxen 3D printed solid formulation CN4-v2 was analyzed with Micro-CT imaging, following the methodology reported in section 4.1.2.15. The images acquired are reported in Figure 63, where circular sections were cut out from the whole layer scanned.

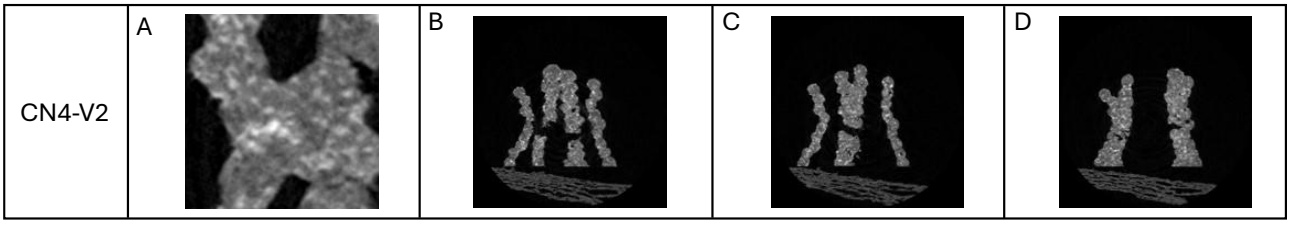

Figure 63. Micro-CT images obtained with 3D printed reservoir formulations (different section views).

With the images displayed in Figure 63, sections of the 3D printed CN4-v2 formulation are reported. The channeled structure characterizing the solid forms is clearly evident. Big channels run vertically, created by the extruded strands of the formulation, which intersect towards the middle of the printlet (C) before returning close to the external perimeter (D).

The holes created internally, at their maximum width, are bigger than the extruded strands, indicating a wide amount of space available for the release media. The exposed surface of the printlet is extremely high, justifying the fast release kinetics reached with this formulation. Figure 63-A is a magnification of the extruded dried formulation. From the picture reported is visible how high density spots are present within the homogeneous hydrogel prepared, probably attributable to the undissolved disaggregant material enclosed within the dried material. The circular shape of the extruded strands is well maintained, and the subsequent deposited layers are easily recognizable. The low degree of printing process optimization carried out could justify the shape flections observable on the perimeter strands, which are slightly bent, resulting in wider edges and shrinked central area of the printlet. Optimization steps of the printing process and subsequent drying could be useful to obtain printed solid forms more refined and comparable to the CAD model prepared. By the way, the small dimensions required by the rodent animal species for which the printed formulations are intended are a big challenger to deal with in terms of printed structure resolution, especially when the printing technologies employed belong to the material jetting family.

4.1.3.12. Solid state investigation of liquisolid formulations

4.1.3.12.1. X-Ray Diffraction (XRD)

Solid state investigation was performed on the liquid-solid formulation that achieved an immediate release, following the methodologies reported in section 3.1.2.4. Since formulation CN4-v2 differed from CN4 only in terms of 3D construct infill density, the solid state characterization was performed on CN4 solid forms, which turned out to be better manageable due to its higher density.

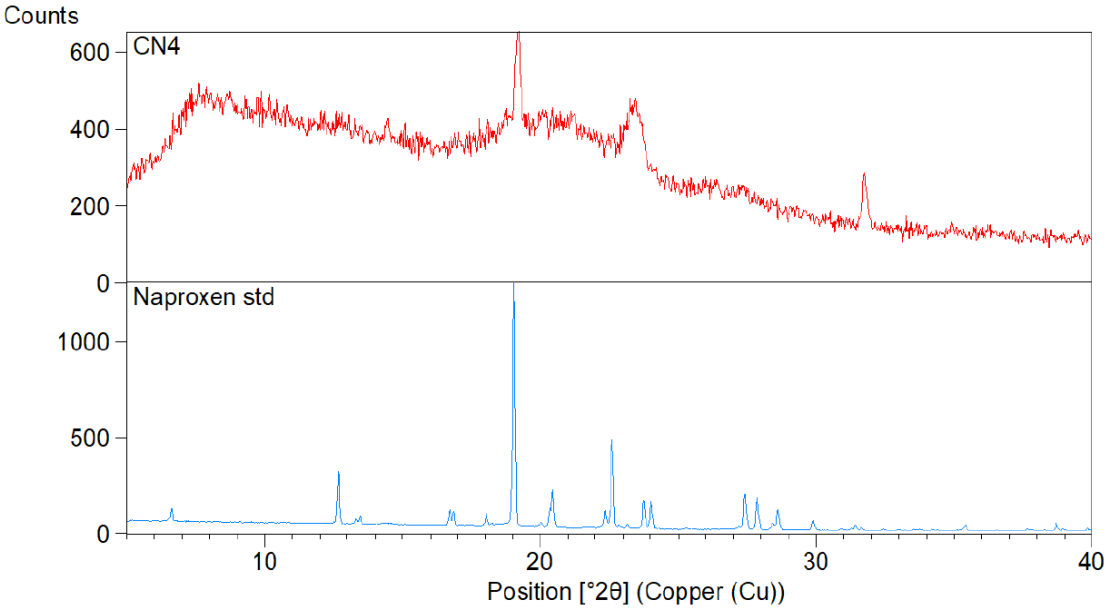

Figure 64. XRD of 3D printed naproxen immediate release formulation (CN4 - red) compared to naproxen std (light blue).

XRD analysis of CN4 3D printed formulation reported in Figure 64, showed the presence of few low intensity peaks, not directly attributable to naproxen standard. The amorphous phase of CN4 was clearly evident, attributable to the high presence of polymeric excipients in the formulation composition. Detailed XRD studies were performed and reported in Figure 72. All the components of CN4 formulation were analyzed with XRD, but only the relevant diffractograms are shown in Figure 72.

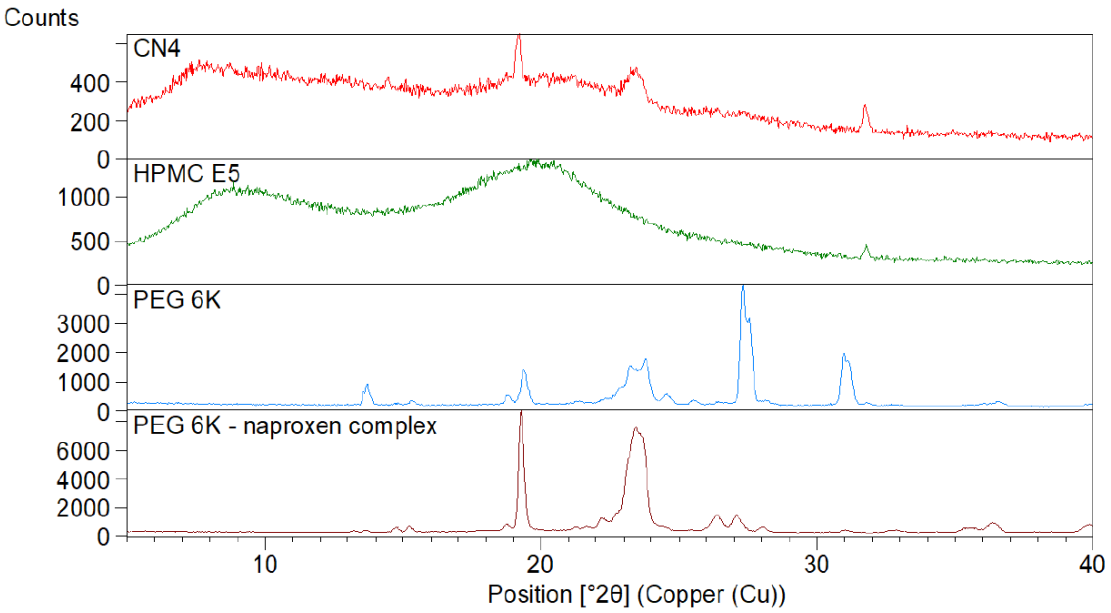

Figure 65. XRD of 3D printed naproxen immediate release formulation (CN4 - red) compared to HPMC E5 (green), pure PEG 6K (light blue) and a complex of PEG 6K and naproxen (maroon).

The diffractogram obtained from XRD analysis of HPMC E5 (green line) exhibited how the small peak present in the 3D printed formulation at 31,8°2Theta was already present in the polymeric starting material, probably due to the presence of an external contaminant. The other peaks present at 19,2 and 23,4°2Theta in the CN4 diffractogram were derived from the formulation process followed during the preparation of the hydrogel. Naproxen addition to the formulation was performed at 85°C (4.1.2.5 and 4.1.2.6), where PEG 6K was already present in a dissolved state. As already disclosed in the work performed by Mura et al. [110], naproxen and PEG 6K chemically interact because of a co-fusion process. Naproxen is highly soluble in melted PEG 6K, forming a weak complex characterized by high dissociation constants. To confirm that, a mixture of naproxen-PEG 6K 10-90 was prepared and heated up to 80°C degrees, until a viscous solution was obtained. The solution was then let to cool down to room temperature, obtaining solidification. The resulting solid was then powdered with mortar and pestle and XRD analysis was performed. The result is reported in Figure 72 (maroon line), showing how the main peaks observed in 3D printed CN4 formulation are derived by the interaction between naproxen and PEG 6K after being melted together.

4.1.3.12.2. Differential Scanning calorimetry (DSC)

The observed interaction between naproxen and PEG 6K co-fused is further confirmed by the DSC analysis, reported in Figure 66.

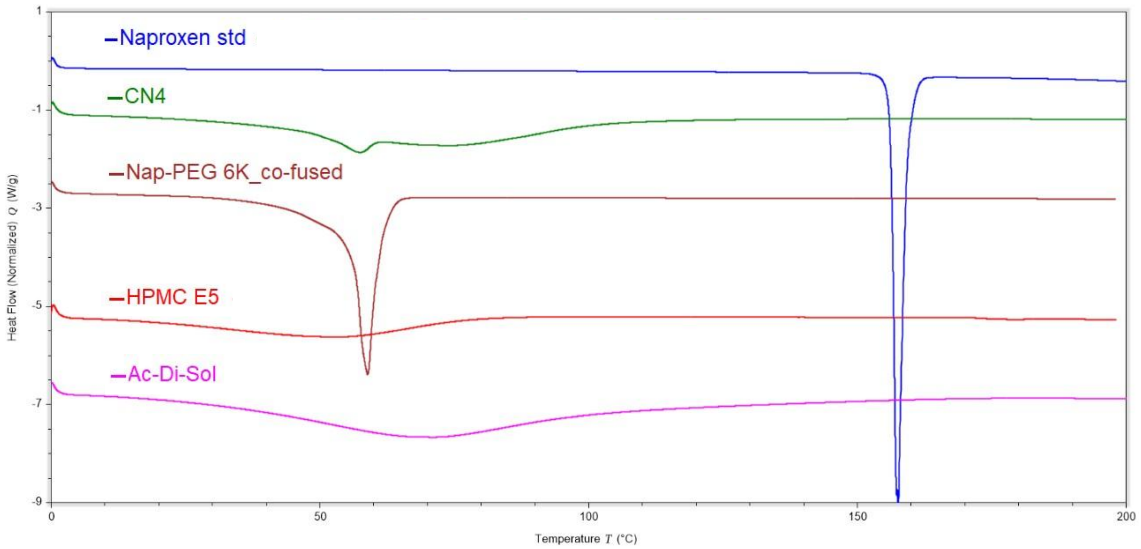

Figure 66. DSC of printed CN4 formulation (green) compared to naproxen standard (blue), Naproxen-PEG 6K co-fused material (maroon), HPMC E5 (red) and Ac-Di-Sol® (pink).

Naproxen melts around 157°C, while in CN4 formulation the drug melting is not present, confirming the absence of crystalline material in the printlet. CN4 solid formulation showed a small endothermic peak at 57°C, followed by a broad endothermic event between 62°C and 110°C. The first one was produced by the chemical interaction between naproxen and PEG 6K, because it was present at the same temperature in the co-fused mixture prepared on purpose [110]. The latter endothermic event was probably attributable to the melting of the other polymeric excipients present in the formulation, especially Ac-Di-Sol®. The thermal behavior of the formulation confirmed the presence of a chemical interaction between naproxen and PEG 6K, keeping the api stabilized in a dispersed or dissolved state, avoiding presence of crystalline material and helping to speed up the release during the dissolution test (see section 4.1.3.10).

4.1.3.12.3. Scanning Electron Microscopy (SEM)

SEM images of the surface of the 3D printed CN4 formulation are illustrated in Figure 67.

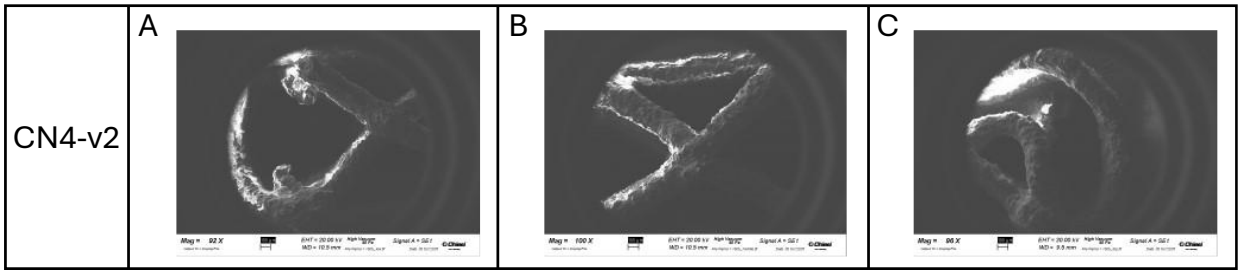

Figure 67. Scanning electron microscopy images obtained with 3D printed CN4-v2 formulation (top views).

SEM images acquired showed the top view of 3D printed CN4-v2 formulation. It is possible to observe how the extruded strands of material are well retained and their circular morphology maintained. The top edges of strands are not well melted to the perimeter (Figure 67-A), meaning that the *gcode* employed in the printing still needs to be improved. The crossing areas of extruded material are well defined and separated, confirming the good resolution achieved with the formulation employed. The filaments appear homogeneous but not smooth, the surface is slightly irregular, probably insoluble excipients included in the formulation composition. The wide channels generated from the slicing process are clearly visible and distinguishable, confirming what observed with Micro-CT and and optical microscopy previous analysis (Figure 61 and Figure 63). Recrystallized naproxen is not present on the external surface of the solid form, confirming XRD and DSC analyses results (sections 4.1.3.12.1 and 4.1.3.12.2).

4.2. Direct Powder Extrusion

The study and development of 3D printed formulations prepared with direct powder extrusion 3D printing technology, was performed in collaboration with UniURB for the first phase.

The content of this section was published [76].

4.2.1. Materials

Naproxen powder from BLD pharm (Reinbek, Germany) was selected as model drug. Polyvinyl alcohol (PVA) in the forms of powder (05 fine, VIVAPHARM®, 4.6-6 mPas, JRS Pharma, Rosenberg, Germany), and micronized powder (EG-03P, 27-33 mPas, Farmalabor, Milan, Italy) was tested. Hydroxypropyl celluloses (HPC-L MW 140 kDa, and HPC-SSL MW 40 kDa) were obtained from Nippon Soda (Tokyo, Japan), while hydroxypropyl methylcellulose (AFFINISOL™, HPMC HME 15LV and AFFINISOL™, HPMC HME 100LV) from DuPont (Wilmington, USA). Kollidon® VA 64 (copovidone) was obtained from Basf (Ludwigshafen, Germany). Polyox WSR N10 (PEO, MW 100 kDa) was purchased from Colorcon (Gallarate, Italy); while mannitol from Farmalabor (Milan, Italy) and PEG 6 kDa from Merck (Darmstadt, Germany). The salts (NaCl, KCl, $Na_2HPO_4*2H_2O$, KH_2PO_4) employed for preparing PBS, methanol and formic acid were purchased from Merck (Darmstadt, Germany). All solvents used were analytical grade.

4.2.2. Methods

4.2.2.1. 3D printer employed

M3DIMAKER™ (FabRx, London, UK) was the 3D printer involved in the project execution, equipped with a direct powder extrusion nozzle only. The printhead employed was a single-screw powder extruder with a nozzle diameter of 0.2 mm. Printbed temperature was set to 80°C and the extrusion temperature adjusted depending on the various properties of the formulations (170-180°C). Infill density was kept at 100% and layer height at 0.4 mm. The default speed employed was 5 mm/s during extrusion while travel speed was set at 50 mm/s. Three layers of skirt were added to provide continuity to the flow of material.

4.2.2.2. Selection of printable cellulose-based polymeric excipients

Prior printing, each batch (5 g) was prepared by weighing the components, drying overnight at 40°C, and finally the blend was homogeneously shaker mixed for 15 minutes at 100 rpm

(Galena Top powder mixer, Ataena, Ancona, Italy). The prepared blend was directly fed into the printing unit (Tumaker NX Pro, Gipuzkoa, Spain) prior preheating the equipment approximately for 15 minutes. After each trial, the printhead was disassembled and cleaned preventing cross-mixing between the formulations.

Firstly, the extrudability was evaluated, considering formulations “extrudable” when a good flowability and a uniformity of filaments coming out from the nozzle were observed. Subsequently, the extrudable formulations were considered “printable” when the layer-by-layer deposition of the molten material led to the production of the desired design.

The matrix excipient was first blended with 10% w/w of the selected model drug corresponding to an administrable rodent dose of 1.5 mg/unit during preclinical studies. If the formulation was not extrudable or the printability was not adequate, different percentages of additional excipients were considered according to the necessities. Mannitol, PEO 100 kDa or PEG 6 kDa were added as plasticizers to control the flowability of the material and-or as binders to enhance the layer-layer adhesion. Table 49 reports the composition of each formulation tested with 10% w/w of naproxen.

Table 49. Composition of the powder blends containing 10% w/w of naproxen.

Formulation	Matrix Excipient	Polyox WSR N10	Mannitol	Kollidon VA 64	PEG6000
F28	PVA 05 fine	-	-	-	-
F29	PVA Farmalabor	-	-	-	-
F30	HPC-L	-	-	-	-
F31	HPC-SSL	-	-	-	-
F32	Kollidon® VA 64	5%	-	-	-
F33		20%	-	-	-
F34	Affinisol™ HPMC HME 15LV	-	10%	-	-
F35		-	-	-	-
F36		-	10%	-	-
F37		10%	-	-	-
F38		-	-	-	10%
F39		-	10%	-	5%
F40	Affinisol™ HPMC HME 100LV	-	-	-	-
F41		-	10%	-	-
F42		10%	-	-	-
F43		-	-	10%	-
F44		10%	-	10%	-
F45		-	-	20%	-
F46		-	-	40%	-

4.2.2.3. Optimization of the printing process

The 3D printing process was carried out similarly to what performed with caffeine formulations. The same printer was employed, and the printing parameters are described within section 3.2.2.3.

4.2.2.4. Powder blend uniformity

Powder blend uniformity was evaluated following the same methodology already reported in section 3.2.2.4, applied with caffeine blends.

4.2.2.5. Solid state characterization

The solid state characterization of naproxen 3D printed formulations with DPE technology was performed using the same instruments and methodologies already used with caffeine formulations. For XRD see section 3.2.2.5.1, for DSC and TGA see section 3.2.2.5.2, for SEM analysis see section 3.2.2.5.3 while for FTIR refer to section 3.2.2.5.4.

4.2.2.6. Uniformity of dosage units

Mass uniformity was assessed according to the method described in the European Pharmacopoeia (Eur. Ph. XI Ed.) for uncoated tablets of mass < 80 mg; the deviation is set at ±10% from the average. A total of 20 dosage units, taken randomly, were analysed.

4.2.2.7. Drug content

For naproxen-loaded mini printlets, the effective drug loading was quantified using UV-Vis (Shimadzu UV-1900i, Shimadzu, Tokyo, Japan) dissolving the printed formulations in PBS. The analysis was conducted in spectrum mode, and the peak absorbance was evaluated at 230 nm.

4.2.2.8. In vitro drug release

The cumulative drug release profile of the drug from the 3D printed formulations was evaluated adapting the method described in the European Pharmacopoeia (Dissolution Test, Eur. Ph. XI Ed.). The analysis was carried out following method reported in section 3.2.2.8. Quantification studies were carried out using UV-vis for naproxen. The analytical method is described in section 4.2.2.7. The analysis was carried out in triplicate. Also, for each formulation, size 9 capsules were manually filled with powder blends, and the drug release profile was assessed at the same conditions described above.

4.2.2.9. Mechanical properties

A compression test was performed to assess the mechanical properties of the printlets following method reported in section 3.2.2.9.

4.2.3. Results

4.2.3.1. Selection of printable cellulose-based polymeric excipients

In the identification of the optimal formulation, appreciable flowability is a fundamental prerequisite for good printability performance. Hence, the extrudability and printability were evaluated for each blend.

Most of the formulations were extrudable, however, the filaments obtained from F28 and F29 were rough and brittle, in addition, when increasing the temperature an over-extrusion was observed and the filament browned. Like what observed with caffeine, PVA has not proved adequately processability in combination with the model drugs, probably due to the narrow range between the melting and degradation temperature.

Considering HPC-based formulations, when extruded with incorporation of naproxen (F30 and F31), no additional excipients were needed.

The extrusion of Kollidon® VA 64 proved difficult also with naproxen. Even in the presence of excipients, the formulations tend to adhere to the screw (F32 and F33). The incorporation of mannitol (F34) helped the extrusion, but without providing sufficient flow.

Moving on, two different grades of HPMC at lower and higher molecular weight (15LV and 100LV, respectively) were tested. Formulations containing only the drug (F35 and F40) or with the addition of mannitol (F36 and F41) were easily extrudable, with a good control over the material flow, while the addition of Polyox WSR N10 (F37 and F42) lead to a loss of control over the flow that turned out to be too slow. PEG6000 was also selected as a binder for the HPMC-based formulations (F38) but it led to a very sticky blend that clogged the nozzle during the extrusion. HPMC100LV was also combined with Kollidon® VA 64 at different concentrations, at 10% (F43) high temperatures were required to obtain a sufficient flow from the nozzle, leading to the darkening of the filament, the addition of mannitol (F44), helped lowering the extrusion temperature, thus avoiding the darkening of the filament but a complete lack of flow control was experienced. Higher concentrations of Kollidon® VA 64 were added to the mixture (F45 and F46) but led to the extrusion of a filament that was too stiff and brittle. Overall, the formulations containing HPMC at lower molecular weight resulted in a more controlled and smooth extrusion through the nozzle.

Taking into consideration the extrudability test, a preliminary printing trial was performed with F30, F31, F35, F36, F39, F40 and F41. By comparing the formulations, HPC-L based composition (F30) provided a superior accuracy of the design. Concerning the HPMC15LV-based formulations, the good extrudability didn’t lead to a good outcome of the printing process. This was due to a quick cooling of the filament and complete lack of adhesion to

the printing bed and layer to layer. Hence, the addition of 5% of PEG6000 (F39) was selected to enhance the “stickiness” of the blends resulting in a good layer adhesion and printing accuracy. Thus, formulations F30 and F39 were selected as candidates for the manufacturing of the printlets loaded with the respective model drug. The printed products are represented in Figure 3. After printing, the devices were measured using a digital caliper (Mitutoyo, Japan).

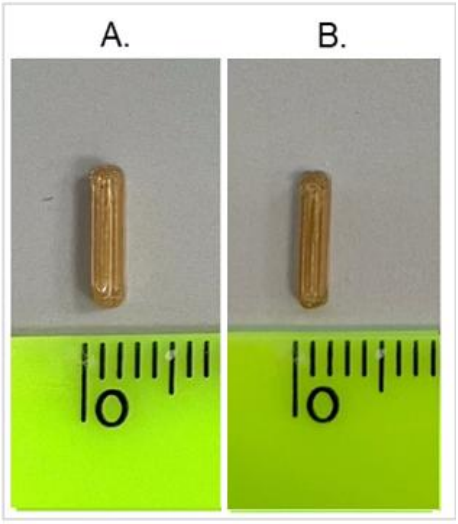

Figure 68. Top view of the printlets: (A) HPC-L-based formulation (F30); (B) HPMC 15LV-based formulation (F39). The scale is expressed in cm.

4.2.3.2. Powder blend uniformity

To evaluate the homogeneity of the powder blends, random samples (triplicate) of the same formulation were collected after mechanical mixing. For all the formulations, HPC-L and HPMC 15LV-based, the resulting intensity of the UV bands overlapped, confirming the homogeneity of the mixtures.

4.2.3.3. Solid state characterization

4.2.3.3.1. Differential scanning calorimetry (DSC) and Thermogravimetric analysis (TGA)

DSC analysis was carried out to assess the thermal stability of the excipients and APIs in the most promising formulations at the operating temperatures and after printing. Thermograms are reported in Figure 69. Naproxen shows its endothermic peak, related to the melting at T_p = 158.14°C [111].

Mannitol and PEG 000 showed their melting peaks at T_p = 168.16°C and T_p = 66.57°C, respectively. Cellulose-based polymers are instead amorphous and glass transition temperatures are hardly detectable as previously reported [77, 78, 79]. Thermograms display a broad endothermic event at low temperatures T < 100°C which can be attributed to the evaporation of the moisture absorbed [80]. The peak is anyway weak as the amount of water incorporated is very low due to the overnight drying of the physical blends.

When considering the physical mixtures and 3D printed formulations, significant changes in the thermal behavior are detectable. These naproxen-based formulations showed a depression, in terms of temperature and intensity, of the peaks relative to the drug and excipients. This phenomenon is well explained in the literature and it's a symptom of a strong physical interaction between the polymer matrices and the drug, suggesting a good miscibility, where the polymer acts as the "solvent" and the drug as the "solute" of the mixture [112]. Indeed, the resulting 3D printed formulations show a complete amorphous state (HPMC 15LV-based printlets present a small endothermic peak probably due to the presence of a low amount of mannitol still in the crystalline form). This is also because the printing temperatures selected are higher than the melting temperature of the drug. DSC thermograms were also confirmed through the XRD analysis and SEM imaging (sections 4.2.3.3.3 and 4.2.3.3.4).

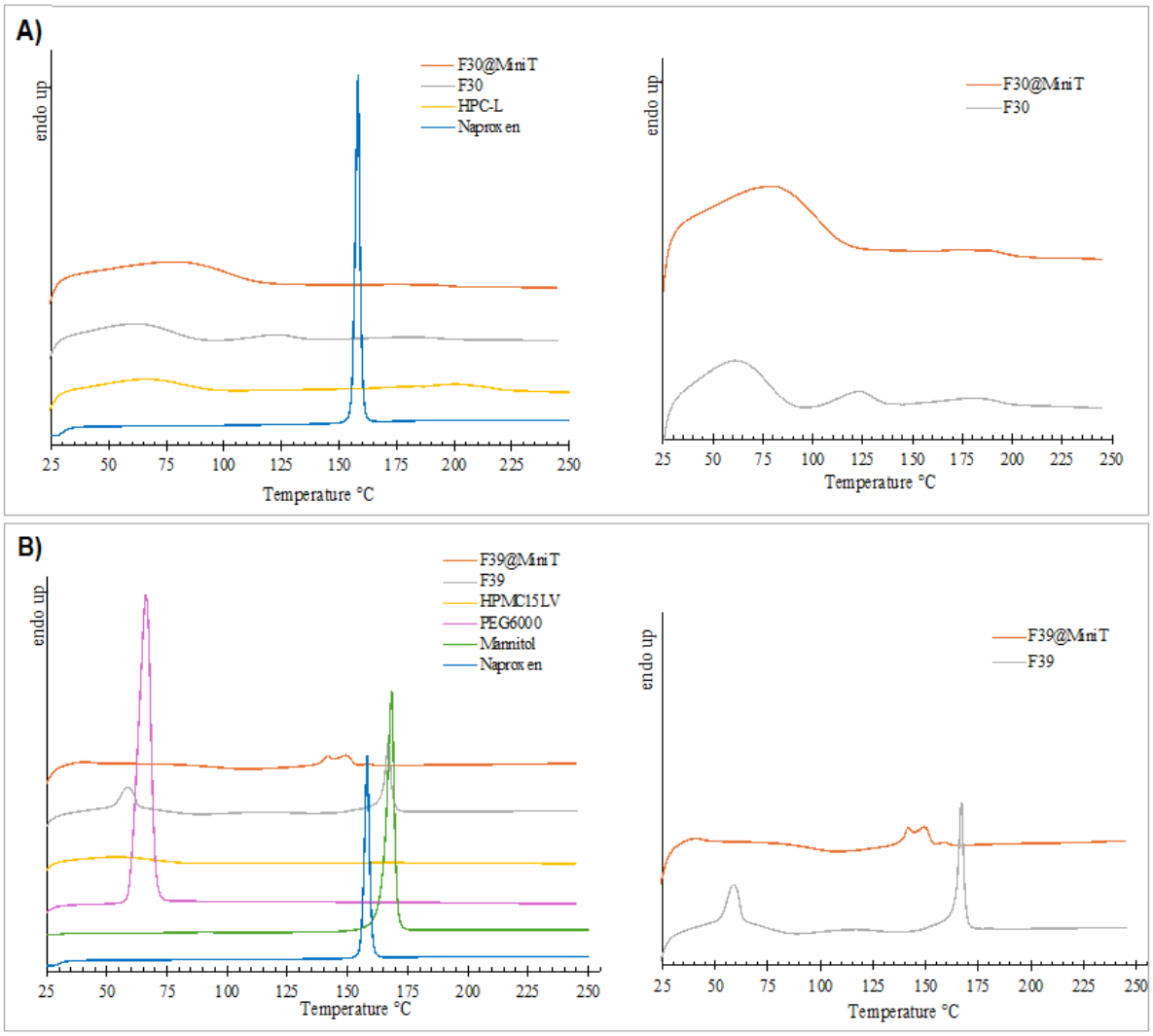

Figure 69. DSC thermograms of naproxen loaded formulations in the two different polymer matrices.

Since the materials are exposed to high temperatures during the 3DP manufacturing process, it is essential that all formulations are processed at conditions that are clearly below the decomposition critical points; ideally, at the lowest feasible processing temperatures [82]. The primary benefit of DPE over FDM is that the powder blends only need to go through the hot stage once because creating the filament is not a required step.

Based on the weight variations, the TGA thermograms of the active ingredients, excipients, physical mixtures and 3D printed formulations were examined (Figure 70). It is evident that the printing temperatures, which range between 170°C and 180°C, are far below these critical points. Until 200°C, indeed, a negligible weight loss was observed for all samples (1.2 – 2.3%, due to the release of the moisture absorbed), demonstrating the chemical stability of the materials during the printing process.

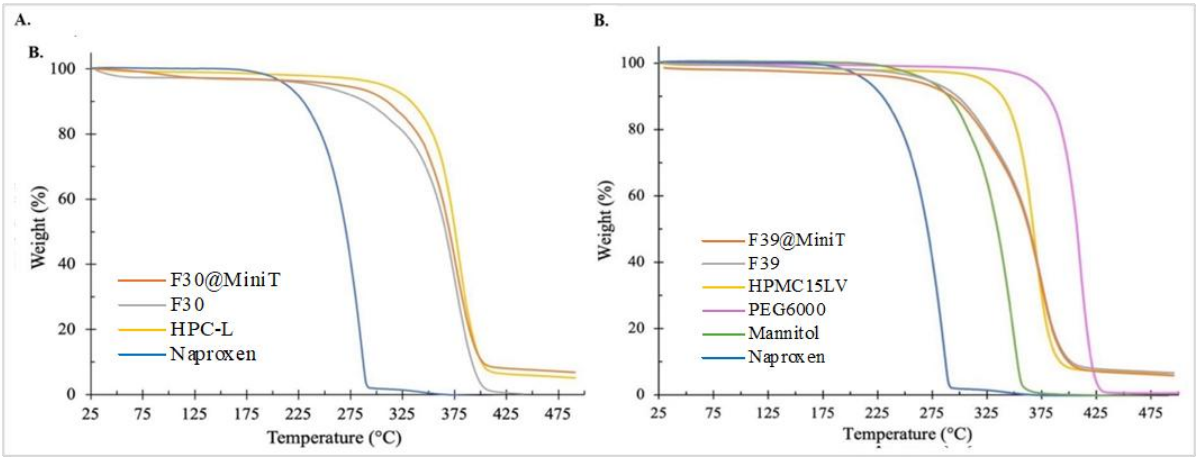

Figure 70. TGA thermograms of naproxen loaded formulations in the two different polymer matrices.

4.2.3.3.2. Fourier-transform infrared spectroscopy (FTIR)

FTIR spectra were collected from analysing the raw materials (excipients and naproxen), the powder blends and final printlets, as shown in Figure 71. All the significant peaks observed in the spectra are confirmed with the ones found in literature. HPC-L and HPMC 15LV show their significant peaks around 3200-3400 cm^{-1}, broadband, due to the O-H stretching vibrations in the pyranose ring of the sugar, at 2926 and 2856 cm^{-1} attributed to the C-H asymmetric and symmetric vibrations, and a broad band at 1050 cm^{-1} due to the C-O-C asymmetric stretches [83]. In the PEG 6000 spectrum, the peak at 1100 cm^{-1} is due to the stretching vibration of C–O–C bonds, while the strong peaks around 2800-2900 cm^{-1} to the stretching vibrations of C-H and OH functional groups, respectively [84, 85]. Mannitol spectrum displays the main peaks at 3310 cm^{-1} (broadband, O-H stretching vibrations), at 1348 cm^{-1} and 1080 cm^{-1} (C-H and C-O stretching vibration respectively) [86]. Naproxen spectrum shows a broad band around 3300-3200 cm^{-1} due to the O-H stretching vibrations and a significant peak at 1555 cm^{-1} characteristic of the stretching vibration of the COOH functional group [113]. Both the spectra of the powder blends and the final 3D printed formulations feature the main peaks of the raw materials (excipients and API), and no unknown peaks appear, nor significant ones disappear, suggesting a good compatibility among the excipients and APIs but also within the manufacturing method.

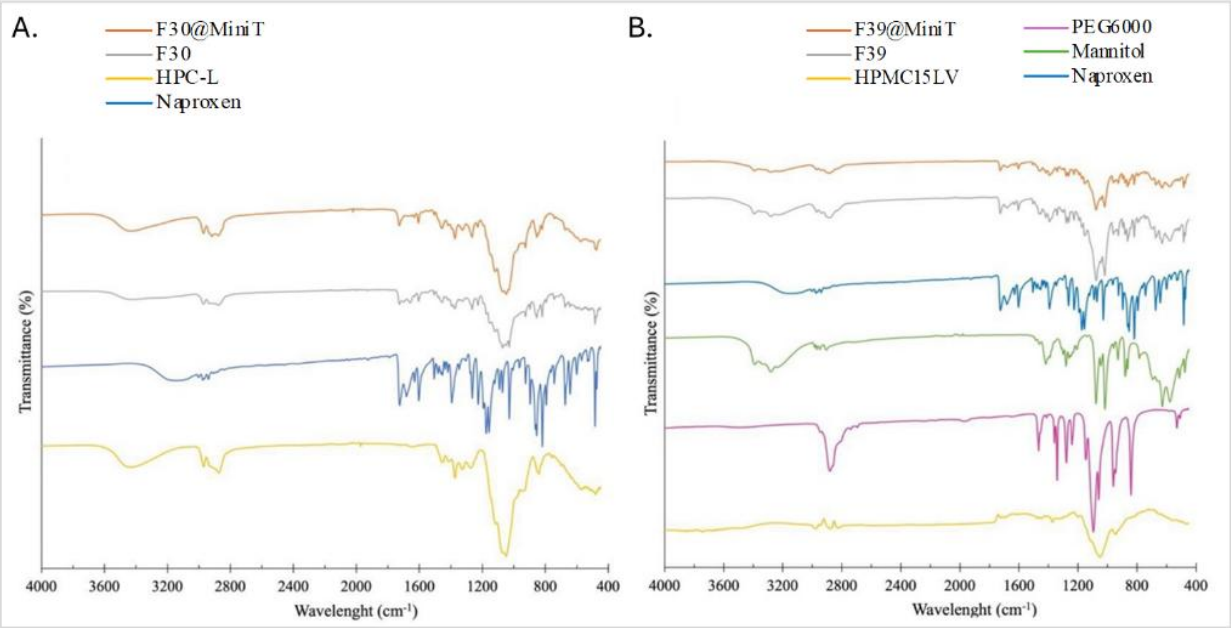

Figure 71. FTIR spectra of the raw materials, physical blends and 3DP formulations. Naproxen-loaded formulations F30 and F39 (A and B) in the two different polymer matrices.

4.2.3.3.3. X-ray diffraction (XRD)

X-Ray diffraction spectra were acquired on the final 3D printed forms, under transmission mode. The analysis of F30 shows a completely amorphous diffraction pattern (Figure 72) while in F39 is still present some crystallinity related to recrystallized delta form of mannitol (Figure 73), as previously noticed during the thermal analysis (see section 4.2.3.3.1).

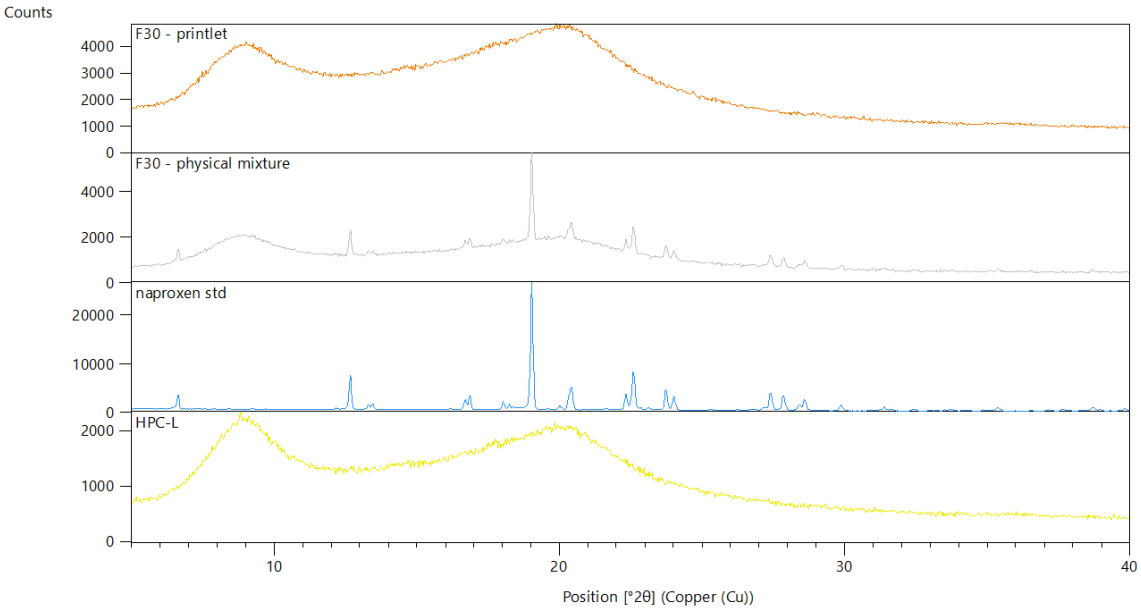

Figure 72. XRPD diffractograms of the raw materials, physical blend and 3D printed formulation F30.

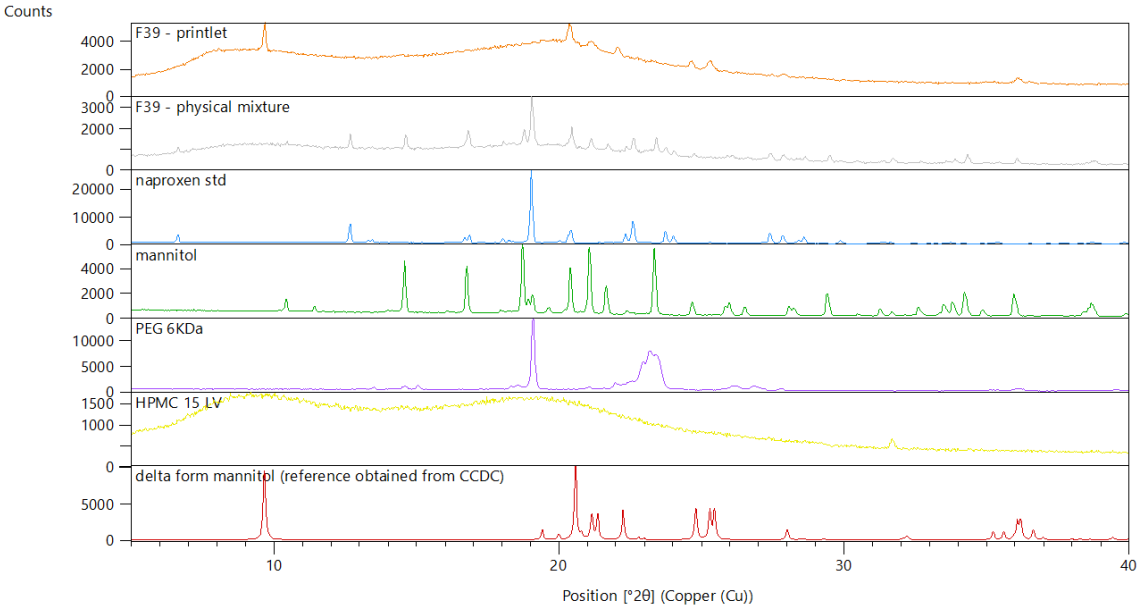

Figure 73. XRPD diffractograms of the raw materials, physical blend and 3D printed formulation F39.

4.2.3.3.4. Morphological characterization by scanning electron microscopy (SEM)

SEM images shown in Figure 74 (first and second panel) revealed a smooth surface for the 3D printed solid forms. The layered structure appears accurate both from the top (left) and lateral view (right), confirming the accuracy of the printing process; indeed, neither

overlapping nor empty spaces are observed. Moreover, in accordance with the results obtained at the XRD analysis where naproxen was not detected in the printlets, in Figure 74-C no recrystallized API was visible within the matrix of the naproxen-loaded printed formulations.

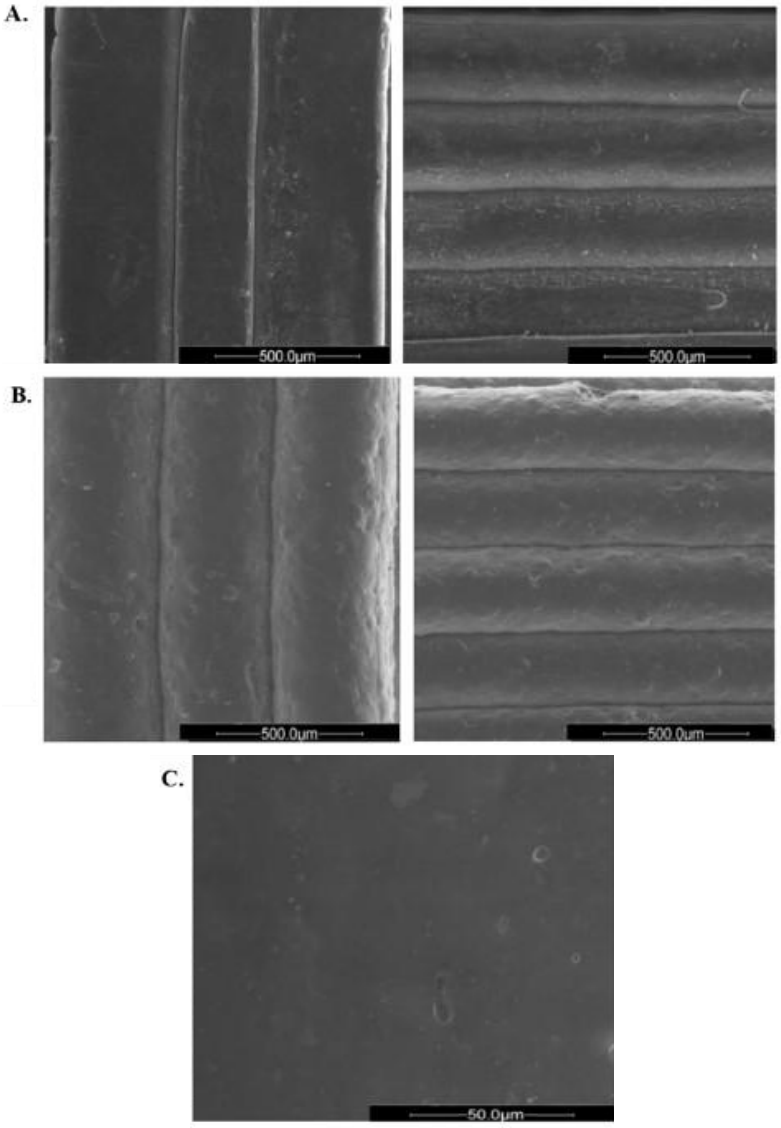

Figure 74. (A) SEM images of top and lateral view of printlet F30. (B) SEM images of top and lateral view of F39 printlet. (C) SEM image showing the presence of crystalline structure.

4.2.3.4. Uniformity of dosage units

Uniformity of mass was assessed for the printlets. The ones obtained from HPC-L-based formulations (F30) showed an average mass of 21.2 ± 1.1 mg. While, for those obtained from HPMC 15LV (F39) the average mass was 24.3 1.7 mg. European Pharmacopoeia states that individual masses of no more than two tablets can differ from the average mass

by more than 10% when it comes to uncoated single-dosage units with an average mass lower than 80 mg. Since only one printlet exceeded the 10% limit, for both the HPC-L and HPMC 15LV-based formulations, the Eur. Ph. requirement was satisfied. Indeed, each batch's relative deviation from the mean mass was low, confirming a good reproducibility of the manufacturing method and satisfying control over the dosage-units' uniformity.

4.2.3.5. Drug content

The effective drug content in the printlets was evaluated through quantitative characterization (UV-Vis) and referred to the theoretical API amount loaded in the powder pre-processing at the 3D printer. Drug loading efficiency was 90.92% for HPC-L based formulation (F30), and 94.78% for HPMC 15LV-based formulation (F39). Overall, the amount of naproxen loaded in the final 3D printed forms was satisfying and considered acceptable even though a loss of drug is present due to the manufacturing method with very limited amount of material to work with.

4.2.3.6. In vitro drug release

The release profile of naproxen from the different cellulose-based matrices were evaluated through dissolution studies, in accordance with the Eur. Ph. XI. As shown in Figure 75, the release ratio of naproxen from HPC-L formulation was slow, obtaining 24.9 ± 1.7% of dissolved drug after 60 minutes (orange plot). A further slowing in the release is observed in the formulation containing HPMC15LV as the main excipient, 5.4 ± 1.4% (green plot). The different release compared to caffeine matrixial formulations (see section 3.2.3.6), is not to be look at the presence of mannitol as it works only as a plasticizing agent and does not affect the release profile of the drug from the matrix, where 10% of mannitol was added to formulation F30 and further printed (pink plot). The dissolution tests were also carried out on capsules size 9 filled with the physical blends and the resulting data compared with the ones obtained for the 3D printed formulations as shown in Figure 75, dotted plots. Comparing the two manufacturing methods (3D printed forms and conventional size 9 capsules), no significant variation was observed within the release kinetics of the oral dosage forms.

Probably, due to the nature of matrixial formulations, where naproxen was homogeneously mixed with cellulosic polymer, the release profile from these formulations was driven by drug solubility and polymer swellable-soluble characteristics [49, 55]. For this reason, with an

insoluble drug like naproxen [91], this type of formulation printed with a 100% infill (see section 4.2.2.1) was not useful for the scope of reaching a fast release and needed to be changed.

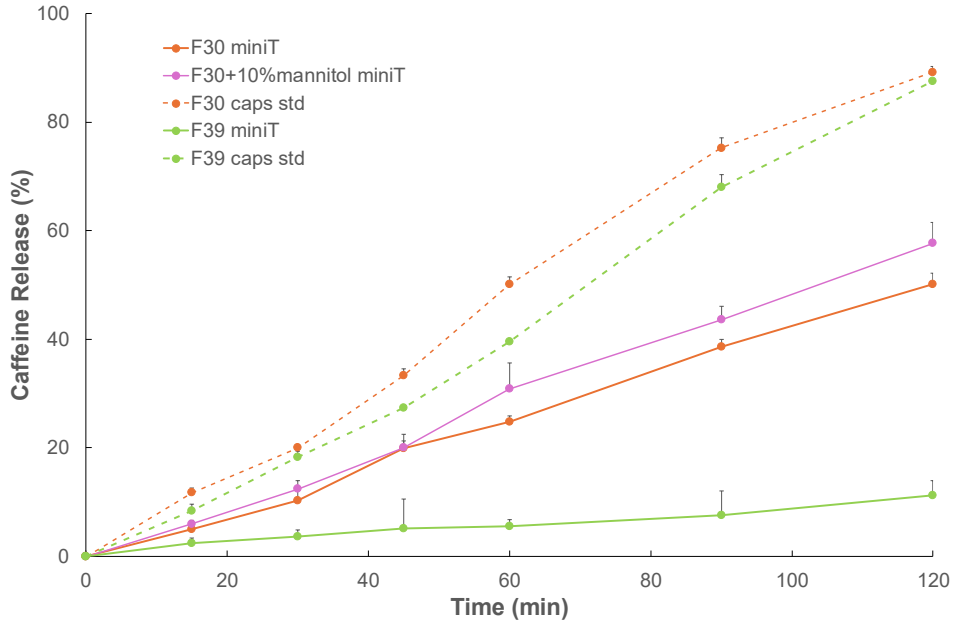

Figure 75. Drug release profiles of size 9 capsules filled with physical blends vs 3D printed formulations.

4.2.3.7. Mechanical properties

A compression test was performed on the 3D printed formulations to evaluate their mechanical behaviour. In Table 50, for each formulation, the peak force (N), UCS (MPa), YM (KPa), and YP (MPa) are listed. The 100% strain was obtained without any breakage occurring in formulation F30, while formulation F39 broke due to delamination when 90% of strain was reached, demonstrating the high toughness and resistance of the 3D printed forms. Moreover, within formulation F39 a more rigid structure was observed, along with an increase in the YM, probably due to 10% of mannitol [88]. This direct correlation is frequently observed during mechanical tests. YM measures the resistance of a material to elastic deformation under load, thus a stiff material has a high YM and changes its shape only slightly under deforming stresses [88]. Overall, the strength needed to reach a strain of 100% was similar for all the tested formulations. In particular, for F15 a lower UCS was registered along with a lower value for the YM, underlining the higher elasticity and plasticity of the 3D printed formulation.

Table 50. Mechanical characteristics of the naproxen printlets.

Formulation	Peak Force (N)	UCS (MPa)	YP (MPa)	YM (MPa)
F30	210.21 ± 9.07	16.74 ± 2.68	2.06 ± 1.74	0.14 ± 0.10
F39	217.93 ± 6.55	17.35 ± 1.72	4.03 ± 1.98	0.21 ± 0.08

4.3. Conclusions

In this part of the study semi-solid extrusion (SSE) and direct powder extrusion (DPE) were evaluated for the fabrication of an immediate release formulation. For this purpose, naproxen as model drug was used, preparing solid oral dosage forms. Within the SSE approach great efforts were accomplished to formulate the poorly water soluble drug into hydrogels useful for the scope of the project. Several formulations were prepared using solubility enhancers like cyclodextrins or surfactants, but all of them were discarded because the reached drug solubilities in water were not adequate to prepare hydrogels suitable for the further printing process. Lipidic excipients were then evaluated: O/W emulsions were investigated and printed, without achieving appropriately defined printed solid forms. Moreover, naproxen turned out to be recrystallized within the formulation. On the other hand, liposomal hydrogels were successfully prepared and printed, keeping naproxen encapsulated. However, the obtained *in vitro* release rate from 3D printed liposomal solid formulation did not meet the requirement for an immediate release. After that, further efforts were put on 'liquisolid' matrix formulations. Several formulations were prepared, printed and finally analyzed. Beyond the composition of the formulations, another parameter turned out to be highly relevant to achieve the immediate release of naproxen, the solid form infill density. Modifications of the infill density of the CAD model deeply altered the release kinetics of the printed formulations. In the end, the appropriate balance was reached between formulation composition and solid form infill density, demonstrating the ability to achieve immediate drug release kinetics with naproxen, in simulated gastric fluid. Moreover, the 3D printed solid formulation was characterized in terms of solid state and the behavior of naproxen was depicted. Its ability to chemically interact with the excipients of the formulation was studied and identified, unveiling the presence of an amorphous dispersed phase which helped to achieve the immediate release, avoiding chemical degradations of the api. These results underscore the potential of SSE-based methods for generating rapidly dissolving oral formulations suitable for preclinical pharmacokinetic investigations.

In contrast, DPE matrix formulations were successfully prepared and printed but the obtained solid formulations resulted to be not optimized. As a result, they did not yield favorable *in vitro* release profiles, indicating limited suitability for immediate release applications under the current experimental conditions. This finding highlights the necessity for further optimization of DPE 3D models, process parameters and excipient selection to enhance drug release performance.

Drug loading and content uniformity analyses of SSE solid formulations revealed variability between batches, suggesting that meticulous process optimization is required to ensure consistent dosing and reproducibility. On the other hand, DPE printed formulations resulted to have reached the target of drug loading, with a suitable homogeneity between printlets, displaying a good starting point for future modifications of other printing parameters.

Overall, the results affirm the feasibility of using SSE-based 3D printing for the production of naproxen oral dosage forms with immediate release properties, while further refinement is necessary for DPE-based matrices to meet *in vitro* performance criteria. Translation of *in vitro* results onto *in vivo* preclinical models will be also another important task, since physiological environment could always apport substantial changes to administered solid forms' performance. These findings provide a foundation for future work aimed at optimizing 3D printing strategies for tailored drug delivery in preclinical research.

5. Conclusions

This research project set out to systematically evaluate the applicability of 3D printing technologies within the pharmaceutical field, with a particular focus on preclinical research phases. Specifically, the study concentrated on assessing a printer capable of operating via two distinct extrusion techniques: semi-solid extrusion (SSE) and direct powder extrusion (DPE). The SSE technology relies on the extrusion of semi-solid formulations, such as gels or pastes, whereas DPE utilizes solid mixtures processed at elevated temperatures to enable deposition onto the printing platform. Both technologies were used to produce solid dosage forms of two model drugs with differing physicochemical properties: caffeine (BCS Class I) and naproxen (BCS Class II).

The central objective was to modulate the release kinetics of the two model drugs under simulated gastric conditions. Thus, the aim was to achieve sustained release for caffeine formulations and immediate release for naproxen formulations, while ensuring the final dosage forms met strict dimensional of preclinical requirements. The oral forms were designed for potential administration to rodent models, typically involving low doses in miniaturized dosage forms. Consequently, the 3D-printed models replicated capsules commonly used for oral administration in rats (size 9), with a target drug load of 1.65 mg per printed unit.

The initial phase of the project focused on caffeine, targeting formulations with sustained release profiles in simulated gastric fluid. Using SSE technology, matrix formulations based on swellable cellulosic hydrogels were first evaluated to modulate drug release kinetics. Although various compositions were tested, none achieved the desired release modulation. The study then shifted towards reservoir-type formulations, prepared using dual print heads loaded with different formulations. This approach successfully yielded solid forms in which the API was localized exclusively within an inner core, surrounded by hydrogel layers containing only polymers. These formulations delivered sustained release kinetics *in vitro* compared to commercial capsules filled with pure API, as demonstrated on both research-grade dissolution apparatus and USP-compliant testers, following pharmacopeial methods. The 3D-printed forms exhibited appropriate drug loading and dimensions suitable for administration in rodents, accurately mimicking size 9 capsules.

In parallel, DPE technology was used to prepare matrix formulations based on swellable cellulosic polymers. The resulting prints matched the size of standard capsules and were loaded with the correct amount of API. However, *in vitro* dissolution kinetics in simulated

gastric fluid did not show significant modulation of drug release compared to commercial caffeine capsules.

Selected SSE and DPE formulations were subsequently administered *in vivo* to rats and compared with commercial size 9 capsules containing only caffeine. Two SSE formulations (CC3 and CH5) and one DPE formulation (F9) were evaluated. Interestingly, despite exhibiting limited sustained release *in vitro*, the DPE formulation proved most effective at prolonging drug release *in vivo*. Among the SSE formulations, only CH5 demonstrated a slight improvement over commercial caffeine capsules in achieving sustained release profiles.

In the second phase of this project, the application of semi-solid extrusion (SSE) and direct powder extrusion (DPE) 3D printing technologies was systematically explored for the formulation of immediate release oral dosage forms, with naproxen selected as the model drug. The SSE approach encompassed a range of formulation strategies, including the use of solubility modulators such as cyclodextrins and lipid excipients for the preparation of micellar suspensions. Additionally, liposomal formulations were developed to enable the encapsulation of naproxen within lipid bilayers. Despite these efforts, the resulting formulations proved unsuitable for the production of solid forms with immediate release properties.

Consequently, the investigation pivoted towards liquisolid formulations incorporated into hydrogels. This strategy enabled the successful fabrication of solid dosage forms with appropriate dimensions, which exhibited immediate drug release kinetics in simulated gastric fluid. The rapid release was attributed, in part, to the low-density structure achieved through precise 3D model design. However, further optimisation was deemed necessary, as the active pharmaceutical ingredient loading in these solid forms fell below the targeted dose.

Conversely, DPE technology facilitated the production of matrix-based solid dosage forms with suitable size and drug content for potential administration to rodent models. Nevertheless, *in vitro* release testing in simulated gastric fluid did not demonstrate immediate release, underscoring the need for continued investigation into formulation composition and 3D processing parameters to achieve the desired performance. Overall, these findings highlight both the promise and the challenges inherent in harnessing advanced 3D printing technologies for the development of tailored pharmaceutical dosage forms, and they provide a strong foundation for future research aimed at further refining these innovative approaches.

In summary, this project aimed to systematically investigate the potential of advanced 3D printing methods, specifically SSE and DPE extrusion, for the fabrication of oral solid dosage forms suitable for preclinical studies in rodents. The research successfully established proof-of-concept for both sustained and immediate release applications, despite the reduced dimensions of the designed printable object, demonstrating the adaptability of these technologies to address diverse pharmaceutical challenges. While key milestones were achieved, such as the production of miniaturized dosage forms with appropriate dimensional and drug loading characteristics, certain hurdles remain, particularly with respect to optimizing formulation compositions and drug release profiles for DPE-based matrices. Nonetheless, the value added to industrial research is significant, as the work underscores the flexibility and precision offered by 3D printing in creating tailored drug delivery systems, facilitating advances of proprietary projects to development phases.

The minimal quantities of materials required, coupled with the rapid adaptability of both dosage and release kinetics in relation to the reduced dimensions of the solid dosage forms produced, render this formulation technology a considerable asset for preclinical research phases. The capacity to swiftly tailor formulations to meet specific experimental needs not only conserves valuable resources but also allows for the efficient screening of compounds. This efficiency is particularly advantageous when working with limited quantities of active pharmaceutical ingredients or when rapid iteration is necessary to optimize drug delivery profiles. Such flexibility is instrumental in facilitating accelerated progression to later development stages, or conversely, in promptly identifying compounds that are unlikely to advance, thereby safeguarding both financial and temporal resources, assets of paramount importance in the highly dynamic pharmaceutical industry.

Furthermore, it is worth highlighting that the application of these 3D printing technologies was preliminarily evaluated through the formulation of proprietary compounds within the company. This strategic approach not only demonstrated the practical feasibility and versatility of the technologies under real-world conditions but also established a robust foundation for their potential integration into future internal projects. The knowledge and methodologies developed through this work are thus poised to support the advancement of forthcoming initiatives involving proprietary APIs, reinforcing the value that innovative 3D printing approaches can offer to industrial pharmaceutical research and development.

References

[1] SCHLANDER, Michael, et al. How much does it cost to research and develop a new drug? A systematic review and assessment. *Pharmacoeconomics*, 2021, 39.11: 1243-1269.

[2] MILLIKEN, Rachel L., et al. Application of 3D printing in early phase development of pharmaceutical solid dosage forms. *International journal of pharmaceutics*, 2024, 653: 123902.

[3] ANTOLOVIĆ, Roberto; JELIĆ, Dubravko; MARKOVIĆ, Darko. Preclinical Research in Drug Discovery. In: *Drug Interactions in Gastroenterology: A Clinical Guide*. Cham: Springer Nature Switzerland, 2025. p. 13-28.

[4] AWAD, Atheer, et al. Reshaping drug development using 3D printing. *Drug discovery today*, 2018, 23.8: 1547-1555.

[5] AWAD, Atheer, et al. Clinical Benefits of 3D Printing in Healthcare. *3D Printing of Pharmaceutical and Drug Delivery Devices: Progress from Bench to Bedside*, 2024, 187-210.

[6] SHAH, Amit K.; AGNIHOTRI, Sunil A. Recent advances and novel strategies in pre-clinical formulation development: an overview. *Journal of controlled release*, 2011, 156.3: 281-296.

[7] GAO, Y.; GESENBERG, C.; ZHENG, W. Oral formulations for preclinical studies: principle, design, and development considerations. In: *Developing solid oral dosage forms*. Academic Press, 2017. p. 455-495.

[8] GRIGNARD, Elise, et al. Considerations for the development of *in vitro* dissolution tests to reduce or replace preclinical oral absorption studies. *European Journal of Pharmaceutical Sciences*, 2017, 99: 193-201.

[9] SEOANE-VIAÑO, Iria, et al. Translating 3D printed pharmaceuticals: From hype to real-world clinical applications. *Advanced Drug Delivery Reviews*, 2021, 174: 553-575.

[10] https://www.torpac.com/rat.htm

[11] LI, Ping; ZHAO, Luwei. Developing early formulations: practice and perspective. *International Journal of Pharmaceutics*, 2007, 341.1-2: 1-19.

[12] TRENFIELD, Sarah J., et al. 3D printing pharmaceuticals: drug development to frontline care. *Trends in pharmacological sciences*, 2018, 39.5: 440-451.

[13] KHALED, Shaban A., et al. 3D printing of tablets containing multiple drugs with defined release profiles. *International journal of pharmaceutics*, 2015, 494.2: 643-650.

[14] JENNOTTE, Olivier, et al. Three-dimensional printing technology as a promising tool in bioavailability enhancement of poorly water-soluble molecules: a review. *International Journal of Pharmaceutics*, 2020, 580: 119200.

[15] REDDY DUMPA, Nagi; BANDARI, Suresh; A. REPKA, Michael. Novel gastroretentive floating pulsatile drug delivery system produced via hot-melt extrusion and fused deposition modeling 3D printing. *Pharmaceutics*, 2020, 12.1: 52.

[16] MELOCCHI, Alice, et al. 3D printing by fused deposition modeling of single-and multi-compartment hollow systems for oral delivery–A review. *International journal of pharmaceutics*, 2020, 579: 119155.

[17] ISO/ASTM 52900:2021(en) Additive manufacturing — General principles — Fundamentals and vocabulary, International Organization for Standardization, https://www.iso.org/obp/ui/#iso:std:iso-astm:52900:ed-2:v1:en (accessed 22.08.2025).

[18] AUEL, Tobias, et al. 3D printing of pharmaceutical dosage forms: Recent advances and applications. *Advanced Drug Delivery Reviews*, 2025, 217: 115504.

[19] GOOLE, Jonathan; AMIGHI, Karim. 3D printing in pharmaceutics: A new tool for designing customized drug delivery systems. *International journal of pharmaceutics*, 2016, 499.1-2: 376-394.

[20] ZHANG, Jiaxiang, et al. Pharmaceutical additive manufacturing: a novel tool for complex and personalized drug delivery systems. *AAPS PharmSciTech*, 2018, 19.8: 3388-3402.

[21] KOZAKIEWICZ-LATAŁA, Marta, et al. Binder jetting 3D printing of challenging medicines: from low dose tablets to hydrophobic molecules. *European Journal of Pharmaceutics and Biopharmaceutics*, 2022, 170: 144-159.

[22] CUI, Mengsuo, et al. Opportunities and challenges of three-dimensional printing technology in pharmaceutical formulation development. *Acta Pharmaceutica Sinica B*, 2021, 11.8: 2488-2504.

[23] MELNYK, Larissa A.; OYEWUMI, Moses O. Integration of 3D printing technology in pharmaceutical compounding: Progress, prospects, and challenges. *Annals of 3D Printed Medicine*, 2021, 4: 100035.

[24] PITZANTI, Giulia, et al. 3D Printing: an appealing technology for the manufacturing of solid oral dosage forms. *Journal of Pharmacy and Pharmacology*, 2022, 74.10: 1427-1449.

[25] KIM, Ji Hoon; KIM, Kyeongjin; JIN, Hyo-Eon. Three-dimensional printing for oral pharmaceutical dosage forms. *Journal of Pharmaceutical Investigation*, 2022, 52.3: 293-317.

[26] KONTA, Andrea Alice; GARCÍA-PIÑA, Marta; SERRANO, Dolores R. Personalised 3D printed medicines: which techniques and polymers are more successful?. *Bioengineering*, 2017, 4.4: 79.

[27] MUHINDO, Derick, et al. Recent advances in the applications of additive manufacturing (3D printing) in drug delivery: a comprehensive review. *Aaps Pharmscitech*, 2023, 24.2: 57.

[28] CHOU, Wai-Houng; GAMBOA, Alexander; MORALES, Javier O. Inkjet printing of small molecules, biologics, and nanoparticles. *International Journal of Pharmaceutics*, 2021, 600: 120462.

[29] IÇTEN, Elçin, et al. Dropwise additive manufacturing of pharmaceutical products for amorphous and self emulsifying drug delivery systems. *International journal of pharmaceutics*, 2017, 524.1-2: 424-432.

[30] FINA, Fabrizio, et al. Selective laser sintering (SLS) 3D printing of medicines. *International journal of pharmaceutics*, 2017, 529.1-2: 285-293.

[31] WANG, Ning; SHI, Huixin; YANG, Shude. 3D printed oral solid dosage form: Modified release and improved solubility. *Journal of Controlled Release*, 2022, 351: 407-431.

[32] RODRÍGUEZ-POMBO, Lucía, et al. Simultaneous fabrication of multiple tablets within seconds using tomographic volumetric 3D printing. *International Journal of Pharmaceutics: X*, 2023, 5: 100166.

[33] D'ÁVILA, Marcos Akira; MANZINI, Bruna Maria; DÁVILA, José Luis. Material Properties and Selections for Additive Manufacturing (AM). In: *3D & 4D Printing Methods for Pharmaceutical Manufacturing and Personalised Drug Delivery: Opportunities and Challenges*. Cham: Springer International Publishing, 2023. p. 131-148.

[34] PITZANTI, Giulia; LAMPROU, Dimitrios A. Vat photopolymerization methods for drug delivery applications. In: *3D & 4D Printing Methods for Pharmaceutical Manufacturing and Personalised Drug Delivery: Opportunities and Challenges*. Cham: Springer International Publishing, 2023. p. 181-194.

[35] XU, Xiaoyan, et al. Vat photopolymerization 3D printing for advanced drug delivery and medical device applications. *Journal of Controlled Release*, 2021, 329: 743-757.

[36] KARAKURT, Ilbey, et al. Stereolithography (SLA) 3D printing of ascorbic acid loaded hydrogels: A controlled release study. *International Journal of Pharmaceutics*, 2020, 584: 119428.

[37] VLACHOU, Marilena; SIAMIDI, Angeliki; PROTOPAPA, Chrystalla. Extrusion-based 3D printing methods for oral solid dosage forms. In: *3D & 4D Printing Methods for Pharmaceutical Manufacturing and Personalised Drug Delivery: Opportunities and Challenges*. Cham: Springer International Publishing, 2023. p. 195-218.

[38] NYAVANANDI, Dinesh; NARALA, Sagar; REPKA, Michael A. Hot-Melt Extrusion Paired Fused Deposition Modeling 3D Printing: Development of Pharmaceutical Medications. In: *3D Printing: Emerging Technologies and Functionality of Polymeric Excipients in Drug Product Development*. Cham: Springer International Publishing, 2023. p. 169-194.

[39] GOYANES, Alvaro, et al. Direct powder extrusion 3D printing: Fabrication of drug products using a novel single-step process. *International journal of pharmaceutics*, 2019, 567: 118471.

[40] WANG, Honghe, et al. Preparation of core-shell controlled release tablets using direct powder extrusion 3D printing techniques. *Journal of Drug Delivery Science and Technology*, 2023, 88: 104896.

[41] AGUILAR-DE-LEYVA, Ángela, et al. 3D printing direct powder extrusion in the production of drug delivery systems: state of the Art and future perspectives. *Pharmaceutics*, 2024, 16.4: 437.

[42] JACOBI, Daniel; PYO, Sung Min. Overview of Pharmaceutical 3D Printing Technologies. In: *3D Printing: Emerging Technologies and Functionality of Polymeric Excipients in Drug Product Development*. Cham: Springer International Publishing, 2023. p. 3-27.

[43] FANOUS, Marina, et al. Simplification of fused deposition modeling 3D-printing paradigm: Feasibility of 1-step direct powder printing for immediate release dosage form production. *International journal of pharmaceutics*, 2020, 578: 119124.

[44] SEOANE-VIAÑO, Iria, et al. Semi-solid extrusion 3D printing in drug delivery and biomedicine: Personalised solutions for healthcare challenges. *Journal of controlled release*, 2021, 332: 367-389.

[45] RAHMAN, Jhinuk; QUODBACH, Julian. Versatility on demand–The case for semi-solid micro-extrusion in pharmaceutics. *Advanced Drug Delivery Reviews*, 2021, 172: 104-126.

[46] KHALED, Shaban A., et al. Desktop 3D printing of controlled release pharmaceutical bilayer tablets. *International journal of pharmaceutics*, 2014, 461.1-2: 105-111.

[47] MORONI, Sofia, et al. 4D printed multipurpose smart implants for breast cancer management. *International Journal of Pharmaceutics*, 2023, 642: 123154.

[48] VUONG, Quan V.; ROACH, Paul D. Caffeine in green tea: its removal and isolation. *Separation & Purification Reviews*, 2014, 43.2: 155-174.

[49] BORANDEH, Sedigheh, et al. Polymeric drug delivery systems by additive manufacturing. *Advanced drug delivery reviews*, 2021, 173: 349-373.

[50] GIRI, Bhupendra Raj; POUDEL, Surendra; KIM, Dong Wuk. Cellulose and its derivatives for application in 3D printing of pharmaceuticals. *Journal of Pharmaceutical Investigation*, 2021, 51.1: 1-22.

[51] REPKA, Michael A.; LANGLEY, Nigel. *3D Printing*. 2023.

[52] LAMPROU, Dimitrios (ed.). 3D & 4D Printing Methods for Pharmaceutical Manufacturing and Personalised Drug Delivery: Opportunities and Challenges. 2023.

[53] JAIN, Sourabh; YADAV, S. K.; PATIL, U. K. Preparation and evaluation of sustained release matrix tablet of furosemide using natural polymers. *Research journal of pharmacy and technology*, 2008, 1.4: 374-376.

[54] PRAJAPAT, Priyanka; AGRAWAL, Dilip; BHADUKA, Gaurav. A brief overview of sustained released drug delivery system. *Journal of Applied Pharmaceutical Research*, 2022, 10.3: 05-11.

[55] COLOMBO, Paolo. Swelling-controlled release in hydrogel matrices for oral route. *Advanced Drug Delivery Reviews*, 1993, 11.1-2: 37-57.

[56] HÖLZL, Katja, et al. Bioink properties before, during and after 3D bioprinting. *Biofabrication*, 2016, 8.3: 032002.

[57] EL AITA, Ilias; BREITKREUTZ, Jörg; QUODBACH, Julian. Investigation of semi-solid formulations for 3D printing of drugs after prolonged storage to mimic real-life applications. *European Journal of Pharmaceutical Sciences*, 2020, 146: 105266.

[58] SCHWAB, Andrea, et al. Printability and shape fidelity of bioinks in 3D bioprinting. *Chemical reviews*, 2020, 120.19: 11028-11055.

[59] RONY, Farzana Khan, et al. Extrusion-Based 3D Printing of Pharmaceuticals—Evaluating Polymer (Sodium Alginate, HPC, HPMC)-Based Ink's Suitability by Investigating Rheology. *Micromachines*, 2025, 16.2: 163.

[60] ALBERTINI, Beatrice, et al. An investigation into the release behavior of solid lipid microparticles in different simulated gastrointestinal fluids. *Colloids and Surfaces B: Biointerfaces*, 2019, 173: 276-285.

[61] CEREA, Matteo, et al. Oral hydrophilic matrices having non uniform drug distribution for zero-order release: A literature review. *Journal of Controlled Release*, 2020, 325: 72-83.

[62] OKWUOSA, Tochukwu C., et al. On demand manufacturing of patient-specific liquid capsules via co-ordinated 3D printing and liquid dispensing. *European Journal of Pharmaceutical Sciences*, 2018, 118: 134-143.

[63] LIN, Duanquan; KELLY, Alan L.; MIAO, Song. Alginate-based emulsion micro-gel particles produced by an external/internal O/W/O emulsion-gelation method: Formation, suspension rheology, digestion, and application to gel-in-gel beads. *Food Hydrocolloids*, 2021, 120: 106926.

[64] FALCONE, Giovanni, et al. Floating ricobendazole delivery systems: a 3D printing method by co-extrusion of sodium alginate and calcium chloride. *International Journal of Molecular Sciences*, 2022, 23.3: 1280.

[65] ULERY, Bret D.; NAIR, Lakshmi S.; LAURENCIN, Cato T. Biomedical applications of biodegradable polymers. *Journal of polymer science Part B: polymer physics*, 2011, 49.12: 832-864.

[66] ESCUDERO, J. J., et al. Compaction properties, drug release kinetics and fronts movement studies of matrices combining mixtures of swellable and inert polymers. III: Effect of polymer substitution type. *International Journal of Pharmaceutics*, 2012, 434.1-2: 215-223.

[67] BARNES, Howard A. *A handbook of elementary rheology*. Aberystwyth: University of Wales, Institute of Non-Newtonian Fluid Mechanics, 2000.

[68] LEE, Chi H.; MOTURI, Venkat; LEE, Yugyung. Thixotropic property in pharmaceutical formulations. *Journal of controlled release*, 2009, 136.2: 88-98.

[69] BOM, Sara, et al. On the progress of hydrogel-based 3D printing: Correlating rheological properties with printing behaviour. *International Journal of Pharmaceutics*, 2022, 615: 121506.

[70] HERRADA-MANCHÓN, Helena; FERNÁNDEZ, Manuel Alejandro; AGUILAR, Enrique. Essential guide to hydrogel rheology in extrusion 3D printing: how to measure it and why it matters?. *Gels*, 2023, 9.7: 517.

[71] EDWARDS, Howell GM, et al. Metamorphosis of caffeine hydrate and anhydrous caffeine. *Journal of the Chemical Society, Perkin Transactions 2*, 1997, 10: 1985-1990.

[72] GIFT, Alan D., et al. Influence of polymeric excipients on crystal hydrate formation kinetics in aqueous slurries. *Journal of pharmaceutical sciences*, 2008, 97.12: 5198-5211.

[73] MAZEL, Vincent, et al. Polymorphic transformation of anhydrous caffeine under compression and grinding: a re-evaluation. *Drug development and industrial pharmacy*, 2011, 37.7: 832-840.

[74] DICHI, Emma; LEGENDRE, Bernard; SGHAIER, Mehrez. Physico-chemical characterisation of a new polymorph of caffeine. *Journal of Thermal Analysis and Calorimetry*, 2014, 115.2: 1551-1561.

[75] LEYK, Edyta; WESOLOWSKI, Marek. Miscibility and solubility of caffeine and theophylline in hydroxypropyl methylcellulose. *Pharmaceutics*, 2021, 13.11: 1836.

[76] FRATINI, Costanza, et al. Direct powder extrusion (DPE) 3D-printing of mini-tablets for preclinical studies in rodents. *International Journal of Pharmaceutics*, 2025, 675: 125542.

[77] LUEBBERT, Christian; STOYANOV, Edmont; SADOWSKI, Gabriele. Phase behavior of ASDs based on hydroxypropyl cellulose. *International journal of pharmaceutics: X*, 2021, 3: 100070.

[78] PÖSTGES, Florian, et al. Phase homogeneity in ternary amorphous solid dispersions and its impact on solubility, dissolution and supersaturation–Influence of processing and hydroxypropyl cellulose grade. *International Journal of Pharmaceutics: X*, 2023, 6: 100222.

[79] LARSEN, Bjarke Strøm, et al. Impact of drug load and polymer molecular weight on the 3D microstructure of printed tablets. *European Journal of Pharmaceutical Sciences*, 2024, 192: 106619.

[80] PATEL, Nirali G.; SERAJUDDIN, Abu TM. Moisture sorption by polymeric excipients commonly used in amorphous solid dispersion and its effect on glass transition temperature: I. Polyvinylpyrrolidone and related copolymers. *International Journal of Pharmaceutics*, 2022, 616: 121532.

[81] FANOUS, Marina, et al. Development of immediate release (IR) 3D-printed oral dosage forms with focus on industrial relevance. *European Journal of Pharmaceutical Sciences*, 2020, 155: 105558.

[82] PFLIEGER, Thomas, et al. Influence of design parameters on sustained drug release properties of 3D-printed theophylline tablets. *International Journal of Pharmaceutics*, 2024, 658: 124207.

[83] ZALTARIOV, Mirela-Fernanda, et al. Hydrohypropyl cellulose/polyurethane blends. The behavior after accelerated ageing. A FTIR study. *Cellul. Chem. Technol*, 2020, 54.9-10: 903-914.

[84] ZAHIR, Md Hasan, et al. Preparation of a Sustainable Shape-Stabilized Phase Change Material for Thermal Energy Storage Based on Mg2+-Doped CaCO3/PEG Composites. *Nanomaterials*, 2021, 11.7: 1639.

[85] SHAO, Xinru, et al. Effect of bovine bone collagen and nano-TiO2 on the properties of hydroxypropyl methylcellulose films. *International Journal of Biological Macromolecules*, 2020, 158: 937-944.

[86] BURGER, Artur, et al. Energy/temperature diagram and compression behavior of the polymorphs of D-mannitol. *Journal of pharmaceutical sciences*, 2000, 89.4: 457-468.

[87] LI, Xiaoqiang, et al. Electrospun polyvinyl-alcohol nanofibers as oral fast-dissolving delivery system of caffeine and riboflavin. *Colloids and Surfaces B: Biointerfaces*, 2013, 103: 182-188.

[88] RODRÍGUEZ-POMBO, Lucía, et al. Simultaneous fabrication of multiple tablets within seconds using tomographic volumetric 3D printing. *International Journal of Pharmaceutics: X*, 2023, 5: 100166.

[89] JARADAT, Eman, et al. Microfluidics technology for the design and formulation of nanomedicines. *Nanomaterials*, 2021, 11.12: 3440.

[90] TIONG, Ngiik; ELKORDY, Amal A. Effects of liquisolid formulations on dissolution of naproxen. *European Journal of Pharmaceutics and Biopharmaceutics*, 2009, 73.3: 373-384.

[91] JUNQUERA, E.; AICART, E. A fluorimetric, potentiometric and conductimetric study of the aqueous solutions of naproxen and its association with hydroxypropyl-β-cyclodextrin. *International journal of pharmaceutics*, 1999, 176.2: 169-178.

[92] ERDEN, Nurhan; ÇELEBI, Nevin. A study of the inclusion complex of naproxen with β-cyclodextrin. *International journal of pharmaceutics*, 1988, 48.1-3: 83-89.

[93] LEE, Beom-Jin; LEE, Jeong-Ran. Enhancement of solubility and dissolution rate of poorly water-soluble naproxen by complexation with 2-hydroxypropyl-β-cyclodextrin. *Archives of pharmacal research*, 1995, 18.1: 22-26.

[94] JOHANNESSON, Jenny, et al. 3D-printing of solid lipid tablets from emulsion gels. *International journal of pharmaceutics*, 2021, 597: 120304.

[95] MOHSIN, Kazi; LONG, Michelle A.; POUTON, Colin W. Design of lipid-based formulations for oral administration of poorly water-soluble drugs: precipitation of drug after dispersion of formulations in aqueous solution. *Journal of pharmaceutical sciences*, 2009, 98.10: 3582-3595.

[96] AL-ASHAWY, Marwa, et al. Polymeric Emulsions of Polyethylene Glycol in Water Prepared by Flow-induced Phase Inversion Emulsification: The Effect of Polymer Molecular Weight. *Jordan Journal of Chemistry (JJC)*, 2021, 16.3: 147–152-147–152.

[97] ALSKAR, Linda C.; PORTER, Christopher JH; BERGSTROM, Christel AS. Tools for early prediction of drug loading in lipid-based formulations. *Molecular pharmaceutics*, 2016, 13.1: 251-261.

[98] GOYANES, Alvaro, et al. 3D printing of modified-release aminosalicylate (4-ASA and 5-ASA) tablets. *European journal of pharmaceutics and biopharmaceutics*, 2015, 89: 157-162.

[99] UBOLDI, Marco, et al. Investigation on the use of fused deposition modeling for the production of IR dosage forms containing Timapiprant. *International Journal of Pharmaceutics: X*, 2023, 5: 100152.

[100] BLUME, Gabriele; CEVC, Gregor. Liposomes for the sustained drug release in vivo. *Biochimica et Biophysica Acta (BBA)-Biomembranes*, 1990, 1029.1: 91-97.

[101] THOMAS, Nicky, et al. Characterising lipid lipolysis and its implication in lipid-based formulation development. *The AAPS journal*, 2012, 14.4: 860-871.

[102] ZEMA, L., et al. Different hpmc viscosity grades as coating agents for an oral time and/or site-controlled delivery system: an investigation into the mechanisms governing drug release. *Journal of pharmaceutical sciences*, 2007, 96.6: 1527-1536.

[103] CONTI, Stefania, et al. Matrices containing NaCMC and HPMC: 1. Dissolution performance characterization. *International Journal of Pharmaceutics*, 2007, 333.1-2: 136-142.

[104] ROCHE, Agnès, et al. Preliminary study on the development of caffeine oral solid form 3D printed by semi-solid extrusion for application in neonates. *AAPS PharmSciTech*, 2023, 24.5: 122.

[105] SUÁREZ-GONZÁLEZ, Javier, et al. Individualized orodispersible pediatric dosage forms obtained by molding and semi-solid extrusion by 3D printing: A comparative study for hydrochlorothiazide. *Journal of Drug Delivery Science and Technology*, 2021, 66: 102884.

[106] FUNK, Nadine Lysyk; FANTAUS, Stephani; BECK, Ruy Carlos Ruver. Immediate release 3D printed oral dosage forms: how different polymers have been explored to reach suitable drug release behaviour. *International Journal of Pharmaceutics*, 2022, 625: 122066.

[107] D'SOUZA, Anisha A.; SHEGOKAR, Ranjita. Polyethylene glycol (PEG): a versatile polymer for pharmaceutical applications. *Expert opinion on drug delivery*, 2016, 13.9: 1257-1275.

[108] ROWE, Raymond C., et al. *Handbook of pharmaceutical excipients*. Pharmaceutical press, 2020.

[109] GARCÍA-HERRERO, Víctor, et al. Improvement of the surface hydrophilic properties of naproxen particles with addition of hydroxypropylmethyl cellulose and sodium dodecyl sulphate: *In vitro* and in vivo studies. *International journal of pharmaceutics*, 2017, 529.1-2: 381-390.

[110] MURA, P., et al. Properties of solid dispersions of naproxen in various polyethylene glycols. *Drug development and industrial pharmacy*, 1996, 22.9-10: 909-916.

[111] SOVIZI, M. R. Thermal behavior of drugs: investigation on decomposition kinetic of naproxen and celecoxib. *Journal of thermal analysis and calorimetry*, 2010, 102.1: 285-289.

[112] KISSI, Eric Ofosu, et al. Influence of drug load on the printability and solid-state properties of 3D-printed naproxen-based amorphous solid dispersion. *Molecules*, 2021, 26.15: 4492.

[113] LÖBMANN, Korbinian, et al. A theoretical and spectroscopic study of co-amorphous naproxen and indomethacin. *International journal of pharmaceutics*, 2013, 453.1: 80-87.